LUND UNIVERSITY

Endoplasmic Reticulum Dynamic Structural Changes in Neurons: The Fission-Fusion Phenomena

Kucharz, Krzysztof

2010

Academic dissertation

Endoplasmic Reticulum Dynamic Structural Changes in Neurons: The Fission-Fusion Phenomena

by

Krzysztof Kucharz

This thesis will be defended on December 13th, 2010 at 09:00
in Segerfalksalen, Wallenberg Neuroscience Centre, Lund, Sweden.

Faculty opponent:
Professor Eric Hanse

LUND UNIVERSITY

Organization	Document name
LUND UNIVERSITY Department of Clinical Sciences Laboratory for Experimental Brain Research	DOCTORAL DISSERTATION
	Date of issue 2010-12-13
	Sponsoring organization Lund University
Author(s) Krzysztof Kucharz	

Title and subtitle

Endoplasmic Reticulum Dynamic Structural Changes in Neurons: The Fission-Fusion Phenomena.

Abstract

The endoplasmic reticulum (ER) is crucial for protein synthesis and protein maturation, is involved in cell stress and serves in neurons as the major intracellular Ca2+ store. Neuronal ER forms a continuous network of cisterns and tubules extending from soma to a subset of dendritic spines. The continuity of ER structure is important for maintaining ER basic functions and necessary for proteins and ions to diffuse and equilibrate within its lumen.

We show that ER in neurons can undergo rapid fission (=fragmentation) and subsequently fusion. This phenomenon was previously unknown in neurons. Our findings show that ER fission is induced during N-methyl D-aspartate (NMDA) receptor-mediated Ca2+ entry to the cell in murine primary cultures and hippocampal slice cultures. Using different pharmacological approaches, we demonstrate, that ER fission is triggered independently on Ca2+ from ER stores. Subsequently, we show that mild hypothermia, reported to be protective in experimental stroke models, enhances ER fragmentation. Finally, we validate the occurrence of rapid neuronal ER fission in an animal cardiac arrest model of cerebral ischemia.

We assessed ER structure using confocal microscopy live cell and tissue imaging, 2-photon laser scanning microscopy and transmission electron microscopy (TEM). The fluorescence imaging was performed on murine primary cultures cotransfected to express cytosolic and ER-specific markers; hippocampal slices from transgenic mice expressing ER-specific marker; as well as in transgenic living animals. To characterize the fission-fusion in a quantitative way, we developed a new data analysis method based on fluorescence recovery after photobleaching (FRAP).

Our data show that neuronal ER is a dynamic organelle. We propose a model of ER continuity, where ER is in equilibrium with fission-fusion events. Stimulation of NMDA receptors shifts the equilibrium towards the fragmentation, while inhibiting NMDA receptors promotes the continuous state of ER. We conclude that ER fission-fusion may be of importance in physiology and disease. The molecular machinery regulating the reversible changes in ER morphology remains unknown.

Key words: endoplasmic reticulum, neurons, fission, fragmentation, fusion, calcium, NMDA receptor, confocal microscopy, 2-photon microscopy, FRAP, primary cultures, organotypic slice cultures

Classification system and/or index termes (if any):

Supplementary bibliographical information:	Language
Faculty of Medicine Doctoral Dissertation Series 2010:129	English
ISSN and key title: 1652-8220	ISBN 978-91-86671-45-7
Recipient's notes	Number of pages 112 / Price
	Security classification

Endoplasmic Reticulum Dynamic Structural Changes in Neurons: The Fission-Fusion Phenomena

Krzysztof Kucharz

LUND UNIVERSITY

Doctoral Dissertation

Laboratory for Experimental Brain Research
Department of Clinical Sciences
Faculty of Medicine
Lund University
2010

ISSN 1652-8220

ISBN 978-91-86671-45-7

Lund University, Faculty of Medicine Doctoral Dissertation Series 2010:129

Printed in Sweden by Media-Tryck, Lund, Sweden.

To my family

A process cannot be understood by stopping it.
Understanding must move with the flow of the process, must join it and flow with it.

Frank Herbert, DUNE

CONTENTS

ABBREVIATIONS

aCSF – artificial cerebrospinal fluid
AMPA - α-amino-3-hydroxy-5-methyl-4-isoxazolepropionic acid
CA1, CA2, CA3 – *Cornu Ammoni* hippocampal regions
CICR – Ca2+-induced Ca2+ release
D-AP5 – D-(-)-2-amino-5-phosphonopentanoic acid
DIV – days in vitro
DHPG – 3,5-dihydrophenylglycine
EGFP – enhanced green fluorescent protein
EGTA - ethylene glycol tetraacetic acid
ER – endoplasmic reticulum
FRAP – fluorescence recovery after photobleaching
GaAsP – Gallium-Arsenide-Phosphide (detector)
IICR – IP3R-induced Ca2+ release
IP3R - inositol-3-phosphate receptor
K^+aCSF – high potassium artificial cerebrospinal fluid
mGluR – metabotropic glutamate receptor
MK-801 – 5-Methyl-10,11-dihydro-5H-dibenzo[a,d] cyclohepten-5,10-imine
NMDA – *N*-methyl *D*-aspartate
NMDAR – NMDA receptor
RER – rough endoplasmic reticulum
RyR – ryanodine receptor
SER – smooth endoplasmic reticulum
SPB – Sorensen's phosphate buffer
τ_{eff} – effective half time of FRAP signal recovery
TEM – transmission electron microscopy
UPR – unfolded protein response
VGCC – voltage-gated Ca2+ channels

ORIGINAL PAPERS

This thesis is based on the following papers, which are listed and referred to in the text by their respective Roman numerals (I-III).

I. Kucharz K., Krogh M., Ng A. N., Toresson H.
NMDA receptor stimulation induces reversible fission of the neuronal endoplasmic reticulum.

PLoS ONE 4:e5250. :2009

II. Kucharz K., Wieloch T. and Toresson H. Reversible Endoplasmic Reticulum fission in murine hippocampal pyramidal neurons in organotypic hippocampal slices is dependent on extracellular Ca^{2+}, NMDA receptor activation and is augmented by hypothermia.
Manuscript.

III. Kucharz K., Wieloch T. and Toresson H. Rapid Endoplasmic Reticulum fragmentation in cortical neurons of the mouse brain following cardiac arrest. An in vivo study.
Manuscript.

SUMMARY

The endoplasmic reticulum (ER) is crucial for protein synthesis and protein maturation, is involved in cell stress and serves in neurons as the major intracellular Ca^{2+} store. Neuronal ER forms a continuous network of cisterns and tubules extending from soma to a subset of dendritic spines. The continuity of ER structure is important for maintaining ER basic functions and necessary for proteins and ions to diffuse and equilibrate within its lumen.

We show that ER in neurons can undergo rapid fission (=fragmentation) and subsequently fusion. This phenomenon was previously unknown in neurons. Our findings show that ER fission is induced during *N*-methyl *D*-aspartate (NMDA) receptor-mediated Ca2+ entry to the cell in murine primary cultures and hippocampal slice cultures. Using different pharmacological approaches, we demonstrate, that ER fission is triggered independently on Ca2+ from ER stores. Subsequently, we show that mild hypothermia, reported to be protective in experimental stroke models, enhances ER fragmentation. Finally, we validate the occurrence of rapid neuronal ER fission in an animal cardiac arrest model of cerebral ischemia.

We assessed ER structure using confocal microscopy live cell and tissue imaging, 2-photon laser scanning microscopy and transmission electron microscopy (TEM). The fluorescence imaging was performed on murine primary cultures cotransfected to express cytosolic and ER-specific markers; hippocampal slices from transgenic mice expressing ER-specific marker; as well as in transgenic living animals. To characterize the fission-fusion in a quantitative way, we developed a new data analysis method based on fluorescence recovery after photobleaching (FRAP).

Our data show that neuronal ER is a dynamic organelle. We propose a model of ER continuity, where ER is in equilibrium with fission-fusion events. Stimulation of NMDA receptors shifts the equilibrium towards the fragmentation, while inhibiting NMDA receptors promotes the continuous state of ER. We conclude that ER fission-fusion may be of importance in physiology and disease. The molecular machinery regulating the reversible changes in ER morphology remains unknown.

SUMMARY IN SWEDISH

Det endoplasmatiska retiklet (ER) är nödvändigt för proteinsyntes och posttranslationell proteinmodifiering. ER är också iblandat i cellstress och utgör den största intracellulära kalciumkällan i nervceller. Neuronalt ER bildar ett kontinuerligt nätverk som består av dels rörliknande förbindelser (tubules) och större cisterner. Att nätverket utgör en kontinuerlig lumen är en viktig egenskap som gör att proteiner och kalciumjoner kan röra sig inom ER och utjämna lokala koncentrationsskillnader. Vi visar att ER i nervceller kan genomgå snabb fission (= fragmentering) och därefter fusion. Detta fenomen har tidigare inte rapporterats i neuron. Våra fynd visar att ER-fission i hippokampusneuron i primärkultur eller organotypa kulturer induceras av kalciuminflöde genom en särskild glutamatreceptorklass: NMDA-receptorn. Genom farmakologiska försök har vi visat att ER-fission induceras oberoende av kalciumfrisättning från ER. Dessutom har vi funnit att mild hypotermi leder till ökad fission. Detta är av intresse eftersom mild hypotermi har visat sig ha en skyddande effekt i experimentella stroke-modeller. Slutligen har vi med 2-fotonmikroskopi kunnat visa att snabb ER-fission också sker i hjärnan *in situ* i en djurmodell av hjärtstopp. Vi har studerat ER struktur med ljusmikroskopi (konfokal och 2-foton) i levande nervceller i primärkultur och organotypa kulturer samt i den levande hjärnan. För odlade celler användes transfektion för att få dessa celler att uttrycka fluorescerande proteiner specifikt i ER. För imaging av organotypa kulturer och hjärnan *in situ* genererades olika transgena musstammar med expression av ER-markörerna i olika populationer av neuron. Dessutom har transmissionselektronmikroskopi använts på fixerad vävnad från organotypa kulturer. För att möjliggöra kvantifiering av ER fission och fusion har vi utvecklat en ny dataanalysmetod baserad på ”fluorescence recovery after photobleaching” (FRAP). Våra data visar att ER är en dynamisk modell och vi föreslår en modell för ER-struktur där kontinuiteten av ER hela tiden bestäms av en jämvikt mellan fission och fusion. Aktivering av NMDA-receptorn skiftar jämvikten mot fission medan inhibering av NMDA-receptorn har motsatt effekt. Denna hittills okända strukturella dynamik har sannolikt viktiga funktionella konsekvenser för såväl fysiologiska som patofysiologiska processer vilket diskuteras i denna avhandling.

1. BACKGROUND

Endoplasmic reticulum (ER) is the largest single cellular organelle in neurons. The complexity of neuronal ER structure matches only the diversity of ER cellular functions. The following introduction highlights the most important aspects of ER structure in neurons and the implications of ER structure continuity in neuronal physiology.

1.1. ER structure

1.1.1. Continuity of neuronal ER structure

ER is present in nearly all compartments of a neuron and consists of the nuclear envelope (NE) and peripheral ER. Classically, peripheral ER is divided into two morphologically and functionally distinct domains: smooth (SER) and rough endoplasmic reticulum (RER) (Baumann and Walz, 2001).

While RER is localised mainly to the soma, SER is predominant in axons (Droz et al., 1975; Tsukita and Ishikawa, 1976; Renvoise and Blackstone, 2010), dendrites and can be found in dendritic spines (Martone et al., 1993; Spacek and Harris, 1997; Cooney et al., 2002),

Three-dimensional reconstructions display dendritic ER as a network of interconnected tubules and cisternae, forming a multidimensional continuous reticulum extending from soma through dendritic shaft to the subset of dendritic spines (Martone et al., 1993; Spacek and Harris, 1997; Cooney et al., 2002).

One of the most remarkable aspects of ER structure is the physical continuity of its lumen. The ER lumen continuity is preserved through all compartments of neuron, creating an intracellular endomembranous system in the cell (Droz et al., 1975; Martone et al., 1993; Spacek and Harris, 1997; Baumann and Walz, 2001; Cooney et al., 2002).

1.1.2. Diverse proteins orchestrate ER structure

The thermodynamic properties of a lipid bilayer do not favour the formation of more sophisticated structures, such as the tubular network of SER in dendrites and hence, proteins are needed to shape the ER (Shibata et al., 2009; Park and Blackstone, 2010). Theoretically, lipids with strong monolayer asymmetry are capable of creating a bilayer of high curvature, but based on the

lipid composition of biomembranes, such structures are unlikely to be present in biological systems (Zimmerberg and Kozlov, 2006; van Meer et al., 2008).

Although the functional aspects of ER have been extensively studied through decades, it is not until recently that the theories about the maintenance of complex ER structure have emerged (Shibata et al., 2009; Park and Blackstone, 2010). The first mechanisms proposed to be responsible for shaping the ER tubular structure evolved around the cytoskeleton (Terasaki et al., 1986). Microtubules can affect ER structure by three different mechanisms: the "sliding mechanism" (ER attached to microtubule by motor proteins "sliding" towards microtubule end), the "tip attachment complex (TAC) mechanism" (ER attached to the polymerising plus end of a microtubule) and the "microtubule movement mechanism" (ER attached to moving microtubules) (Waterman-Storer and Salmon, 1998; Du et al., 2004). However, findings from *in vitro* experiments showed that the presence of cytoskeleton elements is not necessary for formation of ER tubular network (Dreier and Rapoport, 2000; Roy et al., 2000), and the current view is that intramembrane proteins are responsible for shaping ER ultrastructure (Shibata et al., 2009; Park and Blackstone, 2010; Renvoise and Blackstone, 2010).

Recent findings implicated that the ubiquitous integral ER membrane proteins: reticulons (Voeltz et al., 2006); receptor expression enhancing protein 5 (REEP5) (Voeltz et al., 2006); REEP1 (Park et al., 2010); atlastin-1 (Hu et al., 2009; Orso et al., 2009) and M1 spastin (Park et al., 2010) may be of particular importance for ER morphogenesis. The common structural feature of these proteins is a double-hairpin hydrophobic domain embedded in the outer leaflet of ER membrane (Zhu et al., 2003; Voeltz et al., 2006; Park et al., 2010). It was proposed, that the hydrophobic domain acts as a molecular wedge generating the tubular structure of ER, however scaffolding mechanisms may contribute as well (Voeltz et al., 2006; Park and Blackstone, 2010; Park et al., 2010). *In vitro* experiments demonstrated that reticulons, REEP1, REEP5, and atlastin-1 are crucial for maintaining the tubular ER structure, and the tubular ER formation is a highly GTP-dependent process (Voeltz et al., 2006; Hu et al., 2009; Orso et al., 2009; Park et al., 2010). A structural model of was proposed, where reticulons, REEP1, atlastin-1 and M1 spastin form functional domain on the ER membrane and induce high curvatures, interacting via REEP1 and spastin with microtubules, thus providing a link between cytoskeleton and integral protein maintenance of ER structure (Park et al., 2010).

Other proteins implicated in playing important role in ER structure maintenance are valosin containing protein (VCP) (Roy et al., 2000) and mitofusin 2 (MFN-2) (de Brito and Scorrano, 2008). VCP was shown to reconstitute *in vitro* low-density microsomes from isolated vesicles into ER-like cisternal network, suggesting an important role for VCP in formation of smooth tubular membrane domains of transitional ER (Roy et al., 2000). MFN-2 protein regulates Ca2+ uptake from ER to mitochondria by

juxtaposing the two organelles. ER in MFN2-/- MEF cells appeared in the form of isolated vesicles, and rescuing the cells with ER-targeted functional MFN-2 variant rendered the ER continuous (de Brito and Scorrano, 2008).

Noteworthy, the mutations in atlastin and spastin are linked with hereditary spastic paraplegia (Hazan et al., 1999; Zhao et al., 2001); and mutations in VCP and MFN-2 with inclusion body myopathy, Paget's disease of the bone and frontotemporal dementia (Viassolo et al., 2008) and Charcot-Marie-Tooth neuropathy type 2A (Zuchner et al., 2004), respectively.

The fact that atlastin-1 and MFN-2 belong to the family of dynamin-like GTPases may provide a link between ER structure maintenance and other GTPases-dependent membrane processes occurring in the cell, such as COPI-, COPII- and clathrin-mediated vesicle trafficking (Kirchhausen, 2000; Pucadyil and Schmid, 2009) or mitochondria fission-fusion (Knott et al., 2008).

Studies on ER employ many different protocols, and although the proteins mentioned above were implicated to be important for ER morphogenesis, there is no evidence that they could mediate dynamic changes of neuronal ER architecture.

1.2. Neuronal ER structure dynamics

Despite its complexity, ER structure is not rigid and displays an ability of structural rearrangements, such as dynamic redistribution within a cell compartment or total remodelling of its architecture. The general knowledge about ER structure dynamics comes primarily from observations in non-neuronal cells and cell lines. Studies show that some cells exhibit dynamic ER structure remodelling in response to intra- or extracellular stimuli. Changes in ER organisation occur upon fertilization in the sea urchin (Terasaki and Jaffe, 1991) and starfish eggs (Terasaki et al., 1996), leading to reduction in ER lumen continuity. Similarly, high intracellular Ca2+ induced ER fission in 3T3 (Subramanian and Meyer, 1997) and HEK cells (Ribeiro et al., 2000).

Although the dynamic redistribution of ER was seen in dendrites, where ER can reversibly enter or exit spines (Toresson and Grant, 2005; Ng and Toresson, 2008), there is limited data on dynamic remodelling of ER ultrastructure in neurons. Formation of ER “lamellar bodies” was observed in Purkinje cells in rats in anoxia conditions (Banno and Kohno, 1996) and after intraventricular administration of glutamate (Banno and Kohno, 1998), however the dynamics of these “lamellar bodies” formation was never assessed. Alteration of ER continuity was observed in primary neuronal cultures stimulated by kainate (Sokka et al., 2007), but the phenomenon was not characterised in detail.

1.3. Neuronal ER function

1.3.1. ER as a site of protein synthesis

It is well established that the primary function of endoplasmic reticulum in all living cells is biosynthesis. In neurons the main site of protein synthesis is the soma, however there is increasing evidence for local protein synthesis occurring in dendritic spines (Steward and Schuman, 2001). ER is the first step in the secretory pathway. Newly synthesised proteins translocate to ER lumen where they are folded and assembled with the assistance of molecular chaperones, undergo processing, and are transported to ER exit sites and further to Golgi (Baumann and Walz, 2001; Lee et al., 2004).

The activity of many ER molecular chaperones depends on high intralumenal concentration of Ca2+, which is needed for the protein folding machinery to work efficiently (Michalak et al., 2002; Brostrom and Brostrom, 2003). A decrease in intralumenal Ca2+ may lead to gradual increase of unfolded proteins in ER lumen, which causes ER stress and subsequently induction of the unfolded protein response (UPR). UPR is manifested by protein synthesis inhibition, and while transient protein synthesis inhibition is considered to be a protective mechanism, if prolonged, leads to cell death (Paschen and Mengesdorf, 2005; Xu et al., 2005). UPR is postulated to be one of the factors contributing to neurodegeneration (DeGracia and Montie, 2004; Paschen and Mengesdorf, 2005).

1.3.2. ER as an intracellular Ca2+ store

Intracellular Ca2+ is a secondary messenger for many cellular processes in the cell and ER is a major intracellular Ca2+ sink and store (Berridge, 1998; Verkhratsky, 2005).

In the resting state, depending on the methods used, the concentration of free Ca2+ in ER lumen is estimated to be in the range of hundreds of micromoles, which is 2 to 3 orders of magnitude higher than in the cytosolic compartment (Verkhratsky, 2004). The effective buffering of Ca2+ in the neuronal ER lumen is achieved by a number of low-affinity, high-capacity Ca2+ binding proteins. The most abundant is calreticulin, which is extremely potent in buffering Ca2+ and possess up to 50 Ca2+ binding sites (Meldolesi, 2001; Verkhratsky, 2005). Other Ca2+ binding protein of significance is BiP (grp78), which, in addition to Ca2+ buffering, is involved in the ER stress response (Bertolotti et al., 2000; Paschen and Mengesdorf, 2005).

The gradient between cytosolic and intralumenal Ca2+ concentration is achieved with the assistance of sarco-endoplasmic Ca2+ ATPases (SERCA) pumps, which sequester Ca2+ into the ER lumen (Verkhratsky, 2005). The activity of SERCA is regulated indirectly by intralumenal Ca2+ concentrations (John et al., 1998; Li and Camacho, 2004).

The release of Ca2+ from ER lumen is mediated by two distinct classes of ER transmembrane receptor channels: inositol-3-phosphate receptors (IP3Rs) and ryanodine receptors (RyRs) (Berridge, 1998; Verkhratsky, 2005). IP3R is activated by inositol-3-phosphate (IP3), a downstream product of e.g. group I metabotropic glutamate receptors (mGluRs) stimulation. In addition, cytosolic Ca2+ levels may augment IP3R responses (Bezprozvanny et al., 1991). The activation of IP3R by IP3 leads to IP3-induced Ca2+ release (IICR) from ER (Berridge, 1998; Verkhratsky, 2005). RyRs are modulated mainly by rises in cytosolic Ca2+ mediated by either extracellular Ca2+ entry via voltage gated Ca2+ channels (VGCC) or receptor-operated channels, but the release of Ca2+ from neighbouring ER Ca2+ channels may contribute as well (Berridge, 1998; Verkhratsky, 2005). Cyclic ADP ribose (cADPR) can sensitise RyR to Ca2+, increasing channel activity (Hua et al., 1994). Activation of RyR in response to elevations in cytosolic Ca2+ levels results in Ca2+-induced Ca2+ release (CICR) from ER store (Berridge, 1998; Verkhratsky, 2005).

The uptake and release of Ca2+ events occur simultaneously and the fine balance between those processes is a basis for maintaining Ca2+ homeostasis in the cell. That is of great importance for neurons, where fluctuations of cytosolic Ca2+ levels are often associated with synaptic activity (Berridge, 1998; Verkhratsky, 2005).

1.4. Implication of ER structure on its functions

1.4.1. Neuronal ER permits movement of proteins and Ca2+ within its lumen

Three-dimensional reconstructions, although helpful to delineate the structure of ER, do not address the properties of the continuous intra-ER aqueous space, i.e. the ability of proteins and ions to distribute within ER lumen.

The first assessments of ER continuity in neurons were done in early 90-ties by monitoring diffusion of the lipophilic fluorescent dye dicarbocyanine (Dil) in ER membranes (Terasaki et al., 1994), but detailed observations came later from studies in non-neuronal cells. The diffusion of green fluorescent protein (GFP) localised to the ER lumen in CHO cells demonstrated that proteins in size of GFP (~30 kDa) distribute within continuous volume of ER (Dayel et al., 1999). Even proteins larger in size, such as elastase-GFP (~60 kDa) could move within ER compartment of 3T3 cells relatively easy, and the speed of protein relocation was estimated to be ~10 μm/min (Subramanian and Meyer,

1997). The increasing evidence for diffusion of proteins within the ER lumen has been strengthened recently, when lentivirally delivered lumenal GFP could distribute freely in ER of different cell lines and neurons (Jones et al., 2008). Further insights shown that ER lumen of astrocytes and neurons in primary cultures and cortical explants permits the movement of a photoactivatable variant of the probe, confirming thus the functional, as well as structural continuity of neuronal ER (Jones et al., 2009).

The fact that proteins can distribute relatively freely within ER lumen does not automatically imply that this is the case for Ca2+. Yet, local uncaging of Ca2+ in ER lumen in pancreatic acinar cells revealed that Ca2+ diffuse within ER volume in distances of ~19 μm within seconds (Park et al., 2000). Recent advances in methods, allowing direct monitoring of ER lumen Ca2+ in neurons, confirmed this observation and it was estimated that Ca2+ can be tunnelled within ER in distances of ~30 μm within a second (Choi et al., 2006). Low-affinity Ca2+ binding proteins in the ER lumen allow more efficient diffusion of Ca2+ compared to cytosol, which buffers Ca2+ movement by high-affinity Ca2+ binding proteins, therefore the continuous ER lumen can be seen as an effective traffic route for Ca2+ in the cell (Petersen and Verkhratsky, 2007).

1.4.2. ER lumen continuity and Ca2+ signalling

The ability of ER lumen to efficiently distribute Ca2+ is important for coordination of spatially separated events in highly polarised cells, therefore ER can be referred to as a signal integrating organelle, which in neurons links synaptic events with distant compartments of the cell (Berridge, 1998; Verkhratsky, 2005; Petersen and Verkhratsky, 2007). Importantly in neurons, the continuous ER lumen allows the replenishment of Ca2+ released from the ER store via IP3R or RyR. The locally depleted ER store can be refilled with Ca2+ from the rest of ER, and during a substantial depletion, with extracellular Ca2+ via store-operated Ca2+ entry mechanism (SOCE) (Bouron, 2000; Baba et al., 2003). The refilling of locally depleted ER Ca2+ store may prevent the aggregation of misfolded proteins, which could occur in low lumenal Ca2+ conditions due to impairment of Ca2+ dependant protein folding machinery (Paschen and Mengesdorf, 2005; Xu et al., 2005). The continuous ER may provide the nuclear envelope with the constant supply of Ca+ to be released via nuclear envelope Ca2+ channels (Fedorenko et al., 2008) and the changes in intralumenal Ca2+ due to the synaptic activity may affect nuclear Ca2+ signalling (Petersen and Verkhratsky, 2007). Nuclear Ca2+ signals are important for regulation of gene expression in the cell, and several cascades regulating transcription have been shown to be Ca2+ dependent, including CREB-mediated gene expression (Bito et al., 1997; Hardingham et al., 2001). Finally, the continuity of ER may help to integrate synaptic signalling with

long-lasting adaptive responses, thus it may the factor contributing to modulation of synaptic plasticity (Bardo et al., 2006).

It is likely then, that alteration of ER network structure that would result in loss of ER lumen continuity would have an impact on ER functions, such as protein secretory pathway, Ca2+ homeostasis and signalling in neurons.

1.5. NMDAR mediated Ca2+ entry as the entry point of the study

NMDARs are one of the subtypes of glutamate receptors that mediate excitatory transmission in the brain. Other subtypes include AMPA receptors, metabotropic glutamate receptors (mGluRs) and kainate receptors. NMDARs are heterotetrameric receptors typically composed of two obligatory NR1 subunits and two NR2 (A-D) subunits (Lau and Tymianski, 2010). NR2A and NR2B are the most common subunits in hippocampus and the ratio of NMDARs containing NR2A or NR2B changes in development (Monyer et al., 1994). NMDARs are ionotropic receptors and their conductance to Ca2+ is highly voltage-dependent. In the resting state the NMDAR channel pore is blocked by magnesium (Mayer et al., 1984). Depolarisation of plasma membrane relieves magnesium block from NMDAR channel pore and upon glutamate and glycine stimulation NMDAR becomes permeable to Ca2+ and potassium, mediating extracellular Ca2+ influx to the cell (Mayer et al., 1984; Johnson and Ascher, 1987; Lau and Tymianski, 2010).

The observations of dynamic ER structure remodelling in response to elevated intracellular Ca2+ levels in non-neuronal cells (Subramanian and Meyer, 1997; Dayel et al., 1999; Park et al., 2000; Ribeiro et al., 2000) as well as in neurons (Banno and Kohno, 1996; Banno and Kohno, 1998; Sokka et al., 2007) lead to hypothesis that these processes may occur during events associated with NMDAR mediated Ca2+ entry in neurons.

2. THE AIMS OF THE STUDY

The main aims of the thesis were:

- to develop protocols for assessing ER dynamic structural changes in neurons in primary cultures, slices and the living brain;

- to assess whether neuronal ER in primary neuronal cultures, tissue slices, and the living brain is capable of rapid structural remodelling – fission;

- to validate, whether ER fission is a reversible process;

- to characterise the key players involved in rapid ER structure remodelling;

- to investigate the properties of fragmented ER.

3. MATERIALS

The experiments described in this thesis were carried out in murine primary neuronal cultures (Paper I), mouse hippocampal organotypic slice cultures (Paper I, II) and *in vivo* mouse brain (Paper III).

3.1. Primary cultures

The ER fission-fusion phenomenon was first detected in hippocampal primary neuronal cultures, therefore this preparation was used for the initial investigation of ER dynamics. To monitor ER structural changes, primary cultures were transfected to coexpress ER lumen and cytosolic fluorescent markers.

3.1.1. Hippocampal primary neuronal cultures preparation

Day 17 pregnant NMRI mice (Scanbur, Taconics) were sacrificed and the isolated uteri put into ice cold PBS (Gibco). Subsequently, the heads were removed and transferred into Petri dishes with ice cold HBSS (Gibco) supplemented with 4.17 mM $NaHCO_3$. The hippocampi were subdissected under a surgical microscope. The tissue was cut with fine scissors, transferred into 15 ml conical tube and disaggregated mechanically by triturating. The cells were washed twice with HBSS with 4.17 mM $NaHCO_3$ (pH = 7.4) and the remaining cell pellet was resuspended in Neurobasal medium with 2% B27, 0.5 mM L-glutamine and 1x pen/strep (all Gibco) supplemented with 25 mM glutamate (Fluka). Cells were seeded at $4x10^5$ cells/ml in 4 well imaging chambers slides (Nunc) coated the previous day with 10 mg/ml Poly-D-lysine and 5 μg/ml laminin (both Sigma). The cultures were maintained at 37°C in 5% CO_2.

3.1.2. Primary cultures transfections

The cells were transfected at 4 day in vitro (DIV) to express the fluorophore of choice using Lipofectamine 2000 (Invitrogen) according to the manufacturer's instructions. The amount of DNA used in lipofection never exceeded 1 mg/ml. The cells were transfected for 3-5 h and the liposome/DNA containing media were replaced with fresh glutamate-free Neurobasal medium supplemented as described above (3.1.1.). Subsequently, cultures were left for 7-

days and afterwards 1/3 of the media volume was changed every 3-4 days.

3.1.3. Fluorophores used in primary cultures

To characterise the dynamic changes of ER morphology in primary cultures, we used genetically encoded fluorophores described below.

3.1.3.1. EGFP and RedER

In order to monitor the general morphology of dendrites and to analyse ER structure simultaneously, the cells were cotransfected with two different plasmids encoding enhanced green fluorescent protein (EGFP) and DsRed2-ER (hereafter also called RedER) marker. EGFP is used as a cytosolic marker, while RedER is a fluorophore localised to ER, containing calreticulin ER-targeting sequence as well as KDEL ER retention signal. The amount of plasmid DNA used for transfection was 0.4 mg/ml for EGFP and 0.6 mg/ml for RedER. Both plasmids were obtained from Clontech.

3.1.3.2. EGFP-ER and DsRed2

To test whether ER fragmentation is not an artefact caused by expression of RedER some cultures were cotransfected to express EGFP-ER, an ER specific marker, while the cytosolic DsRed2 was used to monitor the general morphology of neurons. The amount used in transfection was 0.4 mg/ml for DsRed2 and 0.6 mg/ml for EGFP-ER. DsRed2 was obtained from Clontech, EGFP-ER was a gift from Thomas Oertner, FMI, Basel.

3.2. **Organotypic slice cultures**

The next step was to study the ER fission-fusion phenomena in hippocampal slices representing a more biologically complex system compared to primary cultures, with all cellular constituents of the brain parenchyma except the blood. The transfection of slices with Lipofectamine resulted in very low transfection yield of RedER and led to tissue damage and extensive cell death. To overcome this problem, a transgenic mouse line was generated from B57 black 6 (C57BL/6) mice. The transgenic line expressed cytosolic EGFP and ER lumen RedER under control of the Thy1 neuronal specific promoter.

3.2.1. Generation of Thy1-RedER transgenic mice

The transgene construct was generated to express RedER and cytosolic EGFP from the same transcript by internal ribosome entry site (IRES) mediated EGFP translation. The RedER gene was derived from the same plasmid used in primary cultures (pDsRed2-ER) and cloned into pIRES2-EGFP vector (both Clontech). Next, the RedER-IRES2-EGFP fragment was cloned into pThy-1 vector (gift from Joshua R. Sanes, Washington University). Mainly the RedER signal was used for analysis, since the translation from IRES in animals was weak, resulting in insufficient fluorescence intensity of cytosolic EGFP for imaging procedures. By evaluating RedER fluorescence intensity and distribution in cells, from two constructed transgenic lines, line 27 was found optimal for further analysis.

3.2.2. Preparation of hippocampal organotypic slice cultures

Hippocampal slice cultures were prepared from 7-days old Thy-1 RedER/EGFP line 27 transgenic mice as described (Rytter et al., 2003). The pups were decapitated and brains transferred to ice cold HBSS (Gibco) supplemented with 20 mM HEPES (Sigma), 6 mg/ml D-glucose (Sigma) and pen/strep (Gibco). Hippocampi were subdissected and cut into 250 µm thick slices using McIlwan Tissue Chopper. Next, the tissue sections were transferred to Millicell culture inserts (Millipore), three per insert, and put into 6 well culture plates. Slice cultures were maintained at 35^{o}C, 5% CO_2 in 50% MEM with 25% heat inactivated horse serum, 18% HBSS/$NaHCO_3$ (pH= 7.4) supplemented with 6mg/ml D-glucose, 2% B-27, 4 mM L-glutamine and pen/strep. After 7 DIV slices were grown in maintaining medium (as above) without B-27 supplement. All materials were from Gibco, except D-glucose (Sigma).

3.3. Animal preparation for *in vivo* study

One of our aims was to analyse ER dynamic structure changes in living mouse brain (*in vivo*). In order to do that, a new transgenic mice line had to be generated. The new line expressed ER-targeted EGFP, which was more suitable for *in vivo* multiphoton imaging compared to RedER.

3.3.1. Generation of Thy1-EGFP-ER transgenic mice

Similarly as for Thy-1 RedER/EGFP line, the B57 black 6 (C57BL/6) mice were used to generate the transgenic animals. The transgene was constructed to

express EGFP targeted to ER under neuronal Thy-1 promoter using EGFP gene containing calreticulin ER-targeting sequence and KDEL ER-retention signal (gift from Thomas Oertner; Friedrich Miescher Institute) cloned into pThy-1 vector (gift from Joshua R. Sanes Washington University). The fluorescence signal strength and the cellular expression patterns were assessed in three generated transgenic lines and the Thy1-EGFP-ER-7b line was chosen for further experiments.

3.3.2. Cranial window surgery

In order to assess the dynamics of the ER structure in the living brain a cranial window surgery was performed on transgenic Thy1-EGFP-ER-7b mice. The method was mainly based on protocol developed by Anthony Holtmaat (Holtmaat et al., 2009) with minor modifications. During all steps of surgery the temperature of the animal was maintained at 37^{o}C and monitored using YSI-451 rectal thermistor probe with TC-1000 Mouse Proportional temperature controlling unit connected to 08-13013 mouse small heating pad (all Linton Instrumentation, Norfolk, UK).

Mice under 3.5% isoflurane in oxygen/nitrous oxide (30:70) anaesthesia were transferred onto a custom build operating stage. The head of the animal was shaved and the animal was placed into a stereotactic head frame. The eyes were treated with Viscotears (Novartis, Switzerland) to preserve eye humidity. The anaesthesia was decreased to 1.8-2% isoflurane and the animals were injected with Temgesic (dosage: 0.1 mg/kg; active substance: buprenorfin; Schering-Plough, Germany). The shaved skin was washed with chlorhexidine and iodine. The scalp and periosteum was removed and Marcaine (dosage: 2.5 mg/ml; active substance: bupivacain; AstraZeneca, UK) was administered to the surface of the scar. Subsequently, the exposed edges of the scar were covered with a thin layer of tissue adhesive (Vetbond, 3M). Following that, the animal was injected with Rimadyl (dosage: 5mg/kg; active substance: carprofen, Pfizer) and Dexafort (dosage: 2 mg/kg; active substance: dexamethasone, Intervet, Netherlands)

An area of approximately 4 mm diameter was encircled on the anterior part of right parietal lobe to mark the location for craniotomy, which was performed using dental drill. To prevent tissue damage resulting from the excess of heat generated by the drill, the surface of the scull was flushed with cold saline in 5 minutes intervals during the drilling procedure. Subsequently, the scull bone flap was gently removed to preserve integrity of dura and to prevent excessive bleeding. Immediately after opening the cranium the haemostatic absorbable gelatin sponge (Spongostan®, Ferrosan, Denmark) prewetted with saline was placed on the surface of the brain to maintain brain humidity. Next, sterile liquid low melting agarose (Promega) was applied into the cranial window to remove the presence of air which could obscure the imaging and a sterile 5 mm

diameter circular coverglass (Karl Hecht GmbH & Co KG "Assistent", Germany) was positioned on top of the cranial opening. The rim of the coverglass was secured with Vetbond and the scull was coated with dental cement to stabilise the position of cranial window. Subsequently, a custom-made titanium bar was attached to the scull using dental cement. The purpose of the titanium bar was to firmly attach the mouse head to the stage during imaging.

3.3.3. Animal handling during the imaging

The animals were mounted to imaging insert by the titanium bar. Mice were spontaneously breathing 1.8-2% isoflurane in oxygen/nitrous oxide (30:70) during all steps of imaging. The animals were placed on the heating pad and the rectal temperature was maintained at 37^{o}C.

3.3.4. Potassium-induced cardiac arrest

Cardiac arrest was induced by intravenous injection of 0.5 ml 2 M KCl while the animal was on imaging stage. In all cases the injection resulted in immediate cessation of blood flow.

3.4. Drugs used in study

Glutamate, NMDA, ifenprodil, DHPG and D-AP5 were dissolved in water; ionomycin was dissolved in ethanol and MK-801, KN-93, thapsigargin and staurosporine in DMSO. All drugs were from Tocris Cookson Inc., except glutamate (Sigma).

4. METHODS

4.1. General remarks

The main method used to assess dynamic ER changes was live fluorescence microscopy. This technique allowed monitoring of the dynamic processes occurring in neurons over the time course of the experiments. The imaging was performed on neurons expressing fluorescent proteins in the cytosol or ER lumen. The analysis included collection of time-lapse images, 3D reconstructions of ER structure, and the dynamics of ER was assessed by fluorescence recovery after photobleaching (FRAP) analysis. For each type of biological specimen (neurons, tissue, *in vivo* brain) used in the studies the experimental approach and the imaging procedures had to be developed individually. For additional ER analysis, transmission electron microscopy (TEM) and Ca2+ imaging on primary neuronal cultures were used.

4.2. Live fluorescence imaging techniques

4.2.1. Live cell imaging on primary cultures

The cultures of 17-20 DIV age were used for analysis. Live cell imaging on primary cultures was performed using Zeiss LSM 510 inverted confocal microscope system (Zeiss). To preserve optimal conditions during imaging, the cultures were imaged in heating insert P with incubator S perfused with warm air with 5% CO_2 using objective equipped with a heating ring. Neurons were being imaged with Apochromat 63x N.A. 1.4 objective (Zeiss) in their growth medium. The temperature was maintained at 37^{o}C during all steps of imaging.

4.2.1.1. Imaging of EGFP and RedER in primary cultures

The images were collected as Z-stack series in multi-track mode. Cytosolic EGFP was excited with the 488 nm Argon laser and the emitted fluorescence was detected after a 505–530 nm band pass filter, RedER was excited with the He/Ne 543 nm laser and emission detected after a 560 nm long pass filter.

4.2.1.2. FRAP analysis in primary cultures

Fluorescence recovery after photobleaching (FRAP) was used to assess ER continuity. The fluorescence intensity was measured from selected region of interest (ROI) on a dendrite of spiny, multipolar neuron expressing EGFP and RedER. Multi-track mode was used and the fluorescence from both channels (EGFP and RedER) was recorded for 30 scanning cycles (~40 sec), then subsequently RedER was bleached with 100% He/Ne laser intensity in 80 iterations (~40 sec) and the signal recovery (FRAP) from RedER as well as the signal from EFGP was recorded up to 170 cycles (~250 sec). In addition, simultaneously with bleached ROI, the intensity from another ROI was recorded. The second ROI served to measure background signal strength and was defined always outside the dendrite, but adjacent to bleached (dendrite) ROI. For every neuron, the ROI from the same dendrite area was used in all time points of the experiment.

The time lapse recording of RedER signal defined FRAP curve, whereas the EGFP signal was recorded as control for fluctuations in FRAP due to e.g. focal drift. The final FRAP signal used for the analysis was defined as the ratio between fluorescence intensity of RedER and EGFP after subtracting the background from the two channels respectively.

4.2.2. Live tissue imaging on slices – NMDA experiments

To assess the NMDA induced ER structural changes, a Zeiss LSM 510 confocal microscope was used. The slices were carefully cut out from their culture inserts, placed in an imaging chamber with carbogen gassed artificial cerebrospinal fluid (NaCl: 119 mM, KCl: 2.5 mM, $MgSO_4$: 1.3 mM, NaH_2PO_4: 1 mM, $NaHCO_3$: 26 mM, $CaCl_2$: 2.5 mM, glucose: 11 mM, pH= 7.4) and imaged with Apochromat 63x N.A. 1.4 objective at 37°C.

The RedER signal was collected as described for primary cultures. The expression of EGFP and the signal generated with the LSM 510 setup was weak and not used for further analysis. CA3 pyramidal neurons with typical ER morphology were selected for analysis. The microscope settings used for imaging were as described for primary cultures (4.2.1.).

4.2.2.1. FRAP analysis in NMDA treated slices

For FRAP analysis of ER continuity in slices challenged with NMDA the same protocol was used as for primary cultures, however no EGFP signal was recorded (4.2.1.2).

4.2.3. Live tissue imaging on slices – potassium experiments

To assess structural changes of the ER during potassium induced cell depolarisation, the imaging was performed using Zeiss LSM 710 upright confocal microscope equipped with heated Slice Mini Chamber SMC-1 (Luigs & Neumann). The microscope stage and setup was superior to LSM 510 with regard to slice imaging and therefore LSM 710 was used for further analysis of ER fission-fusion analysis in slices.

Slices were carefully cut out from their membrane insert and transferred onto 50 mm circular Thermo Scientific cover glass in imaging chamber. The chamber was constantly perfused at the flow rate of 4.5 ml/min with carbogen gassed artificial cerebrospinal fluid (aCSF; pH= 7.4) or its variants (see: Paper II, Supplementary Table 1) respective to the type of experiment (see: Paper II, Supplementary Figure 2). The temperature of medium in the imaging chamber was controlled by a Badcontroller V unit (Luigs & Neumann) and the temperature of perfused medium was maintained by HPT-2 in-line tube heater controlled by MTC-20 unit (both npi electronic). The slices were imaged at 35°C (except hypothermia experiments: see Paper II, Supplementary Figure 2)

In all cases, slices were perfused on the stage for at least 5 min before commencing the imaging procedures. Achroplan 10x 0.3 N.A. water immersion objective was used to analyse the general tissue morphology and the inclusion criteria were as follows: pyramidal CA2 or CA3 neurons with normal dendrite morphology, strong expression of RedER (laser power used for imaging <10%) and FRAP signal recovery higher than 70% of its initial signal strength. The slices used for imaging were between 10 and 14 DIV.

4.2.3.1. FRAP analysis on slices – LSM 710

For FRAP analysis, one dendrite of pyramidal neuron with typical ER morphology was chosen from each slice. The experiments were performed using Plan-Apochromat 63x/1.0 NA water immersion objective. The FRAP signal was recorded from RedER in single track mode using 543 nm HeNe laser for excitation and the signal collected after 545-700 nm band pass filter.

Mean RedER fluorescence intensity was measured from a 2 µm x 2 µm square selected region of interest (ROI) on a selected dendrite for 15 scanning cycles (~7.4 sec), bleached for 80 iterations with 100% HeNe laser intensity (~4.6 sec) and FRAP curve was recorded for up to 90 cycles (~17.8 sec). The signal was colleted from a 7.6 µm optical slice (maximum pinhole opening) to minimize the effect of focal drift on FRAP recording. For every neuron, the same dendrite area was used at every FRAP recording in the time course of the respective experiment.

4.2.4. *In vivo* imaging of the mouse brain

To assess the dynamic properties of the ER architecture in the living mouse brain, 2-photon laser scanning microscopy (2PLSM) was used (Svoboda and Yasuda, 2006). The imaging was carried out with multiphoton Zeiss LSM 7MP upright laser scanning microscope equipped using W-Plan Apochromat 20x/1.0 DIC Vis-IR water immersion objective. GreenER was excited by Mai Tai DeepSee Ti:Sapphire pulse laser (Spectra-Physics) tuned to 900 nm and the signal collected in single-track mode using Gallium-Arsenide-Phosphide (GaAsP) spectral detector.

4.2.4.1. FRAP analysis in vivo

In analogy to the experiments performed in primary cultures and slices, FRAP analysis was used to assess the changes of ER continuity in the brain of a living mouse. FRAP was recorded from 10 randomly chosen dendrites (one dendrite per neuron) before and after potassium induced cardiac arrest. The mean fluorescence intensity signal was recorded from a 2 μm x 2 μm selected ROI on a dendrite for 10 scanning cycles (~1.55 sec), bleached for 15 cycles (~0.82 sec) with 100% Mai Tai DeepSee Ti:Sapphire pulse laser intensity. The FRAP curve was recorded for 90 cycles (~15.30 sec). The data was normalized to the initial signal fluorescence intensity strength and presented as mean ± standard deviation of mean.

4.3. Data analysis

4.3.1. The basics of conventional FRAP analysis

The FRAP analysis is usually used to measure the diffusion of molecules within an enclosed volume of a specimen. In our study we applied the FRAP method to quantify the degree of ER fragmentation by monitoring the diffusion of fluorescent molecules within ER lumen. The principles of FRAP used in the ER analysis are represented in Figure 1.

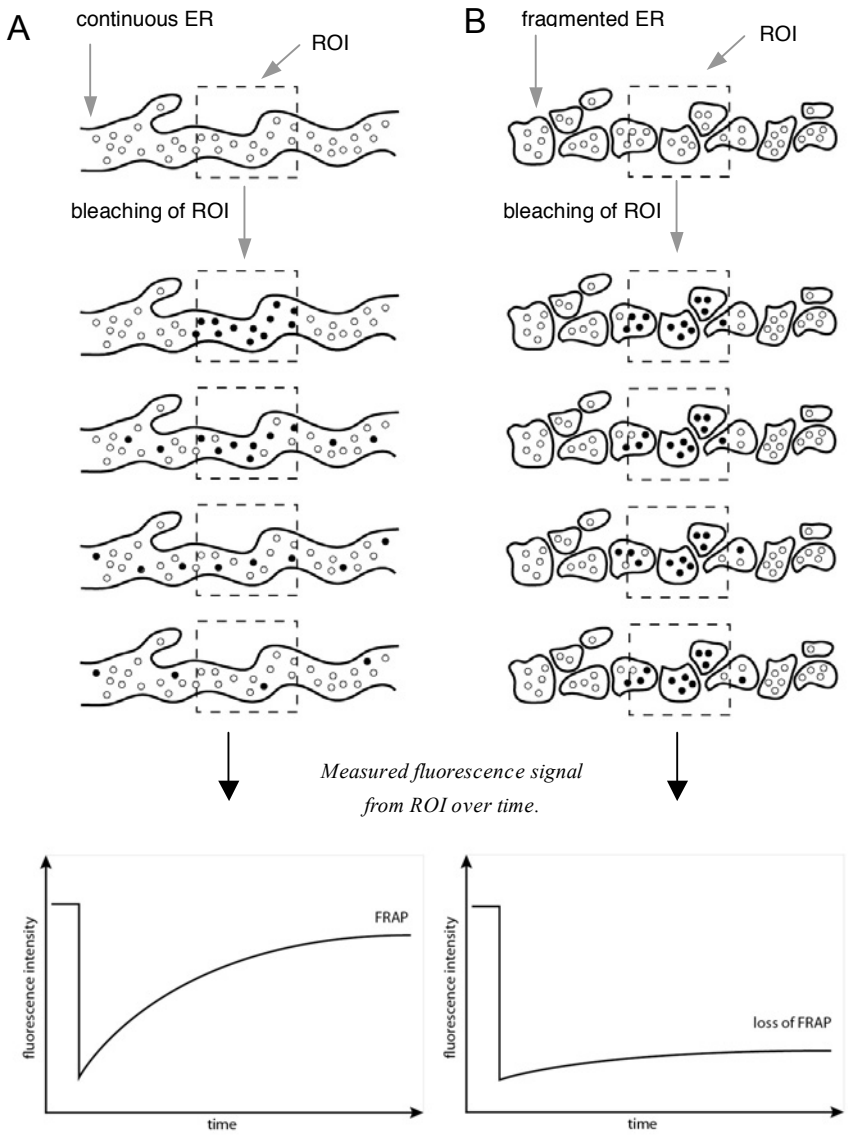

Figure 1: The translation of ER continuity into FRAP signal recovery. A) Continuous structure (i.e. ER volume) allows the equilibration of bleached molecules with unbleached molecules after photobleaching contributing to fluorescence signal recovery measured from selected ROI. B) Non-continuous structure impairs the equilibration of bleached molecules, contributing to loss of FRAP. Black circles represent bleached molecules, white circles are unbleached molecules.

The continuous structure of ER allows the fluorescent molecules to freely equilibrate within its lumen. By defining the region of interest (ROI) and bleaching the molecules within ROI with high laser power, the average fluorescence intensity collected from ROI initially drops, and then subsequently recover over time. The recovery is due to the inflow of non-bleached molecules from outside ROI to bleached area and the exit of bleached molecules from ROI. The exchange of molecules is possible due to the continuous ER lumen. The recorded average fluorescence intensity over time from ROI plots fluorescence recovery after photobleaching curve (Figure 1).

However, the more fragmented ER, the lesser is the diffusion of bleached molecules and the fluorescence intensity recorded from bleached ROI recovers slower, indicating loss of FRAP (Figure 1). This observation is a basis of indirect measurement of ER lumen continuity: the lower the FRAP, the more fragmented ER.

Typically, FRAP data are presented in a form of averaged fluorescence recovery curves, but in most cases no quantitative measurement of FRAP is being provided. Although this representation may be suitable for analysis of binary effects (FRAP vs. lack of FRAP) it doesn't allow the reliable comparison between curves of similar recovery.

Sporadically, the values of mobile and immobile fraction are calculated. Mobile fraction represents the volume (or fraction of molecules) of signal recovery over time and immobile fraction is the volume (or fraction of molecules) that was permanently bleached and will not be replenished with unbleached molecules (Figure 2).

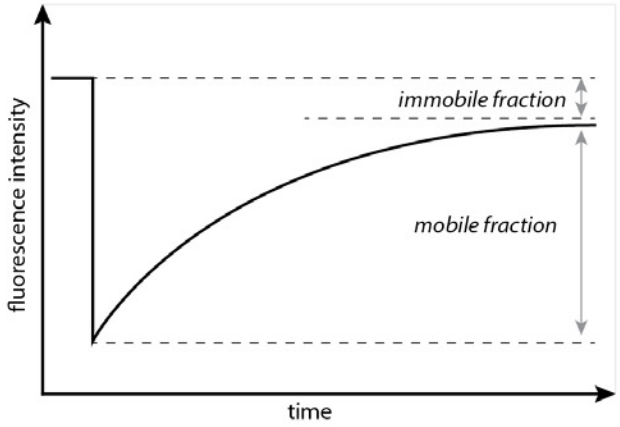

Figure 2: Schematic representation of immobile and mobile fraction on theoretical FRAP curve. Immobile fraction is calculated from a difference between initial signal strength and the asymptote of signal recovery; Mobile fraction is the fraction of signal recovery, calculated from a difference between asymptote of signal recovery and the lowest intensity after rapid photobleaching step.

This approach is valid only for idealised conditions, where the fluorescence recovery reaches clearly defined plateau, no bleaching during scanning procedures occurs and imaging is performed using the same laser power for all of the samples. Being unable to match these criteria, the measurements may produce results that are strongly affected by factors independent of intrinsic properties of investigated specimen.

4.3.2. Modelling ER continuity in FRAP analysis

In our study we aimed at quantifying the data from FRAP experiments by defining τ_{eff} (effective half-time of signal recovery) - a single measurable value that would reliably represent the degree of ER continuity, independently of the factors listed above.

We found that the double exponential growth function provides sufficient fit to the FRAP recovery signal plot. This suggested that the recorded FRAP signal consists of the sum of at least two independent recovery processes. We proposed a model, with the main assumption that ER within ROI consists of at least two volumes (V_1 and V_2), and the RedER molecules (bleached or non-bleached) are exchanged from these volumes with molecules outside ROI with a constant exchange rate of k_1 and k_2, respectively (see: Paper I; Figure 2c). Except V_1, V_2, k_1 and k_2, the recorded fluorescence intensity is affected by the bleaching caused by either scanning procedures, or the rapid photobleaching step. These constants have been defined as *b* and *c* respectively. Together, these 6 parameters were used in defining the mathematical function that can be used to describe the FRAP in each of V1 and V2 volume over time. The function describing signal recovery would consist then of sum of two recoveries;

$$\frac{S(t)}{V} = \frac{S_1(t)}{V_1} + \frac{S_2(t)}{V_2}$$

and each of them would be composed of three equations;

I. $$\frac{S_i(t)}{V_i} = \frac{k_i}{(k_i + b)} + \left(1 - \frac{k_i}{(k_i + b)}\right)\exp(-(k_i + b)t)$$

II. $$\frac{S_i(t)}{V_i} = \frac{k_i}{(k_i + c)} + \left(S_i(t_1) - \frac{k_i}{(k_i + c)}\right)\exp(-(k_i + c)(t - t_1))$$

III. $$\frac{S_i(t)}{V_i} = \frac{k_i}{(k_i + b)} + \left(S_i(t_2) - \frac{k_i}{(k_i + b)}\right)\exp(-(k_i + b)(t - t_2))$$

.

where: i = 1 or 2 (indicating two distinct ER volumes);

$S_i(t)$ = fluorescence signal intensity over time;

V_i = respective ER volume;

k_i = constant of RedER molecules exchange rate;

b = continuous bleaching constant (bleaching due to the scanning procedures);

c = rapid bleaching constant (rapid photobleaching step);

t_1 = time when rapid bleaching starts;

t_2 = time when rapid bleaching ends and signal recovery starts;

t = total time of FRAP recording.

Each of the equations describe distinct segment in FRAP, and together they form a function modelling FRAP curve (Figure 3).

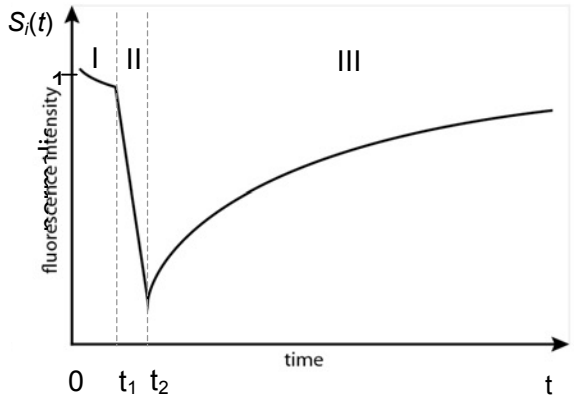

Figure 3: Schematic representation of a FRAP curve fit, which can be divided into three segments (I, II and III). I –fluorescence pre-bleaching scan, where loss of the recorded signal can be attributed to scanning procedures (bleaching constant b); II – rapid bleaching step (with constant bleaching c); III – florescence signal recovery after photobleaching (where constant bleaching b applies).

By fitting the model to the recorded FRAP curves we get the values of 6 constants: b, c, V_1, k_1 and V_2, k_2. The data was fitted using least squares error minimization and the parameters b, c, k1, V1, k2 and V2 were chosen to minimize this sum of squares (see: Paper I; Supplementary Figure 3).

The bleaching constants b and c are not intrinsic to neurons and depend on

settings used during imaging, therefore only V_1, k_1 and V_2, k_2 can be used to define the measurable value of ER continuity. For single ER volume, the half-time of signal recovery can be used as a good measure;

$$\tau_1 = \frac{\ln 2}{k_1} \text{ [s] and } \tau_2 = \frac{\ln 2}{k_2} \text{ [s]}$$

however, FRAP that consists of two compartments contributing to signal recovery does not have a simple half-time of recovery. In order to get a single half-time of recovery (τ_{eff}; effective half-time of recovery);

$$\tau_{eff} = \frac{\ln 2}{k_{eff}} \text{ [s]}$$

a single molecule exchange rate constant (k_{eff}) needs can be calculated from the equation;

$$(V_1 + V_2)\exp(-k_{eff}T) = V_1 \exp(-k_1 T) + V_2 \exp(-k_2 T)$$

where T is a defined time scale.

For all FRAP measurements the fluorescence intensity FRAP data was fitted to the model using least squares error minimization, i.e., the sum of the squares of the deviation of the data point and the predicted value was calculated and the parameters b, c, k1, V1, k2 and V2 were chosen to minimize this sum of squares. The calculated τ_{eff} value was used as a single measurable value of ER continuity (Figure 4).

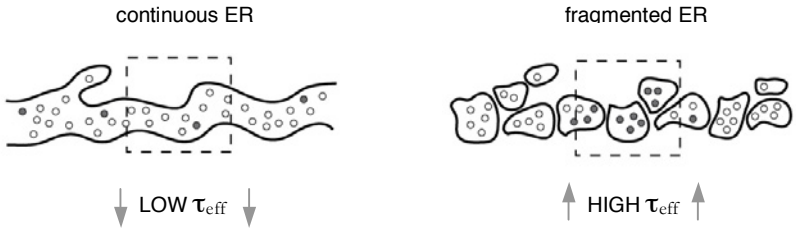

Figure 4: Schematic representation of dendritic ER where τ_{eff} indicates the degree of ER fragmentation.

The lower the molecule exchange constant (k_{eff}) the higher the effective half-time of recovery (τ_{eff}) indicating that ER is more fragmented since the lack of continuity restricts molecules from entering and exiting the bleached volumes of ER contributing to slower FRAP signal recovery.

4.3.3. Statistical analysis

The modelling of ER continuity statistical analysis was performed in R (Ihaka and Gentleman, 1996) (Paper I) and Microsoft Excel 2004 (Paper II). The model for the FRAP curves is described in the result section. For Paper I, the t-tests, paired or unpaired, were performed with distinct variances in the two groups, i.e. without assuming equal variance in the two groups. The standard R function t-test was used. For Paper II, two-tailed t-test was used within the group of single experiment and non-paired two-tailed t-test with Bonferroni correction ($n_{hypotheses} = 3$) for multiple comparisons of τ_{eff} at different time-points. Data in the results section were presented as average ± standard deviation. Box plots in figures show distribution and median. The circled points indicate outliers.

4.3.4. Fluorescence microscopy image processing

Images were exported from the Zeiss AIM software (for LSM 510) or Zeiss ZEN 2010 software (for LSM 710 and 7MP) as 8-bit projected images in TIFF or uncompressed JPEG format. The Z-stack images were projected using maximum intensity projection (except Paper III, Figure 1 where semi transparent intensity projection was used).

Adjustment of images (in LSM or Adobe Photoshop) was limited to changing the contrast and brightness of the whole image.

4.4. Transmission electron microscopy

Due to the limits in resolution of light-based microscopy the ultrastructure of neuronal ER was assessed by transmission electron microscopy (TEM).

4.4.1. Transmission electron microscopy sample preparation

The slices were fixed in their culture inserts with 1.5 % paraformaldehyde and 1.5% glutaraldehyde in 0.1 M Sörensen's phosphate buffer (SPB; 0.1 M NaH_2PO_4/Na_2HPO_4; pH= 7.2) for 1 h. Next, the slices were carefully cut off

from their membrane inserts, washed 3 times in SPB and postfixed for 1h in 1% OsO_4 in SPB. The tissue was washed 3 times SPB and dehydrated in ethanol with gradually increasing concentration (25%, 50%, 75% and 96% for 2x10 min respectively, and 100% for 2x15 min). Following that, the slices were incubated for 2x 20 min in 100% acetone and overnight in 1:1 mixture of acetone and epon resin polybed 812 (Polysciences). The specimen was transferred to pure resin for at least 4 h before the final embedding in new pure resin. The polymerization was at 60^{o}C for 48 h. The embedded specimen was sectioned in an ultratome (Super Nova, Reichert Jung) to 50 nm slices, which were subsequently mounted on slot copper grids previously covered with a thin film of pioloform. Finally, sections were stained in 4% uranyl acetate for 30 min at 40^{o}C and 0.5% lead citrate for 2 min at room temperature and air-dried before the imaging.

4.4.2. Transmission electron microscopy imaging

The TEM micrographs from slices were obtained using Philips CM 10 electron microscope. The pyramidal neurons of CA1 hippocampal region were chosen for analysis. The selection criteria were: neurons with no signs of cell death processes occurring in the cell (i.e. loss of cell membrane integrity or electron-dense chromatine condensation).

The electron micrograph negatives were scanned in 600 dpi in 16-bit grayscale mode and stored as tiff files.

4.5. Supplementary methods used in study

4.5.1. Ca2+ imaging on primary cultures

The method not included in the original papers, but referred to in results and discussion was fluorescence resonance energy transfer (FRET) ratiometric Ca2+ imaging on primary neuronal cultures using genetically encoded cytosolic Ca2+ sensor yellow cameleon 3.60 (YC3.60) indicator (Nagai et al., 2004).

The imaging was performed on 17-20 DIV primary neuronal cultures, transfected with YC3.60 construct (0.5 µg/µl) using the protocol described previously (see: 3.1.2). The imaging was carried out with LSM 510 confocal microscope system (see: 4.2.1). The time-lapse images were collected in single-track mode, the CFP component of YC3.60 was excited with 458 nm Argon laser and the emission detected after 475-525 nm band pass filter. The YFP component FRET emission was collected after 530 nm long pass filter. For every recording, the signal was collected from 3x5 µm ROI on dendrite and from the adjacent background ROI. The background signal was subtracted from

CFP and YFP respectively and the data was presented as YFP/CFP ratio over time.

The components of carbogen gassed Ca2+ free aCSF used to perfuse neurons during imaging were: NaCl 119 mM; KCl 2.5 mM; $MgSO_4$ 1.3 mM; NaH_2PO_4 1 mM; $NaHCO_3$ 26 mM; glucose 11 mM.

5. RESULTS AND DISCUSSION

5.1. ER structure in its basal state is continuous

In all preparations (primary cultures, organotypic slices and mice), FRAP analysis demonstrated that the ER lumen in neurons in the basal state displays a high degree of continuity. Both RedER (Paper I, II) and GreenER (Paper III) could diffuse within ER, accounting for fluorescence signal recovery.

This result is in accord with other studies demonstrating ER lumen continuity by monitoring fluorescent protein diffusion in neurons (Jones et al., 2008; Jones et al., 2009) or structure reconstructions (Martone et al., 1993; Spacek and Harris, 1997; Cooney et al., 2002). Noteworthy, in all of our studies the FRAP signal in naïve neurons never reached its basal state (i.e. 100% of initial fluorescence intensity), suggesting the presence of dendritic ER fractions, where the mobility of proteins is significantly reduced. This can be attributed to ER volumes that maintain continuity with the bulk of ER but are connected only via constricted ER tubular shafts (Martone et al., 1993; Spacek and Harris, 1997; Cooney et al., 2002). Alternatively, lack of complete signal recovery can be explained by the presence of completely isolated ER fragments. Indeed, a "non-continuous" ER fraction can be observed in dendritic shaft in the form of isolated ER vesicles (Martone et al., 1993; Spacek and Harris, 1997). However, it cannot be ruled out, that fluorescent molecules trapped within anterograde or retrograde transport vesicles in ER-Golgi intermediate compartment contribute to the loss of FRAP (Lee et al., 2004).

The morphology of axonal ER was not assessed due to the limited optical resolution of fluorescence microscopy.

5.2. ER can undergo rapid fission

ER fission was visually detected in all types of analysed specimen and the loss of ER continuity was confirmed by FRAP analysis (Paper I-III). The fragmentation of ER was induced by glutamate, NMDA or ionomycin in primary cultures; NMDA and potassium-induced cell depolarisation in slices (Paper I, II) and during cardiac arrest in cortical neurons *in vivo* (Paper III). In all cases, fragmented ER appeared in a form of numerous isolated structures. Interestingly, in every preparation, the average FRAP signal from neurons with fragmented ER displayed some degree of recovery. That could indicate, that with protocols used, the fission is not complete and ER maintains some level of continuity.

TEM was used to assess the ultrastructure of ER in slice cultures exposed to glutamate (Paper I). Both RER in soma and SER in dendrites appeared to be in form of dilated vesicles, substantiating the reduction of ER continuity.

ER fission observed in primary cultures upon bath application of lethal doses of glutamate or NMDA was rapid, occurring in the whole dendritic ER, without further relocation of ER fragments. In slices and in the animal study, an additional phenomenon was observed. A small population of ER vesicles were redistributed after fission in dendritic shaft, forming clusters of fragmented ER. At present, the nature of this mechanism is unknown, however excitotoxic conditions are accompanied by dendritic swelling that could enforce the clustered distribution of ER (Park et al., 1996; Hasbani et al., 2001; Gisselsson et al., 2005; Mizielinska et al., 2009). Microtubules are known to interact with ER affecting its distribution in cells (Waterman-Storer and Salmon, 1998; Du et al., 2004), hence the involvement of cytoskeleton in relocation of ER fragments cannot be excluded. The pattern of ER vesicle clustering was highly reproducible, with similar spatial distribution of ER structures after multiple fission/fusion events (Paper II; Supplementary Figure 3). Interestingly, an analogous spatial pattern was observed for IP3R distribution and "hot"- and "cold-spots" of cytoplasmic Ca2+ waves upon synaptic stimulation (Fitzpatrick et al., 2009), but any functional link between these results remains unknown.

To test whether ER fission is a phenomenon occurring only in neurons of mouse origin, additional experiments were done on rat primary neuronal cultures cotransfected with RedER and EGFP, and the cells displayed ER fragmentation as well (data not shown). In the beginning stage of the study, to rule out the possibility of ER fission being a RedER-specific phenomenon, primary cultures were cotransfected with cytosolic DsRed2 and GreenER, and the NMDA-induced fragmentation was observed as in RedER and cytosolic EGFP model (data not shown). Ultimately, TEM analysis of CA3 region of Thy-1 RedER line 18, where the transgene was not expressed, confirmed that ER fission detected by fluorescence microscopy is not an artefact caused by expression of fluorescent proteins in ER lumen (i.e. unspecific interactions of fluorophore with ER content or aggregation of fluorescent molecules).

5.3. NMDAR stimulation triggers ER fission

The direct evidence of involvement of the NMDAR in inducing ER fission comes from the experiments on primary neuronal cultures (Paper I) and slices (Paper I, II).

In primary cultures, bath application of sublethal or lethal doses of glutamate triggered rapid ER fission, suggesting an important role of glutamate receptors in inducing ER fragmentation. Bath application of NMDA was sufficient to

trigger ER fission and blocking the NMDAR channel with MK-801 resulted in recovery of ER continuity. Furthermore, pretreating the cells with MK-801, and thereby blocking the NMDAR, before applying glutamate or ionomycin (Ca2+ ionophore) did not induce ER fission. ER fission therefore appears to be a highly NMDAR dependent process.

In slices, fragmentation of ER was detected after bath application of NMDA (Paper I) and when perfusing the slices with high-potassium aCSF (Paper II). Inhibiting NMDAR with MK-801 in slices subjected to NMDA lead to ER fusion, similarly, as seen in primary cultures (Paper I). Slices perfused with high-potassium aCSF supplemented with D-AP5 did not exhibit detectable ER fission (Paper II). This supports the notion that Ca2+ entry into the neuron via NMDAR is of particular importance for ER fragmentation, but the involvement of other extracellular Ca2+ entry routes to ER fission mechanism (i.e. VGCC or Ca2+ permeable AMPA receptors) cannot be excluded.

5.4. Involvement of NMDAR gated Ca2+ in ER fission

The primary rise of Ca2+ content in the cytosol during NMDAR stimulation can be attributed to extracellular Ca2+ gated via NMDA receptors, however other mechanisms may contribute as well. NMDAR-induced depolarisation contributes to activation of voltage-gated Ca2+ channels (VGCC), which become permeable to Ca2+. Increased cytosolic Ca2+ induce RyR-mediated CICR that will give rise to additional Ca2+ in the cytosol. Ultimately, depolarisation may release glutamate from presynaptic terminals and activation of group I mGluRs can trigger IICR in postsynaptic neurons, further increasing cytosolic Ca2+ content (Berridge, 1998; Verkhratsky, 2005). In addition, mitochondria can also contribute to rise in cytosolic Ca2+ (Ganitkevich, 2003). Taken together, rise of cytosolic Ca2+ content in neuron upon NMDAR stimulation has two major sources: extracellular Ca2+ and intracellular Ca2+ stores.

The findings from cell lines have demonstrated that elevated cytosolic Ca2+ levels cause alterations in ER continuity (Subramanian and Meyer, 1997; Ribeiro et al., 2000). In these studies a rise in cytosolic Ca2+ was induced by a Ca2+ ionophore. Our results from primary cultures (Paper I) suggest that it is not the release of Ca2+ from ER stores, or general increase in cytosolic Ca2+ that may play a key role in neuronal ER fission, but exclusively NMDAR gated extracellular Ca2+ influx. Ionomycin, which channels Ca2+ through plasma membrane and hence causes influx of extracellular Ca2+ as well as leak of Ca2+ from internal stores, did not trigger ER fission when NMDAR was inhibited by MK-801. Similarly, no ER fission was observed when NMDAR was inactivated and group I mGluRs were stimulated with glutamate or 3,5-dihydrophenylglycine (DHPG). Stimulation of group I mGluRs is expected to

induce Ca2+ efflux from ER via IICR mechanism, however no visually defined ER fission was observed in this treatment. Likewise, thapsigargin, a SERCA inhibitor, which leads to temporary cytosolic increase of Ca2+ from ER store, did not trigger ER fragmentation. Finally, results from slices (Paper II) incubated in Ca2+ free media or preincubated with D-AP5 showed that rapid ER fission occurs only in presence of extracellular Ca2+ and when NMDAR is active.

Summarising, leak or release of Ca2+ from the ER store did not cause ER fission in any given instance, and therefore cannot be considered as a key player in inducing loss of ER continuity.

5.5. Other pharmacological approaches

Ca2+ is a second messenger for many processes in neurons, therefore activation of NMDAR and subsequent Ca2+ influx triggers many intracellular signalling pathways, including possibly those that induce of ER fission. We used different pharmacological approaches to characterise the signalling pathways underlying ER fragmentation. The importance of protein kinases for induction of ER fission machinery was tested using different kinase inhibitors, however, neither KN-93 (inhibitor specific to CamKII) nor staurosporine (broad-spectrum kinase inhibitor) induced or prevented ER fragmentation (Paper I). ER fission was also not inhibited by ifenprodil, a selective NR2B subunit containing NMDA receptor inhibitor, yet the contribution of NR2B containing NMDARs to ER fission cannot be excluded, since the effect could be obliterated by other NMDA receptors.

5.6. The reversibility of ER fragmentation

Most strikingly, our data demonstrate that ER fission can be a reversible process, leading to restoration of ER lumen continuity and cell viability (Paper I, II). Several data support this conclusion. First, applying the NMDAR agonist MK-801, subsequent to NMDA induced ER fission, terminated the fragmentation process and led to ER fusion in primary cultures and slices (Paper I). Washing out glutamate from neuronal cultures after induction of ER fission resulted in complete restoration of ER continuity and cell survival (data not shown). Similarly in slices, washing out high K+ aCSF, resulted in recovery of ER lumen continuity (Paper II). In addition, the process of fission and fusion in slices could be induced multiple times (Paper II).

The observation, that the dramatic appearance of fragmentation of neuronal ER is not a point of no return, and hence cannot be linked exclusively with cell

death processes, suggests that ER fission and subsequent fusion it may be of importance in physiological conditions.

5.7. The implications of ER fission in physiology

ER of fragmented appearance has been shown to restrict the movement of proteins and ions (Subramanian and Meyer, 1997; Dayel et al., 1999; Park et al., 2000), but lacking pharmacological tools to selectively modulate ER fission we can only speculate on the occurrence and importance of rapid ER fission and fusion in neuronal physiology. Results from primary cultures show that ER fission occurs prior to any visually detectable signs of pathological alteration of dendrite morphology. No dendrite swelling defined by cytosolic EGFP was observed subsequently to induction of ER fission, within first minutes of exposure to glutamate or NMDA in primary cultures (Paper I), suggesting that the loss of ER continuity may be of physiological relevance and not be linked exclusively with cell death. This view may be supported by observations in non-neuronal cells, where the reversible rearrangements of ER structure are part of their physiological activity (Terasaki and Jaffe, 1991; Terasaki et al., 1996).

It is unlikely that under physiological conditions neurons would be exposed to global massive membrane depolarisation, as that induced by bath application of NMDAR agonists (Paper I) or high potassium concentration in slices (Paper II).

It is possible, however, that rapid local increase of cytosolic Ca2+ content may trigger localised ER fission. In that respect, stimuli of the lesser magnitude, i.e. that occurring during physiological NMDAR activation would trigger ER fission restricted to ER present e.g. in dendritic spines. The result from primary cultures suggests that transient stimulation with sublethal concentrations of glutamate may induce localised ER remodelling. In our experimental model, we observed gradual ER fission, which appeared to be initiated in distal parts of the dendrite, possibly in dendritic spines, and progressed towards soma (Paper I; Supplementary Figure 1). However, it is still not known, whether ER fission is triggered exclusively by synaptic or extrasynaptic NMDARs. The experimental approach that could help to answer this question would involve local photo-uncaging of glutamate in proximity to spines (containing and deprived of ER) and in dendrite areas where spines are not present.

It can be hypothesized that ER fission creates localized and isolated domains of ER (fragmented ER) limiting the organelle continuity and thus restricting the exchange of proteins and ions with the rest of ER store pool (continuous ER). In addition, it is still not known whether fragmented ER still contains Ca2+ since local Ca2+ release in fragmented ER may cause depletion of the local

Ca^{2+} store. If fragmented ER is not devoid of Ca2+, it is unclear if the dynamic properties of ER store are not affected. There is no evidence that ER fragmentation would alter the activity of IP3R or RyR, and hence the ability of ER to release Ca2+. Similarly, it is not known whether fragmentation would affect SERCA pumps, and thus the uptake of Ca2+ to the ER store. An attempt was made to clarify these issues, using genetically encoded cytosolic Ca2+ indicator in primary cultures but the results were not conclusive (data not shown).

Fragmented ER induced by physiological neuronal activity, even if localised only to spines, may limit amount of locally available Ca2+ from ER store for release through ER Ca2+ channels. If local ER fragmentation restricts the replenishment of released Ca2+ with Ca2+ from the rest of the ER, then it is plausible that ER fission would affect Ca2+ signalling pathways.

Ca2+ signals in spines are believed to have a crucial role in triggering different forms of synaptic plasticity (Malenka and Bear, 2004), and although there is increasing evidence from pharmacological studies on the contribution of ER Ca2+ store to synaptic plasticity (Bardo et al., 2006), there is generally lack of consensus, which most likely derives from different methodological approaches used in these studies. Therefore, it is difficult, to address ER fission-fusion in context of synaptic plasticity. The influence of ER fission-fusion on synaptic plasticity would have to be analysed separately for every approach used in the studies.

ER fragmentation was not assessed in axons, however non-continuous ER may limit the supply of Ca2+ from ER store in presynaptic terminals affecting thus CICR assisted neurotransmitter release (Bouchard et al., 2003).

Interestingly, data from Paper II point out, that inactivating NMDAR by D-AP5, or incubating the slices in Ca2+ free media render ER more continuous compared to the baseline in naïve neurons. That would strongly support the hypothesis proposed in Paper I of ER being in equilibrium, where physiological stimuli associated with normal neuronal activity keeps certain volume of ER persistently fragmented.

The distribution of RyRs, IP3Rs and SERCA pumps, as well Ca2+ binding proteins in ER is not homogenous (Villa et al., 1991; Walton et al., 1991; Johnson et al., 1993), therefore local ER fission-fusion may affect some neuronal Ca^{2+} signalling pathways more then the others.

5.8. The implications of ER fission in disease

5.8.1. Acute disorders

NMDAR mediated excitotoxicity has been described in many disease models, including experimental stroke (Globus et al., 1988; Lau and Tymianski, 2010). Given that overstimulation of NMDA receptors triggers ER fission as well as detrimental processes in the cell we investigated the occurrence of ER fission in cardiac arrest experimental model of stroke *in vivo*. Cardiac arrest results in cessation of cerebral blood flow, subsequent depletion of brain glucose and ATP (Lowry et al., 1964) and to depolarisation of the neuronal plasma membrane (Hansen, 1985). This leads to an increase of synaptic and extrasynaptic glutamate levels (Benveniste et al., 1984; Globus et al., 1988), a decrease in extracellular (Hansen, 1985) and an increase in intracellular Ca2+ levels (Silver and Erecinska, 1992). Indeed, rapid ER fission was present during cardiac arrest in mice (Paper III), and, given our data showing that ER fission can be reversed in primary cultures and slices, means it is of relevance for brain pathology. Noteworthy, the results presented in Paper III is the first ever assessment of ER structure dynamics in the living brain. ER fragmented within 1-2 minutes of cardiac arrest which correlates with time-course of Ca2+ entry to neurons in ischemic conditions (Silver and Erecinska, 1992). ER fission was a global process observed within all analysed neurons. The temporal relation of ischemic events and ER fission is in accord with our experiments performed in primary cultures and slices (Paper I, II), where it was suggested that NMDAR mediated Ca2+ entry is a key factor inducing ER fragmentation. However, we do not know at present if NMDA receptor blockade affects ER fragmentation in vivo following cardiac arrest. It should be noted, that, global ischemia results in loss of ATP synthesis (Lowry et al., 1964), which can be another factor contributing to regulation of ER fission-fusion machinery. The reversibility of ER fission was not assessed *in vivo*, since the cardiac arrest model used in study was terminal.

5.8.2. Chronic disorders

Altered NMDAR-mediated transmission has been linked with models of Alzhemer's (Chohan and Iqbal, 2006), Huntington's disease (Zeron et al., 2002) and schizophrenia (Olney et al., 1999). Although the properties of ER fission-fusion in chronic diseases are not known, investigating the ER dynamics may provide with new bi-directional insights into ER structural changes and neurodegeneration.

5.8.3. ER fission: detrimental or beneficial process?

The fundamental question is whether neuronal ER fission is detrimental or beneficial. During excessive NMDAR stimulation, ER fragmentation may restrict CICR or IICR-mediated efflux of Ca2+ from ER store to isolated ER volumes, while securing the high Ca2+ concentration in the rest of the ER. The activity of ER lumen-resident molecular chaperones depend on the high intracellular Ca2+ levels, (Michalak et al., 2002), therefore, by fragmenting the ER, neurons could preserve the efficiency of protein folding machinery (Paschen and Mengesdorf, 2005).

It can be postulated, that reversible fragmentation of ER helps neurons to overcome a harmful stimulus, such as intracellular Ca2+ overload occurring during excitotoxicity. Hypothermia has been repeatedly shown to have a protective effect in experimental ischemic stroke (Krieger and Yenari, 2004). In that respect the result of decreasing temperature on ER fission in slices (Paper II) is extremely interesting, where we show that the degree of ER fission is temperature dependent. Although, no difference in fragmented ER morphology could be observed between slices at 35^{o}C and 30^{o}C by visual assessment, FRAP analysis showed that decreasing the temperature augments ER fragmentation. This result was unexpected, since mild hypothermia condition is reported to decrease glutamate release *in vivo* (Baker et al., 1995) and accumulation of intracellular Ca2+ in slice cultures (Takata et al., 1997). Yet, it can be hypothesised, that while NMDAR gated Ca2+ influx triggers ER fission, there are additional temperature-dependent mechanisms that regulate ER fragmentation.

In the transient middle-cerebral artery occlusion (MCAO) experimental model of stroke the depletion of ATP results in permanent depolarization of neurons in the brain infarct core (Nedergaard and Astrup, 1986). The infarct core, which contains irreversibly injured ischemic tissue, is surrounded by the penumbra area with cells that have the potential to recover after transient ischemia (Memezawa et al., 1992). It is plausible that ER fission-fusion events occur in penumbral cells, since the tissue exhibit trains of transient membrane depolarisations with transient elevated K+ and decrease of Ca2+ levels (Harris et al., 1982). Whether the reversible ER fission occurs in penumbra and if it correlates with cell survival *in vivo* during ischemia is yet not known, but the question will be addressed in future experiments in models of transient focal or global brain ischemia.

6. CONCLUDING REMARKS

Summarising the results presented in this study I put up the following statements:

Statement I. Neuronal ER in its basal state is generally continuous. However, subfraction of ER exists, where protein equilibration within the total pool of ER lumen is reduced or abolished.

Statement II. Neuronal ER is capable of dynamic structural changes in response to extracellular stimuli in neuronal primary cultures, organotypic slice cultures and *in situ*. The rapid reorganisation of ER structure results in the reduction of ER lumen continuity.

Statement III. Transient ER fragmentation in neurons is reversible and compatible with cell survival.

Statement IV. Activation of NMDAR is a key mechanism triggering rapid dendritic ER structure remodelling. Extracellular Ca2+ influx via NMDAR is required for ER fragmentation to occur.

Statement V. I propose the model of neuronal ER structure dynamics where ER fission and fusion events occur simultaneously in the cell. In physiological conditions ER fission is balanced by fusion leaving ER continuous. Stimulation of NMDAR shifts the equilibrium of events towards fragmented state of ER, whereas inhibition of NMDAR promotes ER continuity.

Statement VI. Temperature plays an important role in ER fission and can be considered as one of regulatory factors of ER continuity.

Statement VII. ER fission-fusion events may alter neuronal Ca2+ homeostasis, and hence be of importance for physiology and disease.

7. ACKNOWLEDGEMENTS

First and foremost: I would like to express my gratitude to my supervisors Hakan Toresson and Tadeusz Wieloch.

Hakan, thank You for showing me the beauty of ER and imaging and teaching me what good Science is about. Your encouragement on many levels made seemingly impossible things a daily routine. Thanks for saving me from "Burlov Lady" too ☺.

Tadeusz, thank You for Your detailed and constructive comments and for keeping me focused and productive during all those difficult days. Your input broadened my scientific horizons. I am sorry for all these "a" and "the" I unintentionally put you through ☺.

It was a true privilege for me to learn from such insightful minds. Thank you both for listening to my thoughts and ideas, teaching me how to learn and see beyond the fluorescence images. You fused the fragmented.

My collaborators and co-workers: Kerstin, you put your heart into my work and I will never forget our long hours spent at C09; Ai Na, my confocal sister-in-arms, hopefully Mr. LSM710 will be tamed soon; Sol, thanks for the excellent slices, genotyping and all the lighters I (almost) stole; Carin, for letting me prove myself in car-hijacking situations; Eric Carlemalm and Lina Gefors for their excellence in TEM and Morten Krogh for the mathemagic.

All present and former ExpBR lab members: Ana Rita, Elenor, Enida, Eskil, Fredrik, Gunilla, Gustav, Karsten, Magnus, Maria, Roland, Saori, Taku, Tina and Tomas. It was a pleasure to work with you, a true enriched environment for a growing scientist.

I was lucky to be surrounded by people of different nationalities, beliefs, and views on life, science, universe and everything: Ajoy, Ariane & Stuart, Ayse, Carlo, Danish Jan, Elissa, Elvira, Funas, Gurdal, Helene, Hilda, Izabella-Kinga, James, the parachute Joanna, Dexer's Joanna, Jonas, Katia, Kirsten, Lina, Magda, Marco, Martina & Jan, Miguel, Oktar, Pekka, Roman, Sajedeh, Shane, and Teia. You are a wonderful mix of friends.

Special thanks for all the people that made Sweden my home away from home: Kurowski family, Maria and Eric and Anna M.-P. in Lund. "Hi" to Evgenia, Ela, Patricita & A'lvaro, Edo and the Polish gang (remember dry ice?) in Uppsala.

Thanks to my pals in my homeland and their long-lasting friendship (21.45 L4D2?). You know who you are. Special thanks to Jekielka for your personal support. Hopefully see you soon folks!

My former teachers and mentors: Mrs Wikiera who made me realise that biology is more about thinking than memorising; Dr Panz; Prof. Emanuelsson and Prof. Alarcon-Riquelme. You all put a foundation stone under this thesis.

My Loving Family: My Parents and my Big Brother Tomek. *Wasze wsparcie nioslo mnie przez najwieksze trudy w zyciu.*

Finally, I would like to acknowledge Rana. Thank you for your patience and unconditional love. The way your heart beats makes all the difference. *Seni seviyorum, benim tatli sincapim.*

8. REFERENCES

Baba A, Yasui T, Fujisawa S, Yamada RX, Yamada MK, Nishiyama N, Matsuki N, Ikegaya Y (2003) Activity-evoked capacitative Ca2+ entry: implications in synaptic plasticity. J Neurosci 23:7737-7741.

Baker CJ, Fiore AJ, Frazzini VI, Choudhri TF, Zubay GP, Solomon RA (1995) Intraischemic hypothermia decreases the release of glutamate in the cores of permanent focal cerebral infarcts. Neurosurgery 36:994-1001; discussion 1001-1002.

Banno T, Kohno K (1996) Conformational changes of smooth endoplasmic reticulum induced by brief anoxia in rat Purkinje cells. J Comp Neurol 369:462-471.

Banno T, Kohno K (1998) Conformational changes of the smooth endoplasmic reticulum are facilitated by L-glutamate and its receptors in rat Purkinje cells. J Comp Neurol 402:252-263.

Bardo S, Cavazzini MG, Emptage N (2006) The role of the endoplasmic reticulum Ca2+ store in the plasticity of central neurons. Trends Pharmacol Sci 27:78-84.

Baumann O, Walz B (2001) Endoplasmic reticulum of animal cells and its organization into structural and functional domains. Int Rev Cytol 205:149-214.

Benveniste H, Drejer J, Schousboe A, Diemer NH (1984) Elevation of the extracellular concentrations of glutamate and aspartate in rat hippocampus during transient cerebral ischemia monitored by intracerebral microdialysis. J Neurochem 43:1369-1374.

Berridge MJ (1998) Neuronal calcium signaling. Neuron 21:13-26.

Bertolotti A, Zhang Y, Hendershot LM, Harding HP, Ron D (2000) Dynamic interaction of BiP and ER stress transducers in the unfolded-protein response. Nat Cell Biol 2:326-332.

Bezprozvanny I, Watras J, Ehrlich BE (1991) Bell-shaped calcium-response curves of Ins(1,4,5)P3- and calcium-gated channels from endoplasmic reticulum of cerebellum. Nature 351:751-754.

Bito H, Deisseroth K, Tsien RW (1997) Ca2+-dependent regulation in neuronal gene expression. Curr Opin Neurobiol 7:419-429.

Bouchard R, Pattarini R, Geiger JD (2003) Presence and functional significance of presynaptic ryanodine receptors. Prog Neurobiol 69:391-418.

Bouron A (2000) Activation of a capacitative Ca(2+) entry pathway by store depletion in cultured hippocampal neurones. FEBS Lett 470:269-272.

Brostrom MA, Brostrom CO (2003) Calcium dynamics and endoplasmic reticular function in the regulation of protein synthesis: implications for cell growth and adaptability. Cell Calcium 34:345-363.

Chohan MO, Iqbal K (2006) From tau to toxicity: emerging roles of NMDA receptor in Alzheimer's disease. J Alzheimers Dis 10:81-87.

Choi YM, Kim SH, Chung S, Uhm DY, Park MK (2006) Regional interaction of endoplasmic reticulum Ca2+ signals between soma and dendrites through rapid luminal Ca2+ diffusion. J Neurosci 26:12127-12136.

Cooney JR, Hurlburt JL, Selig DK, Harris KM, Fiala JC (2002) Endosomal compartments serve multiple hippocampal dendritic spines from a widespread rather than a local store of recycling membrane. J Neurosci 22:2215-2224.

Dayel MJ, Hom EF, Verkman AS (1999) Diffusion of green fluorescent protein in the aqueous-phase lumen of endoplasmic reticulum. Biophys J 76:2843-2851.

de Brito OM, Scorrano L (2008) Mitofusin 2 tethers endoplasmic reticulum to mitochondria. Nature 456:605-610.

DeGracia DJ, Montie HL (2004) Cerebral ischemia and the unfolded protein response. J Neurochem 91:1-8.

Dreier L, Rapoport TA (2000) In vitro formation of the endoplasmic reticulum occurs independently of microtubules by a controlled fusion reaction. J Cell Biol 148:883-898.

Droz B, Rambourg A, Koenig HL (1975) The smooth endoplasmic reticulum: structure and role in the renewal of axonal membrane and synaptic vesicles by fast axonal transport. Brain Res 93:1-13.

Du Y, Ferro-Novick S, Novick P (2004) Dynamics and inheritance of the endoplasmic reticulum. J Cell Sci 117:2871-2878.

Fedorenko EA, Duzhii DE, Marchenko SM (2008) Calcium Channels in the Nuclear Envelope of Pyramidal Neurons of the Rat Hippocampus. Neurophysiology+ 40:238-242.

Fitzpatrick JS, Hagenston AM, Hertle DN, Gipson KE, Bertetto-D'Angelo L, Yeckel MF (2009) Inositol-1,4,5-trisphosphate receptor-mediated Ca2+ waves in pyramidal neuron dendrites propagate through hot spots and cold spots. J Physiol-London 587:1439-1459.

Ganitkevich VY (2003) The role of mitochondria in cytoplasmic Ca2+ cycling. Exp Physiol 88:91-97.

Gisselsson LL, Matus A, Wieloch T (2005) Actin redistribution underlies the sparing effect of mild hypothermia on dendritic spine morphology after in vitro ischemia. J Cereb Blood Flow Metab 25:1346-1355.

Globus MY, Busto R, Dietrich WD, Martinez E, Valdes I, Ginsberg MD (1988) Effect of ischemia on the in vivo release of striatal dopamine, glutamate, and gamma-aminobutyric acid studied by intracerebral microdialysis. J Neurochem 51:1455-1464.

Hansen AJ (1985) Effect of anoxia on ion distribution in the brain. Physiol Rev 65:101-148.

Hardingham GE, Arnold FJ, Bading H (2001) Nuclear calcium signaling controls CREB-mediated gene expression triggered by synaptic activity. Nat Neurosci 4:261-267.

Harris RJ, Branston NM, Symon L, Bayhan M, Watson A (1982) The effects of a calcium antagonist, nimodipine, upon physiological responses of

the cerebral vasculature and its possible influence upon focal cerebral ischaemia. Stroke 13:759-766.
Hasbani MJ, Schlief ML, Fisher DA, Goldberg MP (2001) Dendritic spines lost during glutamate receptor activation reemerge at original sites of synaptic contact. Journal of Neuroscience 21:2393-2403.
Hazan J, Fonknechten N, Mavel D, Paternotte C, Samson D, Artiguenave F, Davoine CS, Cruaud C, Durr A, Wincker P, Brottier P, Cattolico L, Barbe V, Burgunder JM, Prud'homme JF, Brice A, Fontaine B, Heilig R, Weissenbach J (1999) Spastin, a new AAA protein, is altered in the most frequent form of autosomal dominant spastic paraplegia. Nature Genetics 23:296-303.
Holtmaat A, Bonhoeffer T, Chow DK, Chuckowree J, De Paola V, Hofer SB, Hubener M, Keck T, Knott G, Lee WC, Mostany R, Mrsic-Flogel TD, Nedivi E, Portera-Cailliau C, Svoboda K, Trachtenberg JT, Wilbrecht L (2009) Long-term, high-resolution imaging in the mouse neocortex through a chronic cranial window. Nat Protoc 4:1128-1144.
Hu J, Shibata Y, Zhu PP, Voss C, Rismanchi N, Prinz WA, Rapoport TA, Blackstone C (2009) A class of dynamin-like GTPases involved in the generation of the tubular ER network. Cell 138:549-561.
Hua SY, Tokimasa T, Takasawa S, Furuya Y, Nohmi M, Okamoto H, Kuba K (1994) Cyclic ADP-ribose modulates Ca2+ release channels for activation by physiological Ca2+ entry in bullfrog sympathetic neurons. Neuron 12:1073-1079.
Ihaka R, Gentleman R (1996) A language for data analysis and graphics. J Comput Graph Stat 5:299-314.
John LM, Lechleiter JD, Camacho P (1998) Differential modulation of SERCA2 isoforms by calreticulin. J Cell Biol 142:963-973.
Johnson JW, Ascher P (1987) Glycine potentiates the NMDA response in cultured mouse brain neurons. Nature 325:529-531.
Johnson RJ, Pyun HY, Lytton J, Fine RE (1993) Differences in the subcellular localization of calreticulin and organellar Ca(2+)-ATPase in neurons. Brain Res Mol Brain Res 17:9-16.
Jones VC, McKeown L, Verkhratsky A, Jones OT (2008) LV-pIN-KDEL: a novel lentiviral vector demonstrates the morphology, dynamics and continuity of the endoplasmic reticulum in live neurones. BMC Neurosci 9:10.
Jones VC, Rodriguez JJ, Verkhratsky A, Jones OT (2009) A lentivirally delivered photoactivatable GFP to assess continuity in the endoplasmic reticulum of neurones and glia. Pflugers Arch 458:809-818.
Kirchhausen T (2000) Three ways to make a vesicle. Nat Rev Mol Cell Bio 1:187-198.
Knott AB, Perkins G, Schwarzenbacher R, Bossy-Wetzel E (2008) Mitochondrial fragmentation in neurodegeneration. Nat Rev Neurosci 9:505-518.

Krieger DW, Yenari MA (2004) Therapeutic hypothermia for acute ischemic stroke: what do laboratory studies teach us? Stroke 35:1482-1489.
Lau A, Tymianski M (2010) Glutamate receptors, neurotoxicity and neurodegeneration. Pflugers Arch 460:525-542.
Lee MC, Miller EA, Goldberg J, Orci L, Schekman R (2004) Bi-directional protein transport between the ER and Golgi. Annu Rev Cell Dev Biol 20:87-123.
Li Y, Camacho P (2004) Ca2+-dependent redox modulation of SERCA 2b by ERp57. J Cell Biol 164:35-46.
Lowry OH, Passonneau JV, Hasselberger FX, Schulz DW (1964) Effect of Ischemia on Known Substrates and Cofactors of the Glycolytic Pathway in Brain. J Biol Chem 239:18-30.
Malenka RC, Bear MF (2004) LTP and LTD: an embarrassment of riches. Neuron 44:5-21.
Martone ME, Zhang Y, Simpliciano VM, Carragher BO, Ellisman MH (1993) Three-dimensional visualization of the smooth endoplasmic reticulum in Purkinje cell dendrites. J Neurosci 13:4636-4646.
Mayer ML, Westbrook GL, Guthrie PB (1984) Voltage-dependent block by Mg2+ of NMDA responses in spinal cord neurones. Nature 309:261-263.
Meldolesi J (2001) Rapidly exchanging Ca2+ stores in neurons: molecular, structural and functional properties. Prog Neurobiol 65:309-338.
Memezawa H, Smith ML, Siesjo BK (1992) Penumbral tissues salvaged by reperfusion following middle cerebral artery occlusion in rats. Stroke 23:552-559.
Michalak M, Robert Parker JM, Opas M (2002) Ca2+ signaling and calcium binding chaperones of the endoplasmic reticulum. Cell Calcium 32:269-278.
Mizielinska SM, Greenwood SM, Tummala H, Connolly CN (2009) Rapid dendritic and axonal responses to neuronal insults. Biochem Soc Trans 37:1389-1393.
Monyer H, Burnashev N, Laurie DJ, Sakmann B, Seeburg PH (1994) Developmental and Regional Expression in the Rat-Brain and Functional-Properties of 4 Nmda Receptors. Neuron 12:529-540.
Nagai T, Yamada S, Tominaga T, Ichikawa M, Miyawaki A (2004) Expanded dynamic range of fluorescent indicators for Ca(2+) by circularly permuted yellow fluorescent proteins. Proc Natl Acad Sci U S A 101:10554-10559.
Nedergaard M, Astrup J (1986) Infarct rim: effect of hyperglycemia on direct current potential and [14C]2-deoxyglucose phosphorylation. J Cereb Blood Flow Metab 6:607-615.
Ng AN, Toresson H (2008) Gamma-secretase and metalloproteinase activity regulate the distribution of endoplasmic reticulum to hippocampal neuron dendritic spines. Faseb J 22:2832-2842.

Olney JW, Newcomer JW, Farber NB (1999) NMDA receptor hypofunction model of schizophrenia. J Psychiatr Res 33:523-533.
Orso G, Pendin D, Liu S, Tosetto J, Moss TJ, Faust JE, Micaroni M, Egorova A, Martinuzzi A, McNew JA, Daga A (2009) Homotypic fusion of ER membranes requires the dynamin-like GTPase atlastin. Nature 460:978-983.
Park JS, Bateman MC, Goldberg MP (1996) Rapid alterations in dendrite morphology during sublethal hypoxia or glutamate receptor activation. Neurobiol Dis 3:215-227.
Park MK, Petersen OH, Tepikin AV (2000) The endoplasmic reticulum as one continuous Ca2+ pool: visualization of rapid Ca2+ movements and equilibration. Embo J 19:5729-5739.
Park SH, Blackstone C (2010) Further assembly required: construction and dynamics of the endoplasmic reticulum network. EMBO Rep 11:515-521.
Park SH, Zhu PP, Parker RL, Blackstone C (2010) Hereditary spastic paraplegia proteins REEP1, spastin, and atlastin-1 coordinate microtubule interactions with the tubular ER network. J Clin Invest 120:1097-1110.
Paschen W, Mengesdorf T (2005) Endoplasmic reticulum stress response and neurodegeneration. Cell Calcium 38:409-415.
Petersen OH, Verkhratsky A (2007) Endoplasmic reticulum calcium tunnels integrate signalling in polarised cells. Cell Calcium 42:373-378.
Pucadyil TJ, Schmid SL (2009) Conserved functions of membrane active GTPases in coated vesicle formation. Science 325:1217-1220.
Renvoise B, Blackstone C (2010) Emerging themes of ER organization in the development and maintenance of axons. Curr Opin Neurobiol 20:531-537.
Ribeiro CM, McKay RR, Hosoki E, Bird GS, Putney JW, Jr. (2000) Effects of elevated cytoplasmic calcium and protein kinase C on endoplasmic reticulum structure and function in HEK293 cells. Cell Calcium 27:175-185.
Roy L, Bergeron JJ, Lavoie C, Hendriks R, Gushue J, Fazel A, Pelletier A, Morre DJ, Subramaniam VN, Hong W, Paiement J (2000) Role of p97 and syntaxin 5 in the assembly of transitional endoplasmic reticulum. Mol Biol Cell 11:2529-2542.
Rytter A, Cronberg T, Asztely F, Nemali S, Wieloch T (2003) Mouse hippocampal organotypic tissue cultures exposed to in vitro "ischemia" show selective and delayed CA1 damage that is aggravated by glucose. J Cereb Blood Flow Metab 23:23-33.
Shibata Y, Hu J, Kozlov MM, Rapoport TA (2009) Mechanisms shaping the membranes of cellular organelles. Annu Rev Cell Dev Biol 25:329-354.
Silver IA, Erecinska M (1992) Ion homeostasis in rat brain in vivo: intra- and extracellular [Ca2+] and [H+] in the hippocampus during recovery

from short-term, transient ischemia. J Cereb Blood Flow Metab 12:759-772.
Sokka AL, Putkonen N, Mudo G, Pryazhnikov E, Reijonen S, Khiroug L, Belluardo N, Lindholm D, Korhonen L (2007) Endoplasmic reticulum stress inhibition protects against excitotoxic neuronal injury in the rat brain. J Neurosci 27:901-908.
Spacek J, Harris KM (1997) Three-dimensional organization of smooth endoplasmic reticulum in hippocampal CA1 dendrites and dendritic spines of the immature and mature rat. J Neurosci 17:190-203.
Steward O, Schuman EM (2001) Protein synthesis at synaptic sites on dendrites. Annu Rev Neurosci 24:299-325.
Subramanian K, Meyer T (1997) Calcium-induced restructuring of nuclear envelope and endoplasmic reticulum calcium stores. Cell 89:963-971.
Svoboda K, Yasuda R (2006) Principles of two-photon excitation microscopy and its applications to neuroscience. Neuron 50:823-839.
Takata T, Nabetani M, Okada Y (1997) Effects of hypothermia on the neuronal activity, [Ca2+]i accumulation and ATP levels during oxygen and/or glucose deprivation in hippocampal slices of guinea pigs. Neurosci Lett 227:41-44.
Terasaki M, Jaffe LA (1991) Organization of the sea urchin egg endoplasmic reticulum and its reorganization at fertilization. J Cell Biol 114:929-940.
Terasaki M, Chen LB, Fujiwara K (1986) Microtubules and the endoplasmic reticulum are highly interdependent structures. J Cell Biol 103:1557-1568.
Terasaki M, Jaffe LA, Hunnicutt GR, Hammer JA, 3rd (1996) Structural change of the endoplasmic reticulum during fertilization: evidence for loss of membrane continuity using the green fluorescent protein. Dev Biol 179:320-328.
Terasaki M, Slater NT, Fein A, Schmidek A, Reese TS (1994) Continuous network of endoplasmic reticulum in cerebellar Purkinje neurons. Proc Natl Acad Sci U S A 91:7510-7514.
Toresson H, Grant SG (2005) Dynamic distribution of endoplasmic reticulum in hippocampal neuron dendritic spines. Eur J Neurosci 22:1793-1798.
Tsukita S, Ishikawa H (1976) Three-dimensional distribution of smooth endoplasmic reticulum in myelinated axons. J Electron Microsc (Tokyo) 25:141-149.
van Meer G, Voelker DR, Feigenson GW (2008) Membrane lipids: where they are and how they behave. Nat Rev Mol Cell Bio 9:112-124.
Verkhratsky A (2004) Endoplasmic reticulum calcium signaling in nerve cells. Biol Res 37:693-699.
Verkhratsky A (2005) Physiology and pathophysiology of the calcium store in the endoplasmic reticulum of neurons. Physiol Rev 85:201-279.
Viassolo V, Previtali SC, Schiatti E, Magnani G, Minetti C, Zara F, Grasso M, Dagna-Bricarelli F, Di Maria E (2008) Inclusion body myopathy,

Paget's disease of the bone and frontotemporal dementia: recurrence of the VCP R155H mutation in an Italian family and implications for genetic counselling. Clin Genet 74:54-60.
Villa A, Podini P, Clegg DO, Pozzan T, Meldolesi J (1991) Intracellular Ca2+ Stores in Chicken Purkinje Neurons - Differential Distribution of the Low Affinity-High Capacity Ca2+ Binding-Protein, Calsequestrin, of Ca2+ Atpase and of the Er Lumenal Protein, Bip. Journal of Cell Biology 113:779-791.
Voeltz GK, Prinz WA, Shibata Y, Rist JM, Rapoport TA (2006) A class of membrane proteins shaping the tubular endoplasmic reticulum. Cell 124:573-586.
Walton PD, Airey JA, Sutko JL, Beck CF, Mignery GA, Sudhof TC, Deerinck TJ, Ellisman MH (1991) Ryanodine and inositol trisphosphate receptors coexist in avian cerebellar Purkinje neurons. J Cell Biol 113:1145-1157.
Waterman-Storer CM, Salmon ED (1998) Endoplasmic reticulum membrane tubules are distributed by microtubules in living cells using three distinct mechanisms. Curr Biol 8:798-806.
Xu C, Bailly-Maitre B, Reed JC (2005) Endoplasmic reticulum stress: cell life and death decisions. J Clin Invest 115:2656-2664.
Zeron MM, Hansson O, Chen N, Wellington CL, Leavitt BR, Brundin P, Hayden MR, Raymond LA (2002) Increased sensitivity to N-methyl-D-aspartate receptor-mediated excitotoxicity in a mouse model of Huntington's disease. Neuron 33:849-860.
Zhao X, Alvarado D, Rainier S, Lemons R, Hedera P, Weber CH, Tukel T, Apak M, Heiman-Patterson T, Ming L, Bui M, Fink JK (2001) Mutations in a newly identified GTPase gene cause autosomal dominant hereditary spastic paraplegia. Nat Genet 29:326-331.
Zhu PP, Patterson A, Lavoie B, Stadler J, Shoeb M, Patel R, Blackstone C (2003) Cellular localization, oligomerization, and membrane association of the hereditary spastic paraplegia 3A (SPG3A) protein atlastin. J Biol Chem 278:49063-49071.
Zimmerberg J, Kozlov MM (2006) How proteins produce cellular membrane curvature. Nat Rev Mol Cell Bio 7:9-19.
Zuchner S et al. (2004) Mutations in the mitochondrial GTPase mitofusin 2 cause Charcot-Marie-Tooth neuropathy type 2A. Nat Genet 36:449-451.

OPEN ACCESS Freely available online

PLoS one

NMDA Receptor Stimulation Induces Reversible Fission of the Neuronal Endoplasmic Reticulum

Krzysztof Kucharz[1], Morten Krogh[2], Ai Na Ng[1], Håkan Toresson[1]*

1 Laboratory for Experimental Brain Research, Wallenberg Neuroscience Centre, Department of Clinical Sciences Lund, Lund University, Lund, Sweden, **2** Computational Biology and Biological Physics, Department of Theoretical Physics, Lund University, Lund, Sweden

Abstract

With few exceptions the endoplasmic reticulum (ER) is considered a continuous system of endomembranes within which proteins and ions can move. We have studied dynamic structural changes of the ER in hippocampal neurons in primary culture and organotypic slices. Fluorescence recovery after photobleaching (FRAP) was used to quantify and model ER structural dynamics. Ultrastructure was assessed by electron microscopy. In live cell imaging experiments we found that, under basal conditions, the ER of neuronal soma and dendrites was continuous. The smooth and uninterrupted appearance of the ER changed dramatically after glutamate stimulation. The ER fragmented into isolated vesicles in a rapid fission reaction that occurred prior to overt signs of neuronal damage. ER fission was found to be independent of ER calcium levels. Apart from glutamate, the calcium ionophore ionomycin was able to induce ER fission. The N-methyl, D-aspartate (NMDA) receptor antagonist MK-801 inhibited ER fission induced by glutamate as well as by ionomycin. Fission was not blocked by either ifenprodil or kinase inhibitors. Interestingly, sub-lethal NMDA receptor stimulation caused rapid ER fission followed by fusion. Hence, ER fission is not strictly associated with cellular damage or death. Our results thus demonstrate that neuronal ER structure is dynamically regulated with important consequences for protein mobility and ER luminal calcium tunneling.

Citation: Kucharz K, Krogh M, Ng AN, Toresson H (2009) NMDA Receptor Stimulation Induces Reversible Fission of the Neuronal Endoplasmic Reticulum. PLoS ONE 4(4): e5250. doi:10.1371/journal.pone.0005250

Editor: Fabien Tell, The Research Center of Neurobiology - Neurophysiology of Marseille, France

Received February 13, 2009; **Accepted** March 19, 2009; **Published** April 21, 2009

Funding: Funding was from Vetenskapsrådet (to H.T. and Strong Research Environment NeuroFortis), the Royal Physiographic Society, the Åke Wiberg, Crafoord and Segerfalk foundations (all H.T.). M.K. was supported by the Knut and Alice Wallenberg Foundation through the Swegene Consortium and the strategic foundation CREATE Health Centre. The funders had no role in study design, data collection and analysis, decision to publish, or preparation of the manuscript.

Competing Interests: The authors have declared that no competing interests exist.

* E-mail: hakan.toresson@med.lu.se

Introduction

Activation of glutamate receptors triggers a multitude of intracellular signaling pathways important for many aspects of CNS physiology and disease. Some of these signaling events terminate on the endoplasmic reticulum (ER) and are important for many aspects of brain function [1–8]. The ER is generally considered a continuous organelle and neuronal ER is no exception; even the ER found within dendritic spines is connected to the bulk of the ER in the dendrites and soma [9–12]. The continuity of the ER is important for its normal function as a calcium store as well as for its role in the secretory pathway. The continuous ER lumen permits calcium tunneling so the ER calcium channels can gate significant amounts of calcium in local domains upon stimulation and may also permit the propagation of signals over long distances [13,14]. In the secretory pathway, ER continuity allows mature proteins to move to the specialized ER exit sites from which they are trafficked to the Golgi [15–18].

In spite of the vital importance of ER continuity it is known that under certain conditions the ER in some non-neuronal cell types can undergo dramatic changes in structure leading to loss of continuity. Such dramatically altered ER structure has been reported in living cells such as sea urchin [19] and starfish [20] eggs at fertilization, different non-neuronal cell lines [21–23] and lacrimal cells [24]. Fragmentation (hereafter also called fission) of the ER will most likely have significant effects on most, if not all, aspects of ER function. Importantly, it can be predicted that long-term fragmentation of the ER is likely to be incompatible with cellular survival. Hence, for the fragmentation of the ER described above to qualify as a physiologically relevant phenomenon, it should be balanced by a mechanism mediating fusion of ER vesicles. Such events where ER fission is followed by fusion has been convincingly shown in starfish eggs following fertilization-induced ER fission [20]. The fact that the ER in several cell types undergo fission after physiological stimuli prompted us to explore this question in neurons in primary culture as well as in cultured organotypic slices. We describe that, indeed, the neuronal ER is a dynamic organelle and that the fission machinery is controlled specifically by NMDA receptor activity.

Materials and Methods

Primary hippocampal neuronal cultures

Animals were handled in accordance with Swedish law under permits to HT (M197-07, M223-06). Dissected uteri from embryonic day 17 pregnant NMRI mice were transferred to ice cold PBS (Gibco). Hippocampal subdissection was done in ice cold HBSS (Gibco) with 4.17 mM $NaHCO_3$ (Gibco). Tissue was cut with a fine spring scissors, gently disaggregated by triturating, washed twice with HBSS/$NaHCO_3$ (pH 7.4) and transferred to Neurobasal medium supplemented with 2% B-27, 0.5 mM L-glutamine, 1× pen/strep (all from Gibco) and 25 μM glutamate (Fluka). Cells were plated at 4×10^5 cells/ml in imaging 4 well chamber slides (Nunc) coated with 10 μg/ml Poly-D-lysine

(Sigma) and 5 μg/ml laminin (Sigma). At day in vitro (DIV) 4, cells were transfected to express either EGFP and DsRed2-ER (RedER) (Clontech; 0.4 μg/ml and 0.6 μg/ml respectively) or DsRed2 and EGFP-ER (gift from Thomas Oertner, FMI, Basel) using Lipofectamine 2000 (Invitrogen) according to the manufacturer's instruction. Liposome-containing medium was replaced after 3–5 h by glutamate-free Neurobasal medium supplemented as above.

Generation of Thy1-RedER transgenic mice

The transgene construct was built to express RedER and EGFP from the same transcript by internal ribosome entry site (IRES) mediated EGFP translation. Translation from the IRES was very weak, however, and the EGFP signal too low for imaging. The RedER gene derived from pDsRed2-ER was cloned into pIRES2-EGFP vector linearized with *Nhe*I – *Bgl*II. Both vectors were commercially available from Clontech. The RedER-IRES2-EGFP fragment derived using *Nhe*I/*Not*I sites was cloned into the pThy-1 vector linearized with *Xho*I (gift from Joshua R. Sanes; Washington University) [25].

Slice cultures

Organotypic hippocampal slice cultures were prepared from 7-days old Thy-1 RedER transgenic mice as described [26]. Mice were decapitated and brains were transferred to ice-cold HBSS (Gibco) with 20 mM HEPES (Sigma), 6 mg/ml D-glucose (Sigma) and pen/strep (Gibco). Hippocampi were dissected and cut into 250 μm thick slices using a McIlwan Tissue Chopper. Slices were transferred to Millicell culture inserts (Millipore) in 24-well culture plates. Cultures were maintained at 35°C in 50% MEM (Gibco) with 25% heat inactivated horse serum (Gibco), 18% HBSS/$NaHCO_3$ (pH 7.4) supplemented with 6 mg/ml D-glucose (Sigma), 2% B-27 (Gibco), 4 mM L-glutamine and pen/strep. After 7 days in vitro slices were grown in maintaining medium (as above) without B-27 supplement.

Live cell imaging and FRAP analysis

Live cell imaging was performed with a Zeiss LSM 510 inverted confocal microscope system equipped with heating insert P and incubator S perfused with humidified air with CO_2 (5%). Multi track mode was used and EGFP was excited with the 488 Argon laser line and the emitted light detected after a 505–530 band pass filter. DsRed2 was excited with the HeNe 543 laser and emission detected after a 560 long pass filter. Temperature was maintained at 37°C by heating the air and with a lens heater. Primary cultures were imaged in their growth medium by using the 63× N.A. 1.4 objective. Slices used for collecting images were cut out from their insert and placed in an imaging chamber, perfused with carbogen-bubbled artificial cerebrospinal fluid (NaCl: 119, KCl: 2.5, $MgSO_4$: 1.3, NaH_2PO_4: 1, $NaHCO_3$: 26, $CaCl_2$: 2.5, glucose: 11 (numbers are concentration in mM), pH 7.4) and imaged with the 63× lens at 37°C. Images were exported from the Zeiss LSM software as projected images in TIFF or uncompressed JPEG format. Adjustment of images (in LSM or Adobe Photoshop) was limited to changing the contrast and brightness of the whole image. For FRAP recordings the 10× objective was used to analyze slices in their inserts placed on a glass-bottom petri dish with slice culture medium. For FRAP experiments fluorescence intensity was measured from a selected region of interest (ROI) on a dendrite for 30 scanning cycles (~40 sec), bleached with 100% He/Ne laser intensity for 80 cycles (~10 sec) and FRAP curve was recorded for up to 170 cycles (~250 sec). The same ROI was used at every FRAP recording in the respective experiment. In addition to recording the RedER FRAP signal, for primary cultures, the EGFP signal was recorded in another channel in the multi track mode to serve as a control for fluctuations in the FRAP signal due to e.g. focal drift. Furthermore, a non-bleached ROI was always defined outside the dendrite, but adjacent to the dendrite ROI, to collect background signal (Fig. S2). The FRAP signal used for the analysis was defined as the ratio between the red and the green channel after subtracting the background in the two channels, respectively. For data display, the FRAP signal was normalized by dividing with V_1+V_2 obtained from the equations described below.

Drugs

Glutamate, NMDA, ifenprodil and DHPG were dissolved in water; ionomycin in ethanol; KN-93, MK-801, thapsigargin and staurosporine in DMSO. All drugs were frozen in small aliquots at a concentration of at least 1000× and only thawed once. Glutamate was from Sigma, all others from Tocris Cookson Inc.

Statistical analysis

All statistics and modeling was performed in R [27]. The model for the FRAP curves is described in the result section. The data was fitted to the model using least squares error minimization, i.e., the sum of the squares of the deviation of the data point and the predicted value was calculated and the parameters b, c, k1, V1, k2 and V2 were chosen to minimize this sum of squares. The t-tests, paired or unpaired, were performed with distinct variances in the two groups, i.e. without assuming equal variance in the two groups. The standard R function t-test was used. Data presented in the results section are given as average±standard deviation. Box plots show distribution and median.

Electron microscopy analysis

Organotypic slices for transmission EM analysis were fixed in 1.5% paraformaldehyde and 1.5% glutaraldehyde in 0.1 M Sörensen's phosphate buffer (0.1 M NaH_2PO_4/Na_2HPO_4, pH 7.2) for 1 h followed by washing 3 times in Sörensen's phosphate buffer. Tissue was postfixed in 1% osmium tetroxid in Sörensen's phosphate buffer for 1 h, washed 3 times and dehydrated in ethanol with increasing concentration: 25, 50, 75 and 96% for 2×10 min respectively and 100% for 2×15 min. Prior to embedding, the slices were placed in 100% acetone for 2×20 min and then in a mixture of acetone and epon resin polybed 812 (Polysciences) 1:1 over night. Next day the specimen was transferred to pure resin for at least 4 h before embedding in new pure resin and polymerization at 60°C for 48 h. The embedded specimen was sectioned in an ultratome (Super Nova, Reichert Jung) at 50 nm and mounted on slot copper grids previously covered with a thin film of pioloform. Grids were stained in 4% uranyl acetate for 30 min at 40°C and 0.5% lead citrate for 2 min at room temperature and observed with a Philips CM 10 electron microscope. In total, sections from 4 control and 4 glutamate treated slices were analyzed.

Results

ER fission occurs after stimulation of glutamate receptors

When examining primary hippocampal cultures transfected to express a fluorescent protein directed to the ER lumen (as described in e.g. [12]) we sometimes identified neurons with abnormal ER structure but with otherwise normal neuronal morphology. The ER in these cells was fragmented and existed as vesicles rather than the normal smooth and continuous appearance. To explore ER fragmentation further, we transfected hippocampal cultures to express a fluorescent protein targeted to the ER (EGFP-ER or DsRed2-ER (RedER) where the fluorescent

protein is flanked by an ER-targeting sequence and a KDEL ER retention signal previously shown to label neuronal ER [28–30]) and a cytosolic fluorescent protein of another color (EGFP or DsRed2). When such cultures were treated with 100 μM glutamate at day in vitro 17 or later, the neuronal ER underwent rapid (within 1 to 10 min) fragmentation in 17 out of 19 neurons analyzed (Fig. 1A–C). The dramatic change in ER structure always preceded alterations in dendrite morphology. In most instances the ER of the whole neuron fragmented more or less simultaneously but in some cases a gradual distal to proximal wave of ER fission was noted (Fig. S1). Even concentrations of glutamate as low as 10 μM caused rapid fission of the ER in some neurons (data not shown). Selective stimulation of NMDA receptors with 100 μM NMDA had the same effect on ER structure as glutamate (Fig. 1D–E). After 10 min all 17 neurons had undergone ER fission. The ER vesicles found after glutamate as well as NMDA-induced fission were largely stationary and no evidence of trafficking of ER fragments within dendrites was obtained (not shown and Video S1 (between t = 6 and t = 11 min). Following 24 h of glutamate or NMDA all neurons were dead including those few where no ER fission was observed (data not shown).

Modeling ER continuity

In order to determine whether the fragmented appearance of the ER really represented a break of ER continuity we performed FRAP experiments. For these experiments RedER was used rather than EGFP-ER as bleaching EGFP with the 488 argon laser bleaches DsRed2 and then the cytosolic signal cannot be used to control for focal drift (see methods). Multipolar and spiny neurons were selected and for each cell FRAP was recorded from a dendritic region of interest once prior to and once after the addition of glutamate or NMDA (Fig. S2). The time-point for the second FRAP recording varied for individual neurons between 1–55 minutes after the addition of drug. The reason for this variation in time was to permit collecting data from more than one neuron from each well. Our FRAP analysis clearly shows that ER with a fragmented appearance constitutes ER with broken or much reduced lumenal continuity after glutamate (Fig. 2A) or NMDA (Fig. 2B) treatment. To quantify FRAP results in a reliable way we decided to mathematically model ER continuity. The ER within the FRAP region of interest (ROI) was modeled as consisting of two compartments with volume V_1 and V_2, respectively (Fig. 2C). The compartments have rate constants, k_1 and k_2, respectively, defined as the rate at which a RedER molecule, bleached or unbleached, leaves the compartment and is replaced with a molecule from outside the ROI. Molecules within the ROI are bleached with the rate constant c during the photobleaching step. Our model also takes into account the lower level of photobleaching occurring during the recording scans by assigning the rate constant b to this bleaching. The equation governing the FRAP signal (S) during the recording scans in the compartment i = 1, 2 is:

$$\frac{dS_i}{dt} = -bS_i + k_i(V_i - S_i) \tag{1}$$

The equation during photobleaching is the same except for replacing b with c. In the time interval from $t = 0$ to $t = t_1$, we record the signal, and hence the bleaching rate is b. The total signal is:

$$S = S_1 + S_2$$

In the time interval $t = t_1$ to $t = t_2$, we perform the photobleaching with bleaching rate constant c. And finally, from time $t = t_2$ and onwards, we record again with bleaching rate b. By solving these equations with the initial condition that all molecules are unbleached at time 0, i.e., $S_i = V_i$, we get:

$$\frac{S_i(t)}{V_i} = \frac{k_i}{(k_i+b)} + \left(1 - \frac{k_i}{(k_i+b)}\right)\exp(-(k_i+b)t) \tag{2}$$
$$0 <= t <= t_1$$

$$\frac{S_i(t)}{V_i} = \frac{k_i}{(k_i+c)} + \left(S_i(t_i) - \frac{k_i}{(k_i+c)}\right)\exp(-(k_i+c)(t-t_1)) \tag{3}$$
$$t_1 <= t <= t_2$$

$$\frac{S_i(t)}{V_i} = \frac{k_i}{(k_i+b)} + \left(S_i(t_2) - \frac{k_i}{(k_i+b)}\right)\exp(-(k_i+b)(t-t_2)) \tag{4}$$
$$t_2 <= t$$

We fit this model to all the FRAP curves and it was able to fit the data very well (Fig. S3).

We wanted a single measure of ER continuity that could be used to compare the properties of the ER within neurons with different treatments and at different time-points. Such a measure can be made from the 6 parameters that describe the FRAP curve. The bleaching constants, b and c, however, are not intrinsic to the neurons, but depend on the laser power and other experimental settings. Hence, the continuity measure should be constructed from V_1, V_2, k_1 and k_2. With a single compartment, the rate constant, k, or the half-time of recovery $\tau = \ln 2/k$, is a good measure. In this case we have two compartments, and hence a double exponential recovery, which does not have a simple half-time of recovery. In order to get a single recovery time, a time scale, T, needs to be defined. An effective rate constant, k_{eff}, can then be defined by requiring that a single exponential recovery with rate k_{eff} at time T has the same recovery as the double exponential:

$$(V_1 + V_2)\exp(-k_{eff}T) = V_1\exp(-k_1T) + V_2\exp(-k_2T)$$

The effective half-time of recovery, which depends on the choice of time scale T, is given by:

$$\tau_{eff} = \frac{\ln 2}{k_{eff}}$$

We fit the model to the experimental results from each individual neuron and τ_{eff} was calculated for T = 100 s. Glutamate treatment caused an increase in average τ_{eff} from 43.2±11.6 s to 256.2±242.7 s (n = 19, $p<0.0001$). For NMDA the increase was from 43.6±9.7 s to 87.4±38.4 s (n = 17, $p<0.0001$). The distribution of the data with median τ_{eff} for glutamate and NMDA is shown in Fig. 2D and Fig. 2E respectively. Average τ_{eff} after glutamate was significantly higher than after NMDA ($p = 0.008$).

ER fission is reversible

We had previously observed that spontaneous fission could be followed by fusion (HT unpublished). The observed reversibility of

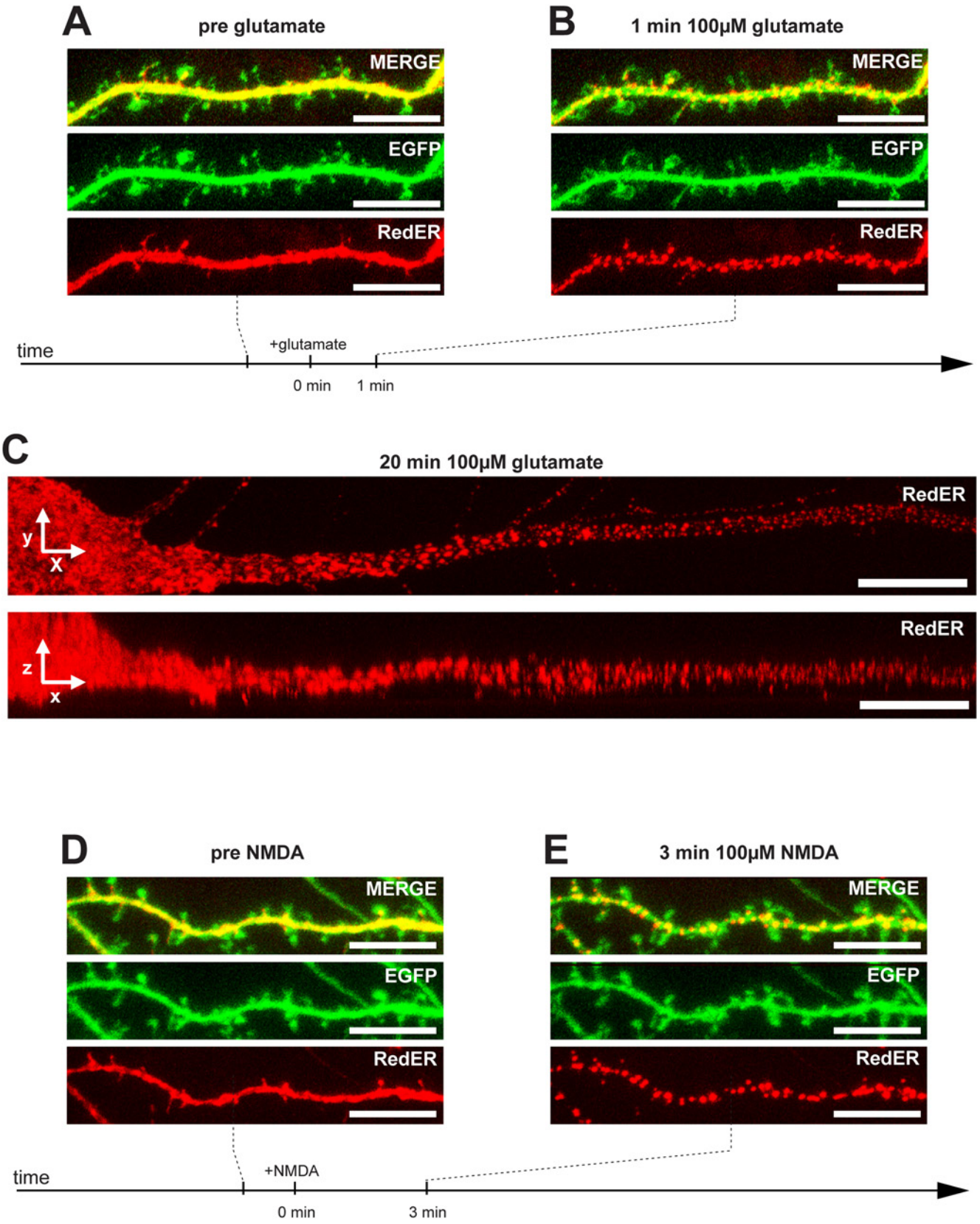

Figure 1. ER fission induced by glutamate or NMDA. (A) Representative image of a dendrite of a living hippocampal neuron transfected to express cytosolic EGFP and RedER showing normal ER morphology. (B) When exposed to 100 μM glutamate, rapid fission of the ER occurred after 1 min. Note the lack of change in dendritic and dendritic spine morphology in the green channel. (C) Image of proximal dendrite exposed to 100 μM glutamate for 20 min clearly showing the fragmented appearance of the ER in the xy (upper panel) and xz (lower panel) dimensions. (D) Representative image of a dendrite with normal morphology. (E) When exposed to 100 μM NMDA, rapid fission of the ER occurred within 3 min. Note the lack of change in dendritic and dendritic spine morphology in the green channel. Scale bar in all panels: 10 μm.
doi:10.1371/journal.pone.0005250.g001

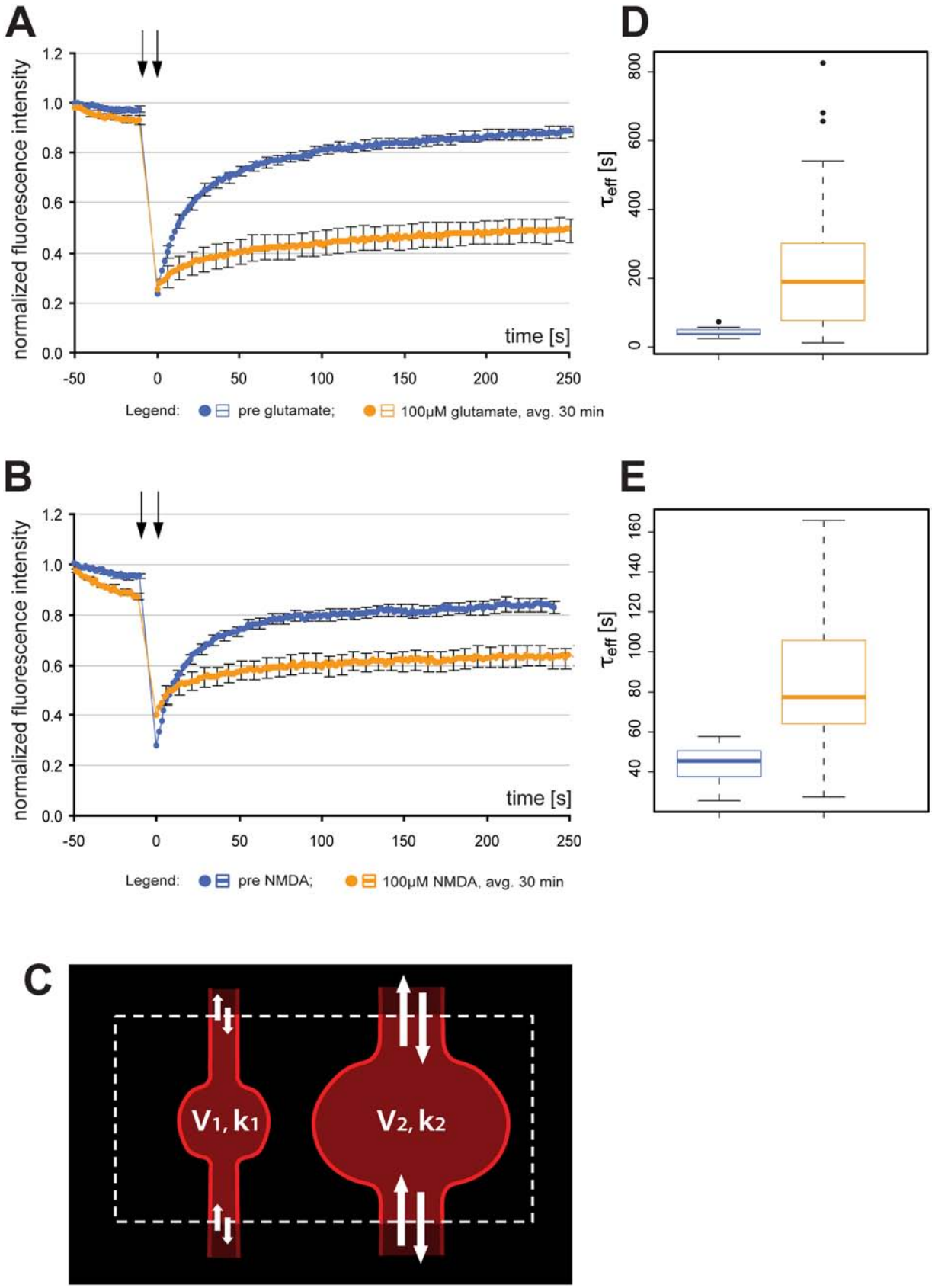

Figure 2. Analysis of ER fission by FRAP. (A and B) Normalized average FRAP signal over time in untreated neurons (blue) and the same neurons after (A) 100 μM glutamate, or (B) 100 μM NMDA (orange). Photobleaching was performed between the arrows. Time = 0 was set to when photobleaching ends and fluorescence starts to recover. Error bars are standard error of the mean (SEM). n = 19 for glutamate; n = 17 for NMDA. (C)

The ER within the ROI (dashed line) was modeled as consisting of two volumes: V_1 and V_2. The RedER molecules move within these volumes with rate constants k_1 and k_2 respectively. (D and E) Box plot of τ_{eff} values of the same neurons shown in A and B. Untreated neurons are blue and the same neurons after (D) 100 μM glutamate or (E) NMDA are orange. Note the difference in scale between D and E. The line in the box is the median and the box represents the 25–75 percentiles. Whiskers extend to the extreme values as long as they are within a range of 1.5× box length. Values outside this range are plotted as outliers. avg.: average.
doi:10.1371/journal.pone.0005250.g002

fragmentation, along with the fact that neurons with fragmented ER often displayed normal neuronal morphology, makes it possible that such ER fission and fusion could have an important function in neurons. In order to further explore this aspect we established an experimental system where neuronal ER fission followed by fusion could be reliably induced without causing cell death. We found that inducing rapid ER fission with 100 μM NMDA followed by the addition of 25 μM of the NMDA receptor antagonist MK-801 2 to 5 minutes after NMDA, allowed ER fusion and cell survival after 24 h (Fig. 3A–C). In some instances ER fusion could be noted as early as 20 min after adding MK-801 (Video S1). After 24 h, ER and overall morphology of the neurons were as prior to NMDA exposure (Fig. 3A–C). Furthermore, we recorded FRAP at three time-points: prior to adding NMDA and MK-801, immediately after the drugs (5–60 min to allow collecting data from several cells in one well) and after 24 h (Fig. 3D). The observed fragmentation was found to correlate with an increase in average τ_{eff} from 35.1±8.0 s to 92.0±44.5 s ($n = 20$, $p<0.0001$). Furthermore, analysis of FRAP data revealed that at 24 h RedER fluorescence recovered from bleaching as prior to adding the drugs. The value for average τ_{eff} at 24 h was 37.6±11.3 s ($p = 0.44$ prior to drugs, $p<0.0001$ after fission). The distribution of the data with median τ_{eff} is shown in Fig. 3E.

ER fission and fusion in hippocampal organotypic slices

As the next step towards exploring the function of neuronal ER fission and fusion we generated transgenic mice expressing the RedER marker under the Thy1 promoter. Of the three founder lines tested, we chose to use lines 18 and 27 both of which showed high expression of the marker in the majority of pyramidal cells of the CA1. Line 27 showed additional RedER expression in a subset of CA3 pyramidal cells (Fig. 4A, B). We established hippocampal organotypic slices from these mice at postnatal day 7. In slices cultured for at least 10 days the ER of the soma and dendrites appeared smooth and continuous (Fig. 4C). Continuity of the dendritic ER lumen was confirmed by FRAP analysis (Fig. 4F and Video S2). Addition of glutamate or NMDA at 100 μM caused rapid ER fission that could be detected visually (Fig. 4D) as well as by FRAP (Fig. 4F and Video S3). Importantly, the same protocol that was developed to permit ER fusion in primary cultured neurons (i.e. 100 μM NMDA followed by 25 μM MK-801) had the same effect on neurons in slices (Fig. 4E, F) (4 out of 4 slices tested).

Ultrastructure of ER fission

While the optical methods used to assess ER structure demonstrate a clear reduction in ER lumenal continuity they cannot be used to determine the actual ultrastructural changes underlying the optical observations. We therefore examined ultrathin sections of organotypic slices with electron microscopy (EM). Untreated slices showed the expected ER structure with wavy membrane tubules and cisterns of smooth ER (SER) in the dendrites (Fig. 5A) and large cisterns of rough ER (RER) in the soma (Fig. 6A). In sections from slices treated with 100 μM glutamate none of the normal ER structures were observed. Within dendrites, normal SER morphology was absent. Instead, vesicles of varying sizes could be seen; often lined up giving the impression of being the result of a fragmentation event (Fig. 5B). In the soma the RER membranes were dilated, fewer ribosomes were attached and the membranes enclosed vesicles rather than the cisterns normally seen (Fig. 6B). EM analysis also revealed that ER in the CA3 region of line 18 (where the transgene is not expressed) was fragmented (not shown) demonstrating that ER fission is not caused by the presence of RedER in the ER.

Mechanisms mediating glutamate induced ER fission

The fact that NMDA rapidly triggered ER fission led us to explore the role of the NMDA receptor. Primary cultures were treated with 25 μM MK-801 for 10 min followed by the addition of 100 μM glutamate. In this instance no fission was observed (Fig. 7A–C) although neuronal morphology was altered with blebbing of dendrites and reduced spine size. In spite of the lack of visible ER fragmentation, FRAP analysis (Fig. 7D) revealed a slight but significant increase in average τ_{eff} from 39.8±7.5 s before adding MK-801 and glutamate to 55.1±21.8 s ($n = 20$, $p = 0.001$) after 10–60 min of drug treatment. After 24 h 19 out of 20 cells had survived and average τ_{eff} was reduced to 36.3±9.5 s, that was not different from time-point one ($p = 0.24$) but significantly lower than after glutamate exposure ($p = 0.008$). The distribution of the data with median τ_{eff} is shown in Fig. 7E.

The fact that no ER fission was seen when the NMDA receptor was blocked suggested to us that influx of calcium could be important for triggering ER fission. Indeed, the addition of 5 μM of the calcium ionophore ionomycin led to ER fission (Fig. 8A, B). FRAP analysis confirmed reduced protein mobility (Fig. 8C) and average τ_{eff} was increased from 39.5±11.1 s to 261.7±242.1 s ($n = 18$, $p<0.0001$). The distribution of the data with median τ_{eff} is shown in Fig. 8D. While such a result is typically interpreted as a general rise in cytosolic calcium is sufficient to trigger the phenomenon under study, secondary effects of ionomycin leading to NMDA receptor activation cannot be excluded. To test this, we incubated the cells with 25 μM MK-801 for 20 min prior to adding 5 μM ionomycin. Interestingly, when the NMDA receptor was blocked, ionomycin treatment did not trigger ER fission (Fig. 8E, F). FRAP experiments showed that MK-801 completely blocked the effect of ionomycin (Fig. 8G) with no change in average τ_{eff} before and after MK-801+ionomycin: 36.9±10.0 s and 38.3±12.1 s respectively ($n = 18$, $p = 0.59$). The distribution of the data with median τ_{eff} is shown in Fig. 8H.

An increase in cytosolic calcium can also be caused by release of ER calcium. However, neither type I metabotropic glutamate receptor activation with 100 μM 3,5-dihydrophenylglycine (DHPG) nor blockade of the sarco- and endoplasmic reticulum ATPase (SERCA) with 200 nM thapsigargin caused fission. NMDA-induced fission was independent of ER calcium levels as it occurred after thapsigargin (Table 1). Numerous downstream signaling events are triggered downstream of NMDA receptor activation. To learn more about the signaling pathways leading to activation of the hitherto unknown ER fission machinery we used pharmacological inhibition of the NMDA receptor as well as several enzymes known to be activated by the NMDA receptor to see if this affected the fission process. Ifenprodil is a non-competitive NMDA receptor antagonist but contrary to MK-801 it specifically inhibits activation of NR2B subunit-containing

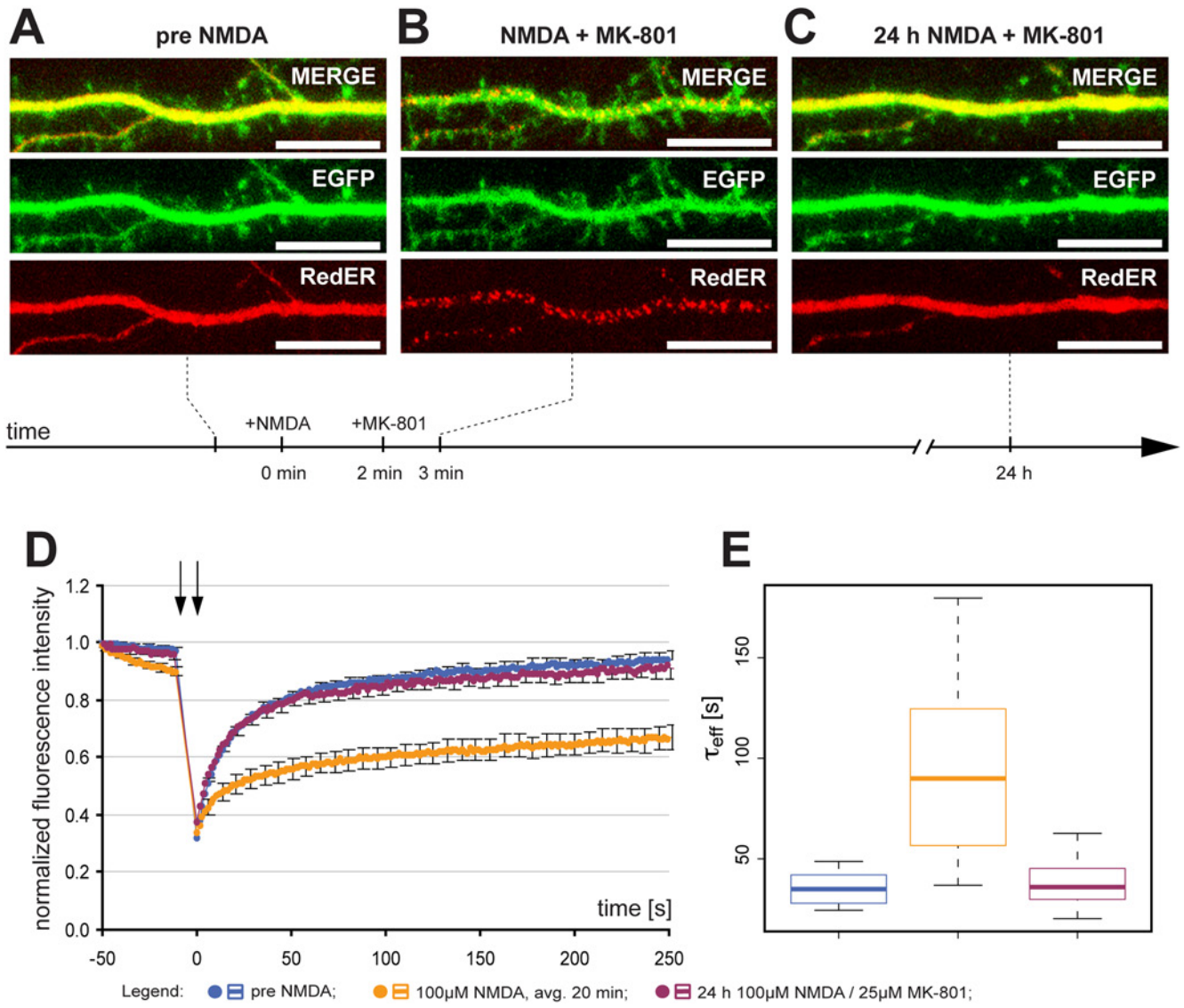

Figure 3. Reversibility of ER fission. (A) Representative image of a dendrite from a neuron with normal dendritic and ER structure. (B) 100 µM of NMDA caused rapid ER fission without any effect on gross dendritic structure. (C) Antagonizing NMDA receptor activation by 25 µM MK-801 allowed for ER fusion and recovery of ER structure by 24 h. (D) Normalized average FRAP signal over time in untreated neurons (blue), the same neurons after NMDA for an average of 20 min (orange) (note that MK-801 was added after 2–5 min) and after MK-801 for 24 h (purple). Photobleaching was performed between the arrows. Time = 0 was set to when photobleaching ends and fluorescence starts to recover. Error bars are SEM. n = 20. (E) Box plot of τ_{eff} values in untreated neurons (blue) and the same neurons after NMDA (orange) and MK-801 (purple). The line in the box is the median and the box represents the 25–75 percentiles. Whiskers extend to the extreme values as long as they are within a range of 1.5 × box length. Scale bar in all panels: 10 µm. avg.: average.
doi:10.1371/journal.pone.0005250.g003

NMDA receptors. 10 µM ifenprodil added 10 min before NMDA did not inhibit ER fission (Table 1). 10 min of 20 µM staurosporine, a broad-spectrum kinase inhibitor was unable to block NMDA-induced ER fission (Table 1). As expected from the staurosporine result, specific inhibition of calcium and calmodulin regulated kinase II (CamKII) by 10 µM KN-93 had no effect on NMDA-induced ER fission (Table 1).

Discussion

Induction of neuronal ER fission

Elevated cytosolic calcium in non-neuronal cells was previously found to cause ER fission [21,22]. Glutamate and NMDA trigger influx of extracellular calcium directly via the NMDA receptor and indirectly by activation of voltage-gated calcium channels. Release of ER calcium will occur by activation of metabotropic glutamate receptors and by calcium induced calcium release [1,7]. Our experiments show that activation of the NMDA receptor is necessary and sufficient for inducing neuronal ER fission in dissociated and organotypic culture. First, glutamate-induced ER fission was inhibited by the NMDA receptor antagonist MK-801. Second, NMDA alone rapidly triggered ER fission. Third, we found that the calcium ionophore ionomycin caused ER fission but that, even in this case, ER fission required NMDA receptor activation. Finally, release of ER calcium triggered by activation of type I mGluRs or store depletion by thapsigargin did not lead to ER fission.

It should be noted that even if NMDA receptor activation was needed for obtaining optically defined ER fragments, glutamate

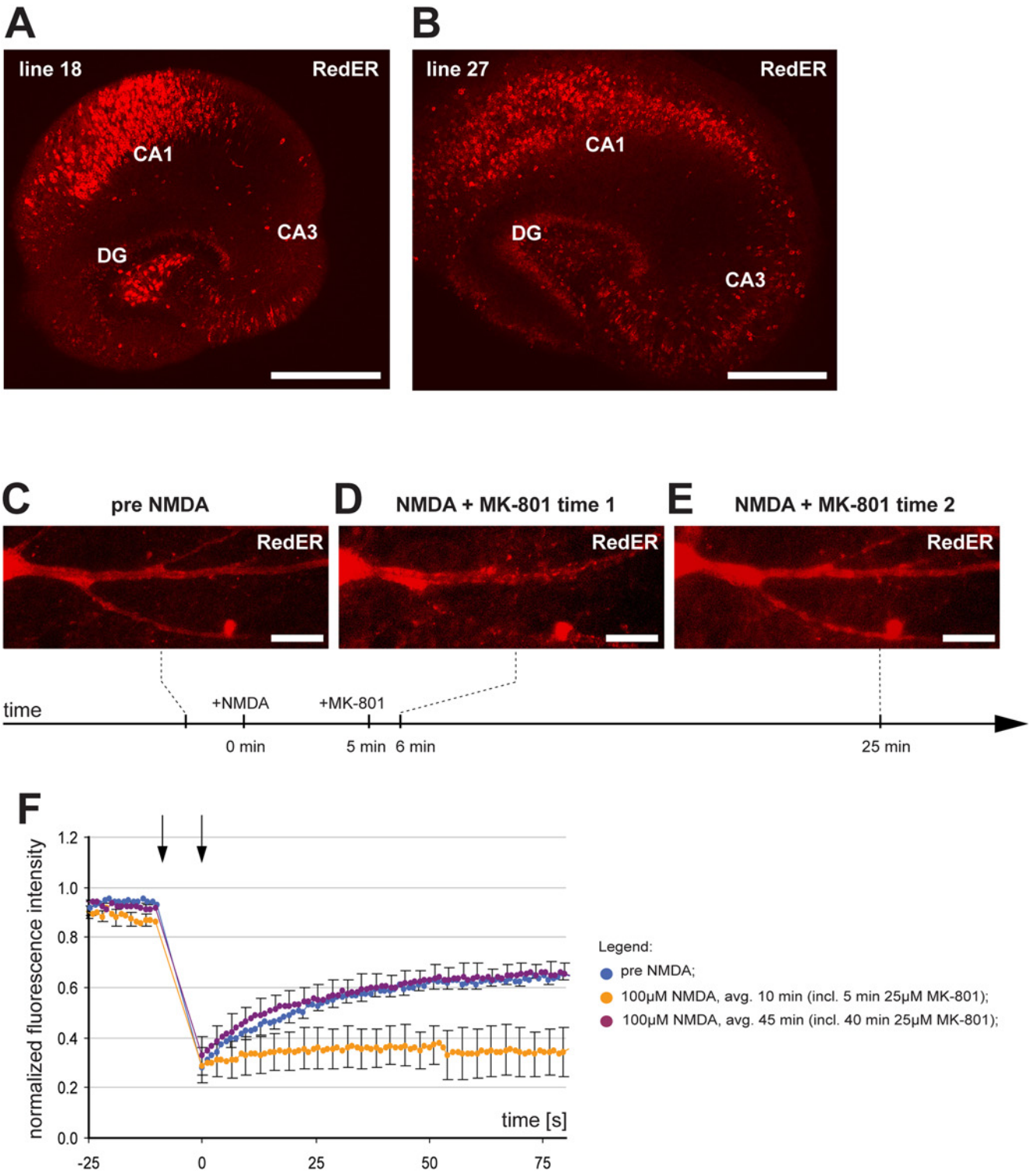

Figure 4. Reversible ER fission in organotypic slices. (A) Hippocampal expression of RedER in Thy1-RedER transgenic mouse line 18. (B) RedER expression in line 27. The expression pattern of the transgene differs slightly in that line 18 has no expression in pyramidal cells of CA3 but does express at high level in the hilus. (C) Representative images of dendritic ER structure in a CA3 pyramidal cell from line 27 with continuous ER prior to any treatment. (D) 100 μM NMDA triggered rapid ER fission. (E) 25 μM MK-801 led to fusion within 25 min. (F) Normalized average FRAP signal over time in untreated neurons (blue), the same neurons after NMDA for 10 min (orange) (note that MK-801 was added after 5 min) and after MK-801 (purple). Photobleaching was performed between the arrows. Time = 0 was set to when photobleaching ends and fluorescence starts to recover. Error bars are SEM. n = 4 neurons in 4 slices. Scale bars: 500 μm in A and B, 10 μm in C-E. avg.: average.
doi:10.1371/journal.pone.0005250.g004

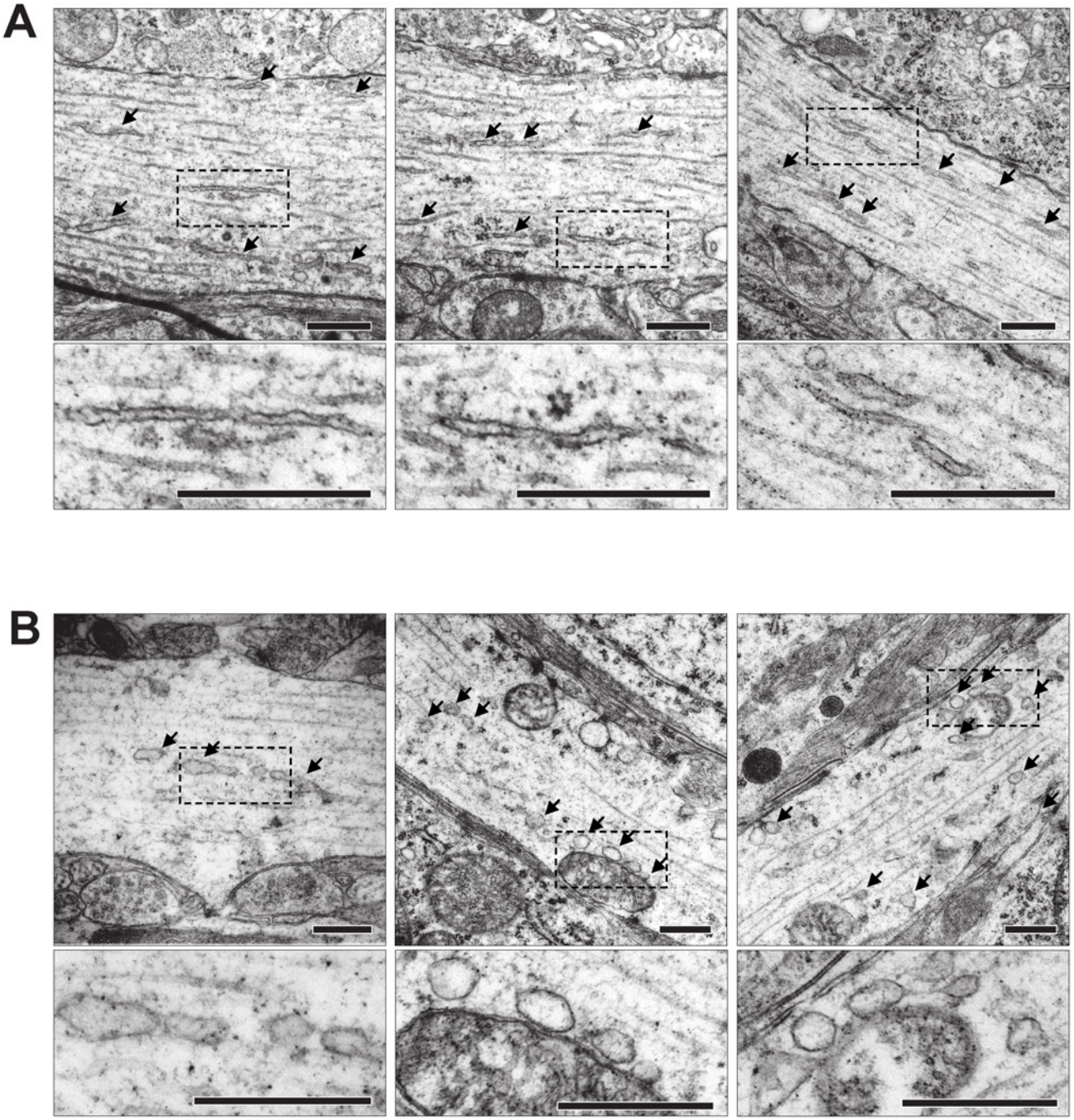

Figure 5. EM analysis of SER in dendrites. (A) Three representative images of dendrites from CA1 and CA3 in organotypic slices. ER profiles are indicated by arrows. (B) The ultrastructure after 100 μM glutamate for 5 min before fixing. No normal SER profiles were seen; instead the dendritic cytosol contains numerous dilated vesicles indicated by arrows. Boxed areas in the low magnification panel are enlarged below. Scale bar in all panels 500 nm.
doi:10.1371/journal.pone.0005250.g005

treatment in the presence of the NMDA receptor antagonist MK-801 did cause a small but significant increase in τ_{eff}. Taken together with the observation that glutamate caused a greater increase in τ_{eff} than NMDA; this may indicate that glutamate has some NMDA receptor-independent effect on ER structure. Nevertheless, we cannot exclude that the increase in τ_{eff} occurring after MK-801+glutamate treatment is a reflection of the rather dramatic but transient changes in neuronal morphology. Furthermore, the fact that τ_{eff} increases more after glutamate than after NMDA could still be an NMDA receptor-mediated effect as glutamate can be assumed to give stronger NMDA receptor activation than NMDA alone (glycine was not co-applied with NMDA).

The observed requirement for NMDA receptor activation to trigger ER fission raises the possibility that specific signaling pathways initiated at the NMDA receptor, rather than a general requirement for high cytosolic calcium, are important. Contrary to MK-801, ifenprodil (another non-competitive NMDA receptor

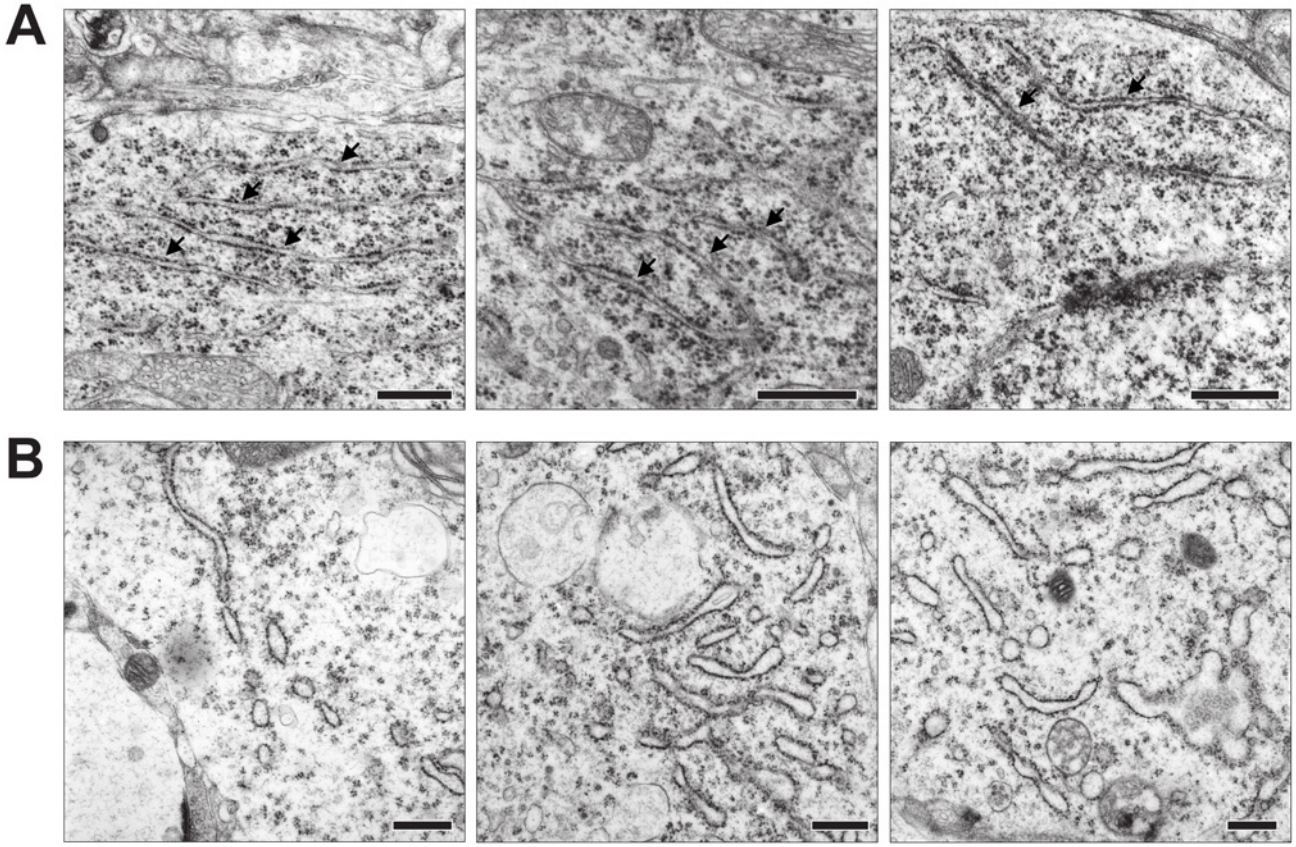

Figure 6. EM analysis of RER in neuronal somata. (A) Three representative images of CA1 and CA3 somata with normal ultrastructure. RER membranes studded with ribosomes are indicated with arrows. (B) The ultrastructure after 100 μM glutamate for 5 min. No normal RER profiles can be seen; instead the cytosol contains numerous dilated vesicles or tubules/cisterns that appear to have fewer ribosomes attached. Scale bar in all panels 500 nm.
doi:10.1371/journal.pone.0005250.g006

antagonist) did not block NMDA induced ER fragmentation. Ifenprodil specifically inhibits NMDA receptors containing NR2B subunits [31]. Hence, activation of NR2A containing NMDA receptors is sufficient for induction of fission. Much of the signaling downstream of the NMDA receptor is mediated by kinases. However, staurosporine, a broad spectrum kinase inhibitor that blocks serine-threonine as well as tyrosine kinases [32] or the more specific CamKII inhibitor KN-93, did not affect NMDA-induced ER fission. Non-kinase calcium-induced signaling events downstream of the NMDA receptor are known. For instance, the small GTPases Ras and Rac can be activated by calcium-dependent guanine-nucleotide exchange factors that localize to spines [33,34]. Alternatively, calcium sensitive parts of the hitherto unknown fission machinery may be localized close to NMDA receptors to induce fragmentation.

Relevance of ER fission

Reorganization of the neuronal ER has been described previously but was not characterized in detail [9,35]. Our results show distinct ER fission, that fragmented ER can fuse and we demonstrate that ER fission is not a point-of-no-return towards cell death. Hence, the poorly known mechanisms of ER fission and fusion are of direct relevance for understanding harmful processes and the development of neuroprotective therapeutic strategies. Indeed, the possibility of neuronal ER fission followed by fusion and cell survival has been suggested to occur after cerebral ischemia followed by reperfusion [36,37]. Interestingly, the same conditions that cause ER fragmentation have been reported to induce stalling and fission of neuronal mitochondria. This process is known in greater detail than ER fission and mutations in several genes of the mitochondrial fission and fusion machinery are known to cause disease [38,39].

While we can safely assume that regaining continuity of the ER is an absolute requirement for cellular survival, an important question remains: Is ER fission a harmful consequence of a harmful stimulus and hence the cell pays a price for ER fusion or is ER fission a protective response that helps the cell overcome a potentially harmful stimulus? The latter is supported by the fact that ER fission has been described in other cell types as a physiological phenomenon [19,20] and we now report that neuronal ER fission occurs in the absence of morphological indicators of cell damage such as dendritic blebbing or loss of spines. What could then be the advantage for a cell to transiently fragment its ER? We hypothesize that the loss of continuity can be seen as creating bulkheads within the ER. Given that neuronal ER calcium can flow freely [40,41], the partitioning caused by fission may serve to limit the release of calcium from the ER lumen under conditions when e.g. part of a neuron's dendritic arbor lies within a region of the brain parenchyma with excess levels of extracellular glutamate. It makes sense to limit release of ER calcium as either its contribution to elevated cytosolic calcium or the depletion of the ER store can contribute to neuronal damage [42–44]. ER fission may also serve to maintain damaged proteins within an area exposed to protein unfolding conditions. Potentially this

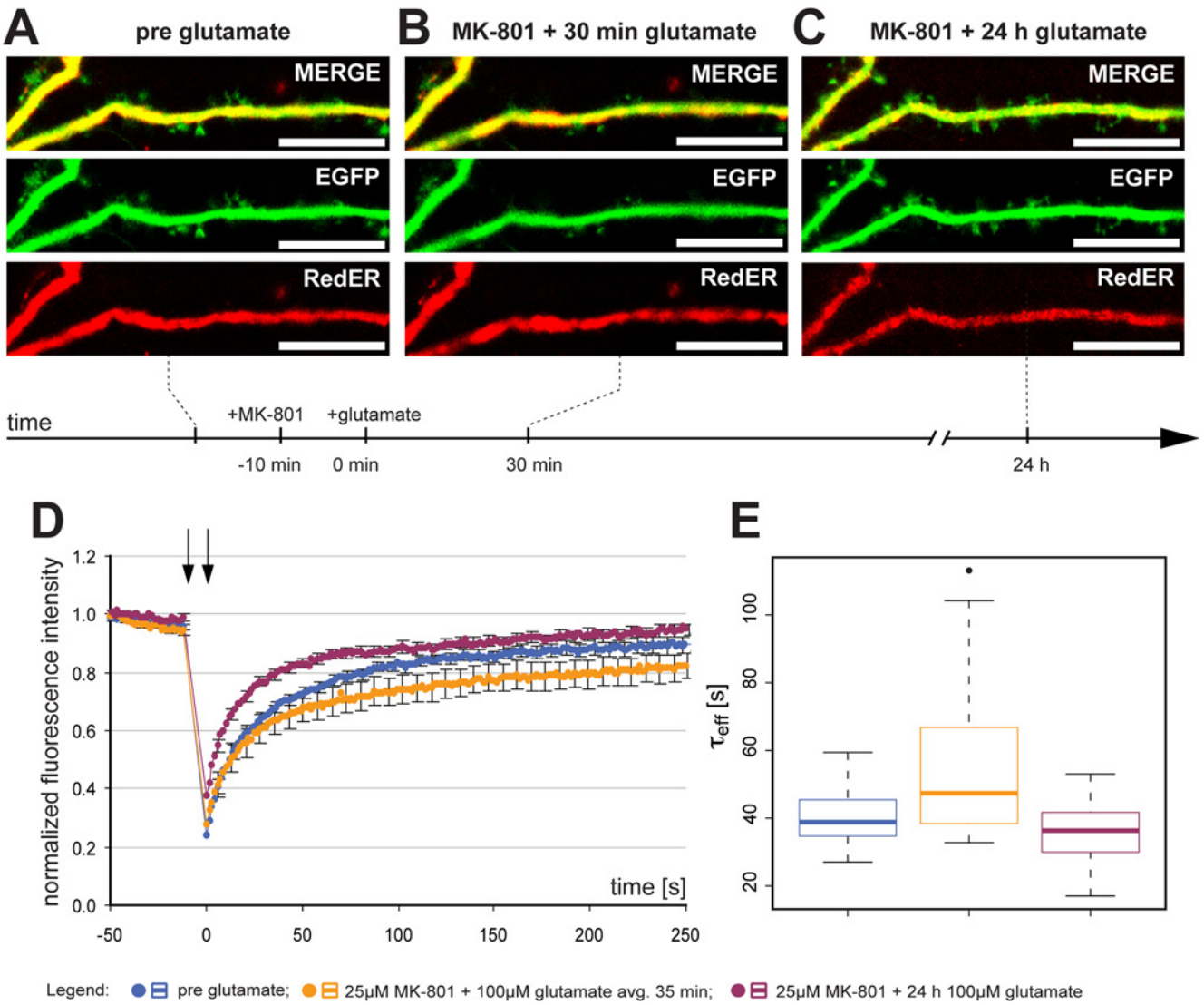

Figure 7. Inhibition of NMDA receptors is sufficient to block glutamate-induced ER fission. (A) Representative image of a dendrite from a neuron with normal dendritic and ER structure. (B) Treatment with 25 μM MK-801 for 10 min prior to 100 μM glutamate prevented ER fission although an effect on gross dendritic structure was seen (reduction in spine length). (C) After 24 h, 19 out of 20 cells had survived and resumed normal morphology. (D) Normalized average FRAP signal over time in untreated neurons (blue), the same neurons after MK-801 and glutamate for an average of 35 min (orange) and after 24 h (purple). Photobleaching was performed between the arrows. Time = 0 was set to when photobleaching ends and fluorescence starts to recover. Error bars are SEM. (E) Box plot of τ_{eff} values in untreated neurons (blue) and the same neurons after glutamate (orange). The line in the box is the median and the box represents the 25–75 percentiles. Whiskers extend to the extreme values as long as they are within a range of 1.5× box length. One neuron was outside this range and plotted as an outlier. Scale bars in all panels: 10 μm. avg.: average.
doi:10.1371/journal.pone.0005250.g007

sequestration of damaged proteins serves to prevent unnecessary induction of the unfolded protein response, which will lead to protein synthesis inhibition [2,6].

The observation in non-neuronal cells that reversible ER fission is a structural correlate of physiological events on the cellular level [19,20] suggests that a similar function in neurons cannot be excluded. Based on current knowledge, transient ER fission can be expected to alter the functional properties of the ER primarily by limiting the movement of ER restricted molecules and ions. Assuming that ER calcium channels function in the fragmented state, the pool of releasable calcium is dramatically altered when ER calcium tunneling [13] is aborted. Moreover, ER structural dynamics may have implications on local protein synthesis in dendrites, a process that has been implicated in synaptic plasticity [45]. In case ER vesicles are capable of supporting protein processing, the fragmented state will support highly localized and stationary protein synthesis, processing and export from the ER.

The ultrastructure of ER fission

By light microscopic visual examination it appears that NMDA receptor stimulation causes the ER to fragment into isolated vesicles. FRAP analyses confirmed a reduction in ER protein mobility. Reduced mobility most likely also applies to calcium ions although presumably on a shorter time scale [40,46]. Nevertheless, in only a few cases could we observe a near complete loss of FRAP (i.e. k_{eff} close to zero) when we bleached a dendrite with fragmented ER. Hence, from this data it cannot be excluded that rather than exclusively forming isolated fragments the ER may

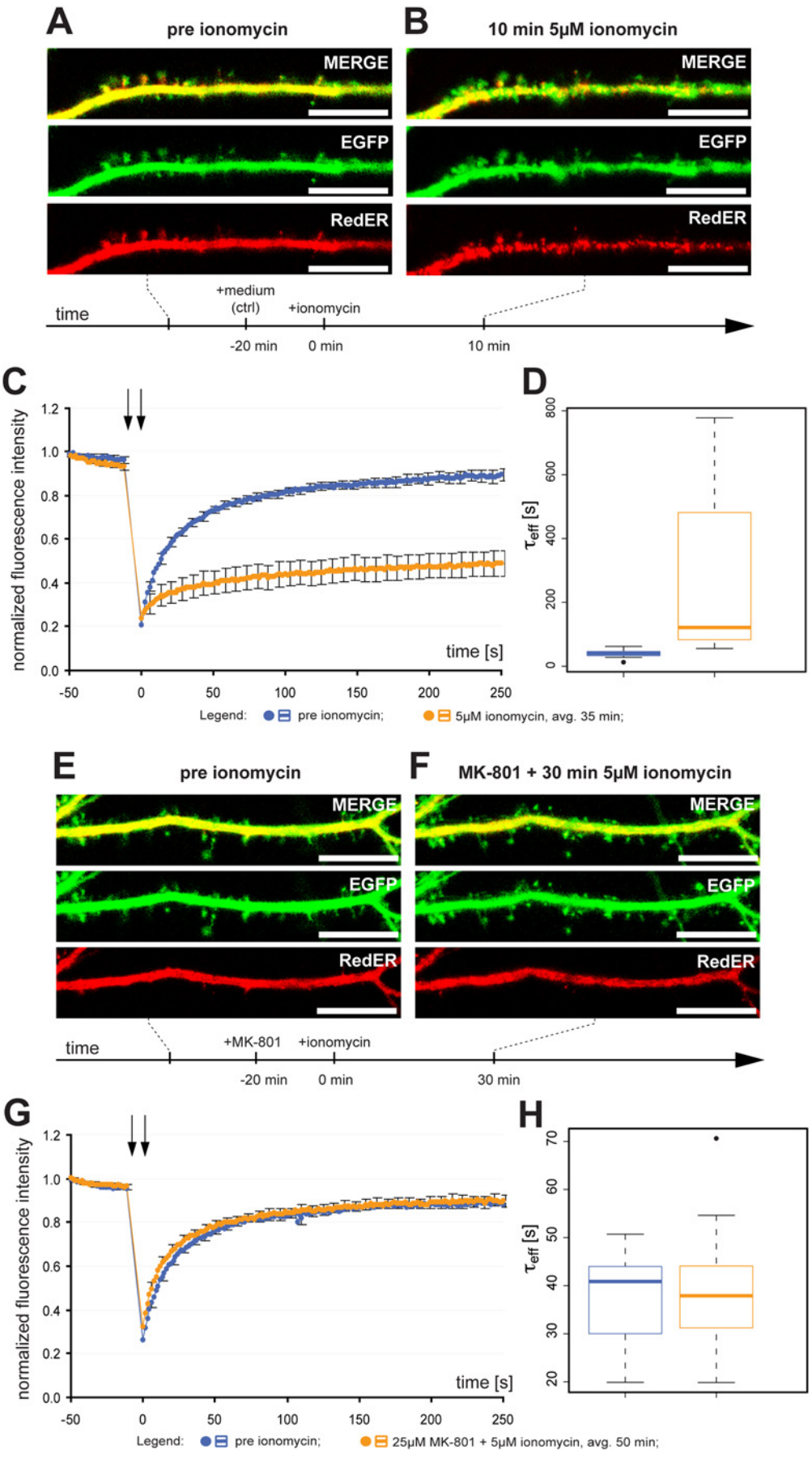
A
pre ionomycin
B
10 min 5µM ionomycin
MERGE
EGFP
RedER
+medium
(ctrl)
+ionomycin
time
-20 min
0 min
10 min
C
normalized fluorescence intensity
time [s]
Legend: pre ionomycin; 5µM ionomycin, avg. 35 min;
D
τeff [s]
E
pre ionomycin
F
MK-801 + 30 min 5µM ionomycin
+MK-801
+ionomycin
30 min
G
normalized fluorescence intensity
time [s]
Legend: pre ionomycin; 25µM MK-801 + 5µM ionomycin, avg. 50 min;
H
τeff [s]

Figure 8. Ionomycin triggers NMDA receptor-mediated ER fission. (A) Representative image of a dendrite from a neuron with normal dendritic and ER structure. (B) Treatment with 5 μM ionomycin for 10 min caused ER fission along with a pronounced effect on gross dendritic structure (dendritic blebbing). (C) Normalized average FRAP signal over time in untreated neurons (blue) and the same neurons after ionomycin for an average of 35 min (orange). Photobleaching was performed between the arrows. Time = 0 was set to when photobleaching ends and fluorescence starts to recover. Error bars are SEM. n = 18. (D) Box plot of τ_{eff} values in untreated neurons (blue) and the same neurons after ionomycin (orange). The line in the box is the median and the box represents the 25–75 percentiles. Whiskers extend to the extreme values as long as they are within a range of 1.5× box length. (E) Representative image of a dendrite from a neuron with normal dendritic and ER structure. (F) Treatment with 25 μM MK-801 for 20 min prior to 5 μM ionomycin prevented ER fission and only caused minor effects on gross dendritic structure. (G) Normalized average FRAP signal over time in untreated neurons (blue) and the same neurons after MK-801 and ionomycin for an average of 50 min (orange). Photobleaching was performed between the arrows. Time = 0 was set to when photobleaching ends and fluorescence starts to recover. Error bars are SEM. n = 18. (H) Box plot of τ_{eff} values in untreated neurons (blue) and the same neurons after ionomycin (orange). The line in the box is the median and the box represents the 25–75 percentiles. Whiskers extend to the extreme values as long as they are within a range of 1.5× box length. One neuron was outside this range and plotted as an outlier. Scale bar in all panels: 10 μm. avg.: average.
doi:10.1371/journal.pone.0005250.g008

additionally form vesicles connected by thin tubules to resemble beads on a string. Data from EM studies of ER fission in other cell types have not provided conclusive evidence to rule out either complete vesiculation or beading of the ER [21,47].

From our EM analysis of ultrastructural changes caused by short-term NMDA and glutamate treatment it can be concluded that somatic RER may indeed maintain connections between ER vesicles. In dendrites we found no evidence for connected ER fragments. However, one must bear in mind that on single sections thin connecting tubules may be missed and hence their existence cannot be ruled out. Thus, the physical basis for the low but existing FRAP after NMDA receptor activation still needs to be elucidated. We do not believe that it was caused by movement of large vesicles into the ROI; as such an event should easily be detected in our time-lapse images. Alternatively, some of the low level FRAP that we observed after fission could be caused by RedER molecules outside the ER proper, as the KDEL retention sequence allows trafficking out of the ER followed by cis-Golgi sorting back to the ER [48]. Additionally, ER vesicles may undergo cycles of fusion-fission and thus permit slow exchange of bleached molecules. Indeed, it can be hypothesized that, what is observed as fragmentation, is the outcome of a shift in the balance between constantly on-going fission and fusion events (Fig. 9).

Supporting Information

Figure S1 Gradual distal to proximal ER fission. In neurons where ER fission did not occur instantaneously fragmentation always occurred gradually from the most distal parts of dendrites towards the soma. The image shows a neuron that was treated with 20 μM glutamate (5 min) and subsequently 25 μM MK801 to attenuate the stimulus. Scale bar: 10 μm.
Found at: doi:10.1371/journal.pone.0005250.s001 (1.91 MB TIF)

Figure S2 Example of FRAP ROI. For all FRAP recordings a rectangular region of interest (ROI) was placed over a dendrite and a square ROI was placed immediately outside the dendrite to collect the background signal. The small boxes show the signal from the FRAP ROI. Scale bar: 10 μm (large image).
Found at: doi:10.1371/journal.pone.0005250.s002 (2.20 MB TIF)

Figure S3 Curve fitting to data points. The FRAP recordings from the 19 neurons in the 100 μM glutamate experiment are shown. The upper panels are recordings prior to glutamate exposure and the lower panels are after 5–60 min of glutamate. The curve fit is in red.
Found at: doi:10.1371/journal.pone.0005250.s003 (1.04 MB TIF)

Video S1 Reversibility of ER fission. Time-lapse recording of a neuron transfected to express RedER exposed to 20 μM glutamate at t = 5 min resulting in rapid ER fission. 25 μM MK-801 was added at t = 11 min and within 20 min the ER vesicles fused. Pixel dimensions: 151×303, frame rate: 25 fps, images collected at 1 Hz.
Found at: doi:10.1371/journal.pone.0005250.s004 (8.31 MB MOV)

Video S2 FRAP experiment on untreated CA1 neuron. Time-lapse recording of a neuron in an organotypic slice expressing RedER under the Thy1 promoter (line 18). Bleaching was performed after the 5th frame (t = 24 s) in the ROI marked with a white rectangle. After bleaching fluorescence recovered rapidly indicating that the ER was continuous. This neuron was not included in the analysis. Pixel dimensions: 366×341, frame rate: 8 fps, images collected at 0.2 Hz.
Found at: doi:10.1371/journal.pone.0005250.s005 (6.17 MB MOV)

Video S3 FRAP experiment on glutamate treated CA1 neuron. Time-lapse recording of a neuron in an organotypic slice

Table 1. Pharmacological manipulation of cytosolic calcium and calcium signaling.

n[a]	drug 1	effect 1 (n[b])	drug 2	effect 2 (n[b])
16	ifenprodil 10 μM/10 min	no ER fission (16)	NMDA 100 μM	ER fission (16)
20	thapsigargin 0.2 μM/60 min	no ER fission (20)	-	-
6	thapsigargin 0.2 μM/10 min	no ER fission (6)	NMDA 100 μM	ER fission (6)
10	KN-93 10 μM/10 min	no ER fission (10)	NMDA 100 μM	ER fission (10)
20	staurosporine 20 μM/20 min	no ER fission (20)	NMDA 100 μM	ER fission (20)
20	DHPG 100 μM/60 min	no ER fission (20)	-	-

Effect on ER structure.
[a]Total number of neurons tested.
[b]Number of neurons displaying the indicated response.
doi:10.1371/journal.pone.0005250.t001

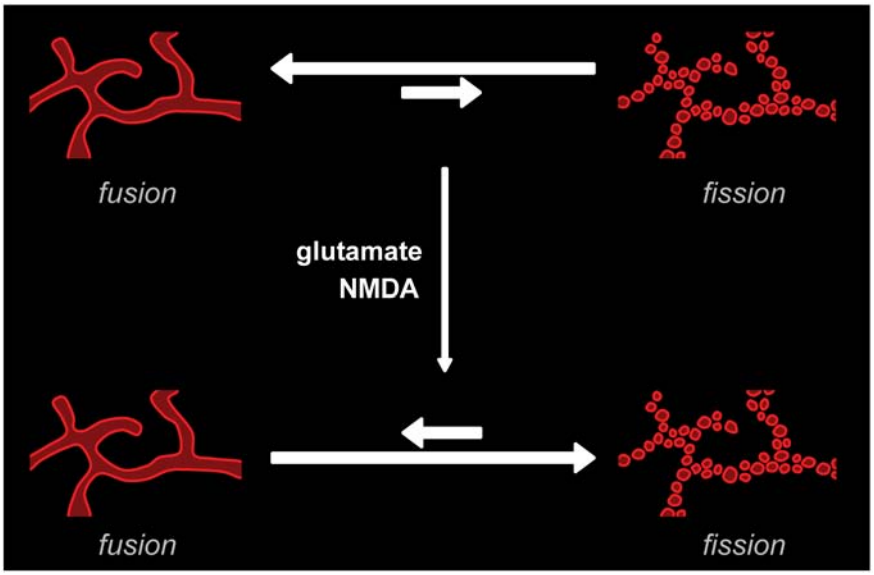

Figure 9. NMDA receptor activation may cause a shift in the balance between fission and fusion events. Rather than viewing the ER as having two static structural states (continuous and fragmented) the ER membranes may be undergoing constant fission and fusion events. In the resting state fusion events balance fission events. After NMDA receptor stimulation this balance may be shifted so that fusion events are more rare than fission events.
doi:10.1371/journal.pone.0005250.g009

expressing RedER under the Thy1 promoter (line 18). 100 μM glutamate was added 5 min prior to recording. Bleaching was performed after the 5th frame (t = 24 s) in the ROI marked with a white rectangle and a clear reduction in FRAP was noted. Pixel dimensions: 365×348, frame rate: 8 fps, images collected at 0.2 Hz.

Found at: doi:10.1371/journal.pone.0005250.s006 (7.36 MB MOV)

Acknowledgments

We are grateful for the support from Tadeusz Wieloch. Thanks to Sol daRocha, Carin Sjölund, Lina Gefors and Eric Carlemalm for technical assistance. Valuable comments were provided by Srikanth Ranganathan, Tadeusz Wieloch and David Nicholls.

Author Contributions

Conceived and designed the experiments: KK HT. Performed the experiments: KK ANN HT. Analyzed the data: KK MK ANN HT. Contributed reagents/materials/analysis tools: MK ANN. Wrote the paper: KK HT.

References

1. Bardo S, Cavazzini MG, Emptage N (2006) The role of the endoplasmic reticulum Ca2+ store in the plasticity of central neurons. Trends Pharmacol Sci 27: 78–84.
2. DeGracia DJ, Montie HL (2004) Cerebral ischemia and the unfolded protein response. J Neurochem 91: 1–8.
3. Lindholm D, Wootz H, Korhonen L (2006) ER stress and neurodegenerative diseases. Cell Death Differ 13: 385–392.
4. Mattson MP (2007) Calcium and neurodegeneration. Aging Cell 6: 337–350.
5. Meldolesi J (2001) Rapidly exchanging Ca2+ stores in neurons: molecular, structural and functional properties. Prog Neurobiol 65: 309–338.
6. Paschen W, Mengesdorf T (2005) Endoplasmic reticulum stress response and neurodegeneration. Cell Calcium 38: 409–415.
7. Verkhratsky A (2005) Physiology and pathophysiology of the calcium store in the endoplasmic reticulum of neurons. Physiol Rev 85: 201–279.
8. Zhang K, Kaufman RJ (2006) The unfolded protein response: a stress signaling pathway critical for health and disease. Neurology 66: S102–109.
9. Terasaki M, Slater NT, Fein A, Schmidek A, Reese TS (1994) Continuous network of endoplasmic reticulum in cerebellar Purkinje neurons. Proc Natl Acad Sci U S A 91: 7510–7514.
10. Martone ME, Zhang Y, Simpliciano VM, Carragher BO, Ellisman MH (1993) Three-dimensional visualization of the smooth endoplasmic reticulum in Purkinje cell dendrites. J Neurosci 13: 4636–4646.
11. Spacek J, Harris KM (1997) Three-dimensional organization of smooth endoplasmic reticulum in hippocampal CA1 dendrites and dendritic spines of the immature and mature rat. J Neurosci 17: 190–203.
12. Toresson H, Grant SG (2005) Dynamic distribution of endoplasmic reticulum in hippocampal neuron dendritic spines. Eur J Neurosci 22: 1793–1798.
13. Petersen OH, Verkhratsky A (2007) Endoplasmic reticulum calcium tunnels integrate signalling in polarised cells. Cell Calcium 42: 373–378.
14. Berridge MJ (1998) Neuronal calcium signaling. Neuron 21: 13–26.
15. Pfeffer S (2003) Membrane domains in the secretory and endocytic pathways. Cell 112: 507–517.
16. Shibata Y, Voeltz GK, Rapoport TA (2006) Rough sheets and smooth tubules. Cell 126: 435–439.
17. Voeltz GK, Rolls MM, Rapoport TA (2002) Structural organization of the endoplasmic reticulum. EMBO Rep 3: 944–950.
18. Antonny B, Schekman R (2001) ER export: public transportation by the COPII coach. Curr Opin Cell Biol 13: 438–443.
19. Terasaki M, Jaffe LA (1991) Organization of the sea urchin egg endoplasmic reticulum and its reorganization at fertilization. J Cell Biol 114: 929–940.
20. Terasaki M, Jaffe LA, Hunnicutt GR, Hammer JA 3rd (1996) Structural change of the endoplasmic reticulum during fertilization: evidence for loss of membrane continuity using the green fluorescent protein. Dev Biol 179: 320–328.
21. Pedrosa Ribeiro CM, McKay RR, Hosoki E, Bird GS, Putney JW Jr (2000) Effects of elevated cytoplasmic calcium and protein kinase C on endoplasmic reticulum structure and function in HEK293 cells. Cell Calcium 27: 175–185.
22. Subramanian K, Meyer T (1997) Calcium-induced restructuring of nuclear envelope and endoplasmic reticulum calcium stores. Cell 89: 963–971.
23. Dayel MJ, Hom EF, Verkman AS (1999) Diffusion of green fluorescent protein in the aqueous-phase lumen of endoplasmic reticulum. Biophys J 76: 2843–2851.
24. Harmer AR, Gallacher DV, Smith PM (2002) Correlations between the functional integrity of the endoplasmic reticulum and polarized Ca2+ signalling in mouse lacrimal acinar cells: a role for inositol 1,3,4,5-tetrakisphosphate. Biochem J 367: 137–143.
25. Caroni P (1997) Overexpression of growth-associated proteins in the neurons of adult transgenic mice. J Neurosci Methods 71: 3–9.
26. Rytter A, Cronberg T, Asztely F, Nemali S, Wieloch T (2003) Mouse hippocampal organotypic tissue cultures exposed to in vitro "ischemia" show selective and delayed CA1 damage that is aggravated by glucose. J Cereb Blood Flow Metab 23: 23–33.

27. Ihaka R, Gentleman R (1996) R: A language for data analysis and graphics. Journal of Computational and Graphical Statistics 5: 299–214.
28. Jones VC, McKeown L, Verkhratsky A, Jones OT (2008) LV-pIN-KDEL: a novel lentiviral vector demonstrates the morphology, dynamics and continuity of the endoplasmic reticulum in live neurones. BMC Neurosci 9: 10.
29. Ng AN, Toresson H (2008) Gamma-secretase and metalloproteinase activity regulate the distribution of endoplasmic reticulum to hippocampal neuron dendritic spines. Faseb J 22: 2832–2842.
30. Horton AC, Ehlers MD (2003) Dual modes of endoplasmic reticulum-to-Golgi transport in dendrites revealed by live-cell imaging. J Neurosci 23: 6188–6199.
31. Williams K, Russell SL, Shen YM, Molinoff PB (1993) Developmental switch in the expression of NMDA receptors occurs in vivo and in vitro. Neuron 10: 267–278.
32. Ruegg UT, Burgess GM (1989) Staurosporine, K-252 and UCN-01: potent but nonspecific inhibitors of protein kinases. Trends Pharmacol Sci 10: 218–220.
33. Farnsworth CL, Freshney NW, Rosen LB, Ghosh A, Greenberg ME, et al. (1995) Calcium activation of Ras mediated by neuronal exchange factor Ras-GRF. Nature 376: 524–527.
34. Fam NP, Fan WT, Wang Z, Zhang LJ, Chen H, et al. (1997) Cloning and characterization of Ras-GRF2, a novel guanine nucleotide exchange factor for Ras. Mol Cell Biol 17: 1396–1406.
35. Sokka AL, Putkonen N, Mudo G, Pryazhnikov E, Reijonen S, et al. (2007) Endoplasmic reticulum stress inhibition protects against excitotoxic neuronal injury in the rat brain. J Neurosci 27: 901–908.
36. Petito CK, Pulsinelli WA (1984) Delayed neuronal recovery and neuronal death in rat hippocampus following severe cerebral ischemia: possible relationship to abnormalities in neuronal processes. J Cereb Blood Flow Metab 4: 194–205.
37. Petito CK, Pulsinelli WA (1984) Sequential development of reversible and irreversible neuronal damage following cerebral ischemia. J Neuropathol Exp Neurol 43: 141–153.
38. Tatsuta T, Langer T (2008) Quality control of mitochondria: protection against neurodegeneration and ageing. Embo J 27: 306–314.
39. Cheung EC, McBride HM, Slack RS (2007) Mitochondrial dynamics in the regulation of neuronal cell death. Apoptosis 12: 979–992.
40. Choi YM, Kim SH, Chung S, Uhm DY, Park MK (2006) Regional interaction of endoplasmic reticulum Ca2+ signals between soma and dendrites through rapid luminal Ca2+ diffusion. J Neurosci 26: 12127–12136.
41. Solovyova N, Verkhratsky A (2003) Neuronal endoplasmic reticulum acts as a single functional Ca2+ store shared by ryanodine and inositol-1,4,5-trisphosphate receptors as revealed by intra-ER [Ca2+] recordings in single rat sensory neurones. Pflugers Arch 446: 447–454.
42. Mattson MP, Zhu H, Yu J, Kindy MS (2000) Presenilin-1 mutation increases neuronal vulnerability to focal ischemia in vivo and to hypoxia and glucose deprivation in cell culture: involvement of perturbed calcium homeostasis. J Neurosci 20: 1358–1364.
43. Wang C, Nguyen HN, Maguire JL, Perry DC (2002) Role of intracellular calcium stores in cell death from oxygen-glucose deprivation in a neuronal cell line. J Cereb Blood Flow Metab 22: 206–214.
44. Wei H, Perry DC (1996) Dantrolene is cytoprotective in two models of neuronal cell death. J Neurochem 67: 2390–2398.
45. Bramham CR, Wells DG (2007) Dendritic mRNA: transport, translation and function. Nat Rev Neurosci 8: 776–789.
46. Park MK, Petersen OH, Tepikin AV (2000) The endoplasmic reticulum as one continuous Ca(2+) pool: visualization of rapid Ca(2+) movements and equilibration. Embo J 19: 5729–5739.
47. Koch GL, Booth C, Wooding FB (1988) Dissociation and re-assembly of the endoplasmic reticulum in live cells. J Cell Sci 91(Pt 4): 511–522.
48. Pelham HR (1988) Evidence that luminal ER proteins are sorted from secreted proteins in a post-ER compartment. Embo J 7: 913–918.

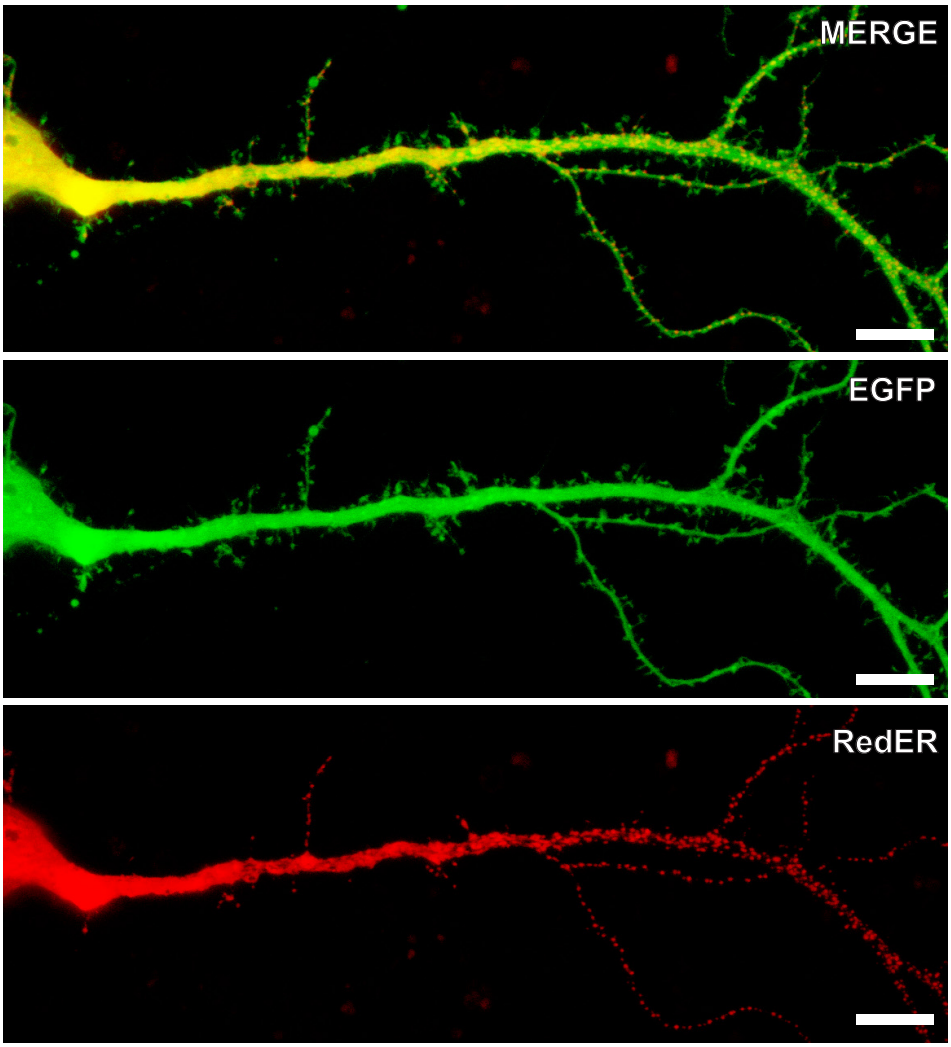

Figure S1. **Gradual distal to proximal ER fission.**
In neurons where ER fission did not occur instantaneously fragmentation always occurred gradually from the most distal parts of dendrites towards the soma. The image show a neuron that was treated with 20 µM glutamate (5 min) and subsequently 25 µM MK-801 to attenuate the stimulus. Scale bar: 10 µm.

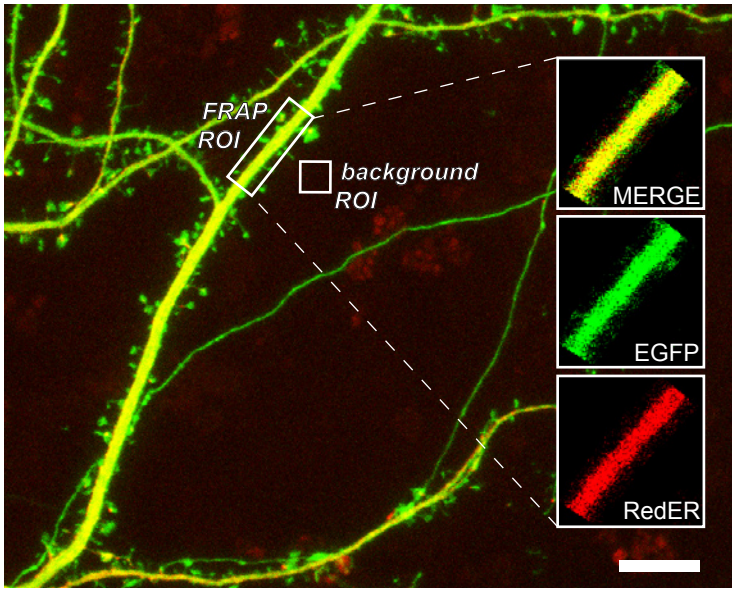

Figure S2. **Example of FRAP ROI.**
For all FRAP recordings a rectangular region of interest (ROI) was placed over a dendrite and a square ROI was placed immediately outside the dendrite to collect the background signal. The small boxes show the signal from the FRAP ROI. Scale bar: 10 µm (large image).

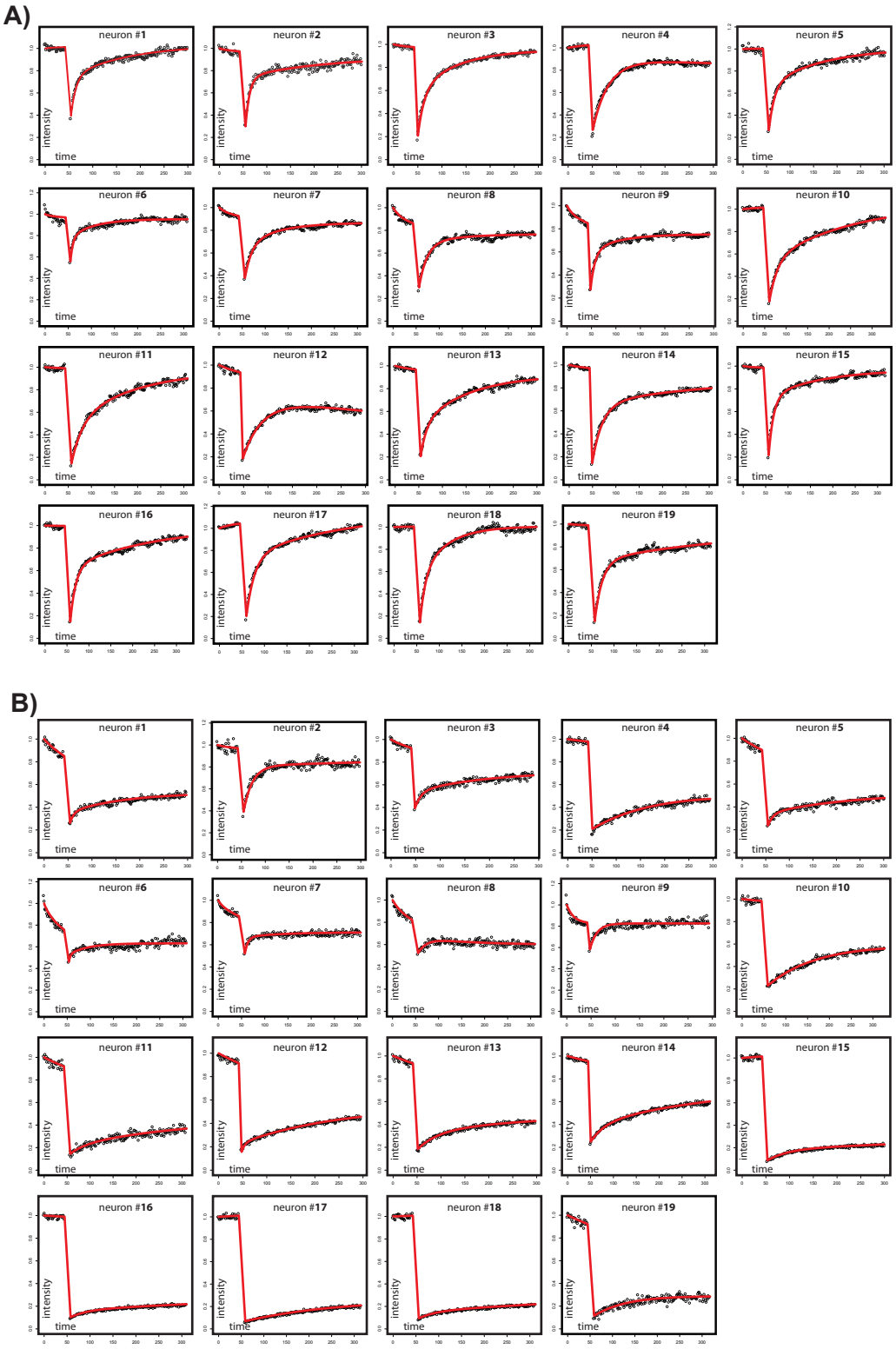

Figure S3. **Curve fitting to data points.**
The FRAP recordings from the 19 neurons in the 100 μM glutamate experiment are shown. The upper panels are recordings prior to glutamate exposure and the lower panels are after 5-60 min of glutamate. The curve fit is in red.

PAPER II MANUSCRIPT

Reversible Endoplasmic Reticulum fission in murine hippocampal pyramidal neurons in organotypic hippocampal slices is dependent on extracellular Ca^{2+}, NMDA receptor activation and is augmented by hypothermia.

Krzysztof Kucharz[1], Tadeusz Wieloch[1] and Håkan Toresson[1]
1: Laboratory for Experimental Brain Research, Department of Clinical Sciences Lund, Lund University, Sweden

Address correspondence to: Hakan Toresson; Associate Professor, PhD; Laboratory for Experimental Brain Research, Department of Clinical Sciences Lund, Lund University, BMC A13, 221 84 Lund, Sweden. Tel: +46 46 222 0613; Fax: +46 46 222 0615; e-mail: hakan.toresson@med.lu.se

ABSTRACT

Endoplasmic reticulum (ER) in cultured neurons is typically a continuous structure, which can undergo rapid fragmentation in response to NMDA receptor (NMDAR) stimulation and if that is transient, subsequently fuse. We aimed at defining the ER fission/fusion phenomena in murine organotypic slice cultures, an experimental model resembling complex brain tissue in vivo. The changes in ER continuity were assessed by Fluorescence Recovery After Photobleaching (FRAP). Using live tissue confocal microscopy we showed that high-potassium induced cell depolarization, which causes release of endogenous glutamate, triggers ER fragmentation. This ER fission is reversible and removal of a high-potassium stimulus results in ER fusion. Furthermore, NMDAR receptor blockade with D-AP5 (50 μM) or removal of calcium ions from the medium prevented ER fission induced by potassium depolarization. Interestingly, when incubation temperature was decreased from 35°C to 30°C, resembling mild hypothermic and neuroprotective conditions in vivo, ER fragmentation was enhanced suggesting that the fragmentation provides protection. We conclude that NMDAR stimulation induces reversible ER fission/fusion, dramatically affecting ER structure, which may alter fundamental ER properties in the cell under physiological conditions or disease.

INTRODUCTION

The endoplasmic reticulum (ER) is a crucial organelle involved in protein synthesis, maturation and cell stress, and serves as the major store of releasable intracellular Ca^{2+} [reviewed in (Burdakov et al., 2005; Paschen and Mengesdorf, 2005; Verkhratsky, 2005)]. Neuronal ER structure is typically considered a continuous organelle organized in the form of a complex interconnected network of cisterns and tubules extending from the soma to subset of dendritic spines (Martone et al., 1993; Terasaki et al., 1994; Spacek and Harris, 1997; Toresson and Grant, 2005). Continuity of ER structure is important for its basic functions and allows directed movement of proteins and diffusional equilibration of ions within its lumen (Dayel et al., 1999; Choi et al., 2006).

It has been shown that some non-neuronal cells exhibit dynamic ER structure remodeling in response to intra- or extracellular stimuli (Terasaki and Jaffe, 1991; Terasaki et al., 1996; Subramanian and Meyer, 1997; Ribeiro et al., 2000; Harmer et al., 2002). Recently a number of proteins have been implicated in regulating ER structure (Park and Blackstone, 2010). Nevertheless, the mechanisms underlying rapid changes in ER morphology remain poorly understood and little is known about the dynamics of the ER structural changes in neurons and its significance in physiology and disease.

In our previous study we demonstrated that dendritic ER undergoes abrupt fragmentation (hereafter also referred to as fission) upon sublethal or lethal NMDA receptor (NMDAR) stimulation. We linked neuronal ER fission with excitotoxic Ca^{2+} influx to the cell and showed that NMDAR activation was necessary for ER fission to occur. Furthermore, we defined rapid loss of ER continuity as a temporary change in ER morphology, where inactivating NMDAR leads to ER fusion and cell survival (Kucharz et al., 2009).

In the present study we aimed at defining signalling pathways involved in reversible ER fission by triggering ER structural changes by neuronal depolarization in murine organotypic hippocampal slices, a preparation used for studies of synaptic plasticity and pathophysiological processes (Holopainen, 2005). The organotypic tissue preparation also allows us to assess the relevance of the fission-fusion process in neurons in an integrated tissue system earlier observed in isolated neuronal cultures (Kucharz et al., 2009). Furthermore, since our previous study showed that blocking NMDAR receptors, which protect neurons against excitotoxicity, inhibited or reversed ER fission, we investigated the effect of decreasing incubation temperature. Mild hypothermia is neuroprotective in many models of transient cerebral ischemia (Krieger and Yenari, 2004) as well as in neuronal cultures (Gisselsson et al., 2010) and organotypic hippocampal slices (Rytter et al., 2005). Several temperature dependent cellular processes have been suggested to mediate the protective effect of hypothermia (Zhao et al., 2007), including changes in actin polymerization-depolymerization (Gisselsson et al., 2010), and effects on intracellular calcium levels (Mitani et al., 1991; Takata et al., 1997). We therefore hypothesized that decreasing incubation temperature from 35 to 30 °C would affect the kinetics of fission-fusion of the neuronal ER.

MATERIALS and METHODS

Imaging setup:

Live cell imaging was performed with a Zeiss LSM 710 upright confocal microscope system equipped with heated Slice Mini Chamber SMC-1 (Luigs & Neumann). The temperature of the imaging chamber was controlled by Badcontroller V unit (Luigs & Neumann). The chamber was constantly perfused with aCSF medium at the flow rate of 4.5 ml/min. The temperature of medium was maintained by HPT-2 in-line tube heater controlled by MTC-20 unit (both npi electronic). The temperature in the chamber was kept at 35°C, unless stated otherwise.

Transgenic mice generation:

For ER fission-fusion analysis the Thy-1-RedER/EGFP transgenic mice were used that express a fluorescent protein DsRed2 targeted to the ER lumen (RedER) and cytosolic Enhanced Green Fluorescent Protein (EGFP) (Supplementary Figure 1). The level of EGFP expression was generally lower compared to RedER and has not been used for main data analysis. The generation of transgene construct and animals was described previously (Kucharz et al., 2009).

Organotypic hippocampal slice cultures:

The 7-days old Thy-1 RedER/EGFP line 27 transgenic mice were decapitated and brains were transferred to ice cold HBSS (Gibco) with 20 mM HEPES, 6 mg/ml D-glucose (both Sigma) and pen/strep (Gibco). The hippocampi were dissected free, sliced into 250 µm thick sections using McIlwan Tissue Chopper and transferred to Millicell culture inserts (Millipore) in 6-well culture plates, three per insert. The slices were grown at 35°C in 50% MEM (Gibco) with 25% heat inactivated horse serum (Gibco), 18% HBSS/$NaHCO_3$ (pH=7.4) supplemented with 6 mg/ml D-glucose (Sigma), 2% B-27 (Gibco), 4 mM L-glutamine and pen/strep. After 7 days of culturing the slices were maintained in medium (as above) without B-27 supplement. Animals were handled in accordance with Swedish law under permits to HT (M275-09).

Slices – live cell imaging:

The slices used for imaging were between 10 and 14 days in vitro. The slices were carefully cut out from the insert membrane and put immediately onto the 50 mm diameter cover glass (Thermo Scientific) in the imaging chamber perfused with carbogen gassed aCSF or its variants (see: results section and Supplementary Table 1); pH=7.4. Slices were perfused on the stage for at least 5 minutes before commencing the imaging. For every slice the general tissue morphology was analyzed under Achroplan 10x 0.3 NA water immersion objective (Zeiss). The inclusion criteria were as follows: pyramidal CA2 or CA3 neurons with normal dendrite morphology, strong expression of RedER (laser power used for imaging <10%) and fluorescence recovery after photobleaching (FRAP) signal recovery higher than 70% of its initial signal strength.

Z-stack image processing:

All presented images were collected as Z-stack series of confocal planes. The pixel dimentions were 0.13x0.13x0.78 µ m. The minimal number of confocal planes used for image reconstruction was 14, the maximum: 40. The confocal planes were projected using maximum intensity projection in ZEN 2008

imaging software (Zeiss), and the images were exported as either uncompressed .jpg or .tiff files. The images were aligned in Photoshop (Adobe) and imported to Illustrator (Adobe).

FRAP:

For analysis of ER continuity one pyramidal neuron (per slice) from CA2 or CA3 region with dendrite of typical ER morphology was chosen. RedER FRAP signal was collected in single track time-lapse mode using 543 nm HeNe laser for excitation and detector set on 545-700 nm band pass for emission. FRAP experiments were performed with Plan-Apochromat 63x/1.0 NA water immersion objective. Mean fluorescence intensity from RedER was measured from a 2 µm x 2 µm selected region of interest (ROI) on a dendrite for 15 scanning cycles (~7.4 sec), bleached with 100% HeNe laser intensity for 80 cycles (~4.6 sec) and FRAP curve was recorded for up to 90 cycles (~17.8 sec). The signal was colleted from 7.6 µm optical slice (maximum pinhole opening) to minimize the effect of focal drift on FRAP recording. For every neuron analyzed the same dendrite area was used at every FRAP recording in the time course of the respective experiment. The data were normalized to the initial intensity strength = 1.

Data analysis:

The FRAP recovery curves have been analyzed using ER continuity model described previously (Kucharz et al., 2009). Briefly, the data were fit into double exponential model curve by squares error minimization. Using the fitted curve and global T=10 sec the effective half time of recovery (τ_{eff}) was calculated. For statistical analysis paired two tailed t-test was used within the group of single experiment and non-paired two tailed t-test with Bonferroni correction ($n_{hypotheses}$ = 3) for multiple comparisons of τ_{eff} at different time-points. The FRAP curves data presented in the results section are average±standard error of mean. Box plots show distribution and median. The circled points indicate outliers.

Drugs:

D-AP5 (Tocris Cookson Inc.) was dissolved in water to 5 mM (100x working solution), frozen in small aliquots and thawed only once prior to use.

RESULTS

The experimental design of all experiments is displayed in Supplementary Figure 2. All slice experiments were run randomly among experimental groups and hence could be analyzed statistically as a single experimental entity.

Potassium-induced depolarization triggers reversible ER fission:

Slices were placed onto the stage and perfused for 5 min with aCSF. Perfusion with aCSF did not alter ER structure; its continuity was maintained even during prolonged incubations in the imaging chamber (up to 60 min, data not shown). From each slice, apical dendrite of an one pyramidal neuron was chosen for further analysis. At first the continuity of dendritic ER was validated by image scan of dendritic ER morphology (Figure 1A) and FRAP analysis (Figure 1B). Slices were left for an additional 5 min in aCSF and then were perfused with K^+aCSF. Exposure to 50 mM K^+ for 1.5 min rendered ER fragmented (Figure 1A) which was reflected by loss of FRAP (Figure 1B). The fragmentation process occurred rapidly after ~25 sec of exposure to K^+aCSF (Supplementary Video 1). Subsequently, K^+aCSF was removed by perfusing the slice and imaging chamber with aCSF. The gradual recovery of ER continuity could be detected after a few minutes in aCSF and within 15 minutes neurons displayed complete ER fusion (Figure 1A, 1B). The calculated effective half-time of FRAP signal recovery (τ_{eff}) from 51 investigated slices (one neuron per slice) that underwent potassium-induced fission was calculated to confirm the temporary loss of ER continuity. The value of average τ_{eff} of untreated neurons was 6.71±1.37 s, while 1.5 min after exposure to high potassium τ_{eff} increased to 17.32±10.31 s ($p<0.001$) clearly indicating ER fragmentation (Figure 1C). The average τ_{eff} after 15 minutes after removal of potassium was 7.07±1.94 s ($p<0.001$) confirming the regain of ER continuity. There was no significant difference in τ_{eff} between the neurons before treatment and after 15 minutes of recovery after high potassium insult ($p=0.5898$).

The ER fission - fusion process is highly reversible and could be induced multiple times (Supplementary Figure 3). In addition ER fission occurred very rapidly in the whole cell, although in some cases we observed that ER fission is a gradual process, progressing towards soma from distal to proximal parts of the dendrite.

Extracellular Ca^{2+} is required for depolarization-induced ER fission:

High potassium depolarization triggers a multitude of effects in neurons, including activation of voltage gated calcium channels (VGCC) and neurotransmitter (e.g. endogenous glutamate) release (Ueda et al., 2000) with subsequent NMDA receptor activation, which leads to increase in cytoplasmic Ca^{2+} content. To assess whether extracellular influx of calcium is critical for inducing ER fission we incubated slices in Ca^{2+} free aCSF. In naïve slices, this treatment neither caused noticeable change in ER morphology as verified optically (Figure 2A) nor did it alter the state of ER continuity as assessed by FRAP analysis (Figure 2B). Subsequently, the slices were exposed for 1.5 min to high potassium in Ca^{2+} free K^+aCSF. Contrary to potassium-induced ER fission in the presence of extracellular Ca^{2+} (Figure 1A) no ER fission was detected in Ca^{2+} free K^+aCSF media (Figure 2A). Moreover, even exposure to high potassium aCSF for a prolonged period of 20 min failed to induce optically defined ER fragmentation (Figure 2A). In some instances we observed the neurons for up to 60 min in K^+aCSF and in no case did they manifest ER fission (data not shown). The ER continuity during prolonged exposure to high potassium was assessed by FRAP analysis (Figure 2B). The average FRAP signal recovery data show that there was no loss of FRAP after 1.5 or 15 minutes of exposure to high potassium in Ca^{2+} free K^+aCSF compared to untreated neurons (n=35). Finally, the analysis of τ_{eff} values proved that there was no statistically significant difference between untreated neurons (τ_{eff} = 5.92±1.45 s) and neurons exposed for 1.5 and 15 min to high potassium insult (τ_{eff} = 5.72±1.89 s and 5.92±2.00 s respectively (Figure 2C)).

NMDAR gated Ca^{2+} is required for depolarization-induced ER fission:

The requirement of extracellular Ca^{2+} influx for ER fragmentation and our earlier results in cultured hippocampal cells demonstrating the involvement of NMDA receptors in the fragmentation process (Kucharz et al., 2009) prompted us to explore the necessity of NMDAR gated Ca^{2+} influx for induction of ER fission. In that regard we performed a series of experiments using the NMDAR antagonist D-AP5. Slices were incubated in their growth medium for 30 min with 50 μM D-AP5 and transferred to the imaging chamber where they were perfused for 5 min with aCSF supplemented with D-AP5. At any given time and instance 50 μM D-AP5 was present in perfused media. The incubation with NMDAR antagonist did not cause optically detectable change in dendritic ER structure (Figure 3A) and the FRAP analysis confirmed the continuous state of ER (Figure 3B). When slices were challenged for 1.5 min with K^+aCSF containing D-AP5 there was no optically detectable ER fission (Figure 3A). However, the average FRAP recovery was lower compared to untreated neurons (Figure 3B). Subsequently to high potassium challenge the slices were perfused again with aCSF supplemented with D-AP5. Dendritic ER preserved its continuity (Figure 3A) and a slight rise in average FRAP recovery was detected (Figure 3B). The τ_{eff} values calculated from FRAP curves confirm the minimal loss of ER continuity during exposure to high potassium. With D-AP5 present, the average of τ_{eff}=7.92±3.83 s of neurons in K^+aCSF was higher compared to τ_{eff}=5.90±1.35 s of untreated neurons and the rise in τ_{eff} was statistically significant ($p<0.05$). Washing out the high potassium for 15 min with aCSF containing D-AP5 resulted in decrease of average τ_{eff} to 6.68±2.66 s (Figure 3C). This value was close to untreated neurons and there was no statistically significant difference between untreated neurons and neurons after 15 min recovery after exposure to high potassium.

The absence of extracellular Ca^{2+} and the presence of D-AP5 increases the basal state of ER continuity:

The analysis of τ_{eff} values of neurons before high K^+ treatment show that neurons in Ca^{2+} free environment as well as neurons exposed to D-AP5 display higher degree of lumenal continuity (Supplementary Figure 4A). There was statistically significant difference between untreated neurons (τ_{eff} = 6.71±1.17 s) and neurons in Ca^{2+} free aCSF (τ_{eff} = 5.92±1.45 s; p=0.020) as well as between untreated neurons (τ_{eff} = 6.71±1.17 s) and neurons exposed to D-AP5 (τ_{eff}=5.90±1.35 s; p=0.014).

Decrease in incubation temperature enhances ER fission:

Decreasing incubation temperature to levels mimicking mild hypothermic condition in vivo (30°C) has been previously reported to be protective against excitotoxic injury of neurons in oxygen-glucose deprivation (OGD) model

of stroke in organotypic slice cultures (Rytter et al., 2005). To test whether mild hypothermia affects ER fission, and hence possibly be of relevance for cell death processes, we carried out the following experiment. First, the slices were placed onto stage and perfused with 35°C aCSF (hereafter referred also as normotermia). After 5 min of incubation with 35°C aCSF the continuity of ER was validated by image scan (Figure 4A) and FRAP analysis (Figure 4B). Subsequently, the temperature in the imaging chamber was lowered and the slices were perfused with 30°C aCSF (denoted hypothermia). After 5 min of incubation at 30°C none of the dendrites choosen for analysis exhibited loss of continuity compared to normotermia condition as validated optically and by FRAP analysis (Figure 4A-B). The comparison of average τ_{eff} of neurons in normotermia and hypothermia shown that decreased temperature did not affect the ER continuity. The difference between τ_{eff} at 35°C (τ_{eff} =6.37±1.22 s) and 30°C (τ_{eff} = 6.80±1.44 s) was not statistically significant (p=0.435, n=36). The slices were left for additional 5 min in 30°C aCSF and subsequently perfused for 1.5 min by 30°C K^+aCSF. Perfusion with high-potassium aCSF induced immediate ER fission as verified optically (Figure 4A). The fragmented state of ER was confirmed by average FRAP signal (Figure 4B) and τ_{eff} analysis (Figure 4C). The average of τ_{eff} in 30°C K^+aCSF was significantly higher (τ_{eff} =28.19 ±19.71 s) as compared to untreated neurons in 30°C aCSF (τ_{eff}=6.80±1.44 s) indicating loss of ER continuity. Next, K^+aCSF was washed away with 30°C aCSF and ER regained its continuity within 15 min as confirmed by image scan, average FRAP and τ_{eff} analysis (Figure 4A-C). There was no significant difference in average τ_{eff} value between the neurons before treatment and after 15 minutes of recovery after high potassium insult (τ_{eff}=6.80±1.44 s vs. τ_{eff}=7.74±2.8 s respectively, p=0.159).

Strikingly, the degree of ER fragmentation at 30°C was considerably higher compared to fragmented ER at 35°C (Supplementary Figure 4B). The difference between average τ_{eff} of neurons in normotermia (τ_{eff} =17.32±10.31 s) and hypothermia (τ_{eff} =28.19±19.71 s) is statistically significant (p<0.01). Noteworthy, there was no statistically significant difference (p=0.578) in τ_{eff} between neurons that recovered after high-potassium insult at 30°C (Figure 4C) and 35°C (Figure 1C).

DISCUSSION

In the present investigation we clearly demonstrate that the ER is a highly dynamic structure in neurons in the organotypic hippocampus slice, and that it can undergo a rapid fission followed by fusion process. We also show that the fission process is dependent on extracellular calcium ions and NMDA receptor activation and temperature affects the degree of ER fragmentation. In the following we will discuss the implication of our result for synaptic transmission and brain pathology.

Induction of depolarisation-induced ER fission:

Our data demonstrate that potassium-induced depolarization of neuronal membranes induces rapid and reversible dendritic ER fission. This addresses an important unanswered question from an earlier study (Kucharz et al., 2009) where it was shown that the ER can undergo rapid fragmentation in primary neuronal cultures in response to sublethal or lethal NMDAR stimulation by either glutamate or NMDA. In that study, loss of ER continuity was induced by bath application of glutamate or NMDA at high concentrations and, although fission could be reversed, the physiological relevance of these findings was not clear. In the present study we posed the question: can ER fission be triggered by endogenous synaptic glutamate release? In the present work the protocol of potassium-induced depolarization of neurons leads to influx of calcium and indeed we show that under these conditions extracellular calcium is a prerequisite for ER fission. With the present protocol, calcium could enter through voltage-gated calcium channels (VGCC) and NMDAR activated by release of endogenous glutamate from presynaptic boutons. It appears that the latter is an important factor contributing to ER fission since it was blocked by NMDAR antagonism by D-AP5. The fact the potassium still induces a certain degree of fragmentation while the NMDA receptor is blocked suggests that calcium entering through VGCC or calcium permeable AMPA receptors may contribute to some degree to ER fragmentation.

In physiological conditions it is unlikely that neurons would undergo such a massive global depolarization as the one induced by perfusing the cells with high potassium aCSF. Instead, local ER fragmentation at “hot spots” or “cold spots” on the dendrites can be envisaged, as described in IP3 receptor activated calcium

release (Fitzpatrick et al., 2009). In some cases we observed that ER fission is a gradual process, progressing towards soma from distal to proximal parts of the dendrite. The areas of the dendrite with the least ER content appeared to fragment first, suggesting that the ER in spines is more susceptible to undergo fission. It is possible that stimuli of the lesser magnitude, i.e. that occurring during physiological NMDAR activation would trigger ER fission restricted spatially to dendritic spines.

ER dynamics and its significance:

It is currently not known whether synaptic activity can modulate ER structure so that e.g. physiological NMDAR activation would trigger local ER fission. Our data, suggest a mechanistic link between synaptically generated calcium transients and ER continuity since the ER appeared more fused (i.e. lower τ_{eff}) in neurons incubated in Ca^{2+} free aCSF than that of neurons in normal aCSF. The fact that neurons incubated with D-AP5 display a similarly decreased average τ_{eff} compared to untreated neurons indicates that it is not the extracellular level of calcium per se that controls ER structure but instead the amount of calcium that is gated to the cytosol mainly through the NMDAR. If these mechanisms operate on the micrometer scale, physiologically induced local ER fission would have far reaching implications for synapse function regulation. It has been shown that the presence of ER in dendritic spine affects postsynaptic calcium transients (Holbro et al., 2009). It is likely, that local fragmentation of ER in spines and the accompanied change in the ER Ca^{2+} tunneling properties would restrict the amount of calcium available for release through spine ER Ca^{2+} channels and, hence locally affect Ca^{2+} signalling and downstream intracellular signalling pathways.
The fact that ER can be divided into functional domains and is not homogenous in distribution of Ca^{2+} channels, such as ryanodine receptors (RyRs), inositol trisphosphate receptors (IP3Rs) and sarco-endoplasmic reticulum Ca^{2+}-ATPase (SERCA), as well as calcium binding proteins (Villa et al., 1991; Walton et al., 1991; Johnson et al., 1993; Fitzpatrick et al., 2009) adds to the complexity of interpretation of the potential effects of local ER fission-fusion and its possible impact on neuronal Ca^{2+} signalling.

Implication for disease:

Although the involvement of mechanisms regulating ER structure in neurodegeneration is not clear, we propose that this phenomenon may play an important role in disease. Our data suggest that disorders associated with deranged Ca^{2+} homeostasis and/or NMDAR activity may well lead to altered activity and structure of the ER. The overstimulation of NMDAR during excitotoxic insults represents the extreme case with rapid ER fission while chronic but smaller elevations of cytosolic calcium may restrict calcium tunneling and alter the calcium signalling properties of the neuron.
An important question in this context is whether ER fission is a protective response to calcium overload or a contributing factor to neuronal pathology and death. In experimental stroke it has been demonstrated that occlusion of the middle cerebral artery leads to depletion of ATP in the core of the ischemic brain region with a permanent membrane depolarization of neurons in this regions (Nedergaard and Astrup, 1986). Surrounding this ischemic core tissue is an area of variable hypoperfusion, the penumbra area, were trains of transient membrane depolarizations occur, with transient elevated extracellular potassium levels and decreased calcium levels (Harris et al., 1982). Our results are highly relevant to events occurring in the penumbra regions and we could envisage that ER transiently fragments in these regions.

Hypothermia has been repeatedly been shown to diminish infarct size when applied during MCAO or immediately after reperfusion (Krieger and Yenari, 2004). Our observation that ER fission is more pronounced at lower temperatures is interesting in the context of neuroprotective properties of mild hypothermia, since the more fragmented the ER, the less tunneling of calcium would be expected to occur. The protective action of hypothermia in excitotoxicity has been linked, among others, with reduced accumulation of intracellular calcium (Takata et al., 1997) and decreased release of glutamate (Baker et al., 1995). The observed increased loss of ER continuity in hypothermia conditions was therefore unexpected since our data indicate that the intracellular calcium levels and/or NMDA receptor activation would be enhanced by the decrease in temperature. In our previous study we suggested that the degree of ER fission is dependent of the amount of NMDAR agonist (Kucharz et al., 2009), however it is possible that other mechanisms, which are

temperature dependent would also contribute to ER fission.

It possible that the impairment of the very processes regulating ER fission and fusion lead to brain pathology, Among the few proteins that have so far been functionally linked to ER structure regulation, several have proven to harbour disease-causing mutations. The mutations in Valosin-containing protein (VCP), mitofusin-2 (MFN2) or atlastin genes have been shown to cause abnormalities in ER, manifested by loss of ER continuity or complete ER fragmentation (Roy et al., 2000; de Brito and Scorrano, 2008; Orso et al., 2009). Correspondingly, the mutations in VCP, MFN-2 and atlastin cause inherited syndrome of inclusion body myopathy with Paget's disease of the bone and frontotemporal dementia (IBMPFD), Charcot-Marie-Tooth inherited motor neuropathy type 2A (CMT2A) and hereditary spastic paraplegia (HSP) respectively (Zhao et al., 2001; Zuchner et al., 2004; Viassolo et al., 2008).

In conclusion, our data show that neuronal ER in highly dynamic in neuronal tissue, capable of adaptive structural changes in response to physiological or pathological stimuli. In its basal state ER maintains some degree of fragmentation, where shortage of extracellular Ca^{2+} or blocking NMDAR enhances ER continuity, while overstimulation of NMDAR causes Ca^{2+} mediated, temperature sensitive ER fission. The pathological alterations of ER dynamic properties, their impact on neuronal cell biology and ultimately the occurrence of ER fission in living brain remain still to be explored.

ACKNOWLEDGEMENTS:

We would like to acknowledge Morten Krogh for his contribution in τ_{eff} values calculations, Sol daRocha for excellent technical assistance and Marco Ledri for suggestions concerning the perfusion system setup.

ABBREVIATIONS:

aCSF – artificial cerebrospinal fluid; CA2, CA3 – *Cornu Ammoni* hippocampal regions; ER – endoplasmic reticulum; FRAP – fluorescence recovery after photobleaching; hypothermia condition – slice cultures at 30°C; K^+aCSF – high potassium artificial cerebrospinal fluid; NMDA – *N*-methyl *D*-aspartate; NMDAR – NMDA receptor; normothermia condition – slice cultures at 35°C; τ_{eff} – effective half time of FRAP signal recovery;

REFERENCES:

Baker CJ, Fiore AJ, Frazzini VI, Choudhri TF, Zubay GP, Solomon RA (1995) Intraischemic hypothermia decreases the release of glutamate in the cores of permanent focal cerebral infarcts. Neurosurgery 36:994-1001; discussion 1001-1002.

Burdakov D, Petersen OH, Verkhratsky A (2005) Intraluminal calcium as a primary regulator of endoplasmic reticulum function. Cell Calcium 38:303-310.

Choi YM, Kim SH, Chung S, Uhm DY, Park MK (2006) Regional interaction of endoplasmic reticulum Ca2+ signals between soma and dendrites through rapid luminal Ca2+ diffusion. J Neurosci 26:12127-12136.

Dayel MJ, Hom EF, Verkman AS (1999) Diffusion of green fluorescent protein in the aqueous-phase lumen of endoplasmic reticulum. Biophys J 76:2843-2851.

de Brito OM, Scorrano L (2008) Mitofusin 2 tethers endoplasmic reticulum to mitochondria. Nature 456:605-610.

Fitzpatrick JS, Hagenston AM, Hertle DN, Gipson KE, Bertetto-D'Angelo L, Yeckel MF (2009) Inositol-1,4,5-trisphosphate receptor-mediated Ca2+ waves in pyramidal neuron dendrites propagate through hot spots and cold spots. J Physiol-London 587:1439-1459.

Gisselsson L, Toresson H, Ruscher K, Wieloch T (2010) Rho kinase inhibition protects CA1 cells in organotypic hippocampal slices during in vitro ischemia. Brain Res 1316:92-100.

Harmer AR, Gallacher DV, Smith PM (2002) Correlations between the functional integrity of the endoplasmic reticulum and polarized Ca2+ signalling in mouse lacrimal acinar cells: a role for inositol 1,3,4,5-tetrakisphosphate. Biochem J 367:137-143.

Harris RJ, Branston NM, Symon L, Bayhan M, Watson A (1982) The effects of a calcium antagonist, nimodipine, upon physiological responses of the cerebral vasculature and its possible influence upon focal cerebral ischaemia. Stroke 13:759-766.

Holbro N, Grunditz A, Oertner TG (2009) Differential distribution of endoplasmic reticulum controls metabotropic signaling and plasticity at hippocampal synapses. Proc Natl Acad Sci U S A 106:15055-15060.

Holopainen IE (2005) Organotypic hippocampal slice cultures: a model system to study basic cellular and molecular

mechanisms of neuronal cell death, neuroprotection, and synaptic plasticity. Neurochem Res 30:1521-1528.

Johnson RJ, Pyun HY, Lytton J, Fine RE (1993) Differences in the subcellular localization of calreticulin and organellar Ca(2+)-ATPase in neurons. Brain Res Mol Brain Res 17:9-16.

Krieger DW, Yenari MA (2004) Therapeutic hypothermia for acute ischemic stroke: what do laboratory studies teach us? Stroke 35:1482-1489.

Kucharz K, Krogh M, Ng AN, Toresson H (2009) NMDA receptor stimulation induces reversible fission of the neuronal endoplasmic reticulum. PLoS One 4:e5250.

Martone ME, Zhang Y, Simpliciano VM, Carragher BO, Ellisman MH (1993) Three-dimensional visualization of the smooth endoplasmic reticulum in Purkinje cell dendrites. J Neurosci 13:4636-4646.

Mitani A, Kadoya F, Kataoka K (1991) Temperature dependence of hypoxia-induced calcium accumulation in gerbil hippocampal slices. Brain Res 562:159-163.

Nedergaard M, Astrup J (1986) Infarct rim: effect of hyperglycemia on direct current potential and [14C]2-deoxyglucose phosphorylation. J Cereb Blood Flow Metab 6:607-615.

Orso G, Pendin D, Liu S, Tosetto J, Moss TJ, Faust JE, Micaroni M, Egorova A, Martinuzzi A, McNew JA, Daga A (2009) Homotypic fusion of ER membranes requires the dynamin-like GTPase atlastin. Nature 460:978-983.

Park SH, Blackstone C (2010) Further assembly required: construction and dynamics of the endoplasmic reticulum network. EMBO Rep 11:515-521.

Paschen W, Mengesdorf T (2005) Endoplasmic reticulum stress response and neurodegeneration. Cell Calcium 38:409-415.

Ribeiro CM, McKay RR, Hosoki E, Bird GS, Putney JW, Jr. (2000) Effects of elevated cytoplasmic calcium and protein kinase C on endoplasmic reticulum structure and function in HEK293 cells. Cell Calcium 27:175-185.

Roy L, Bergeron JJ, Lavoie C, Hendriks R, Gushue J, Fazel A, Pelletier A, Morre DJ, Subramaniam VN, Hong W, Paiement J (2000) Role of p97 and syntaxin 5 in the assembly of transitional endoplasmic reticulum. Mol Biol Cell 11:2529-2542.

Rytter A, Cardoso CM, Johansson P, Cronberg T, Hansson MJ, Mattiasson G, Elmer E, Wieloch T (2005) The temperature dependence and involvement of mitochondria permeability transition and caspase activation in damage to organotypic hippocampal slices following in vitro ischemia. J Neurochem 95:1108-1117.

Spacek J, Harris KM (1997) Three-dimensional organization of smooth endoplasmic reticulum in hippocampal CA1 dendrites and dendritic spines of the immature and mature rat. J Neurosci 17:190-203.

Subramanian K, Meyer T (1997) Calcium-induced restructuring of nuclear envelope and endoplasmic reticulum calcium stores. Cell 89:963-971.

Takata T, Nabetani M, Okada Y (1997) Effects of hypothermia on the neuronal activity, [Ca2+]i accumulation and ATP levels during oxygen and/or glucose deprivation in hippocampal slices of guinea pigs. Neurosci Lett 227:41-44.

Terasaki M, Jaffe LA (1991) Organization of the sea urchin egg endoplasmic reticulum and its reorganization at fertilization. J Cell Biol 114:929-940.

Terasaki M, Jaffe LA, Hunnicutt GR, Hammer JA, 3rd (1996) Structural change of the endoplasmic reticulum during fertilization: evidence for loss of membrane continuity using the green fluorescent protein. Dev Biol 179:320-328.

Terasaki M, Slater NT, Fein A, Schmidek A, Reese TS (1994) Continuous network of endoplasmic reticulum in cerebellar Purkinje neurons. Proc Natl Acad Sci U S A 91:7510-7514.

Toresson H, Grant SG (2005) Dynamic distribution of endoplasmic reticulum in hippocampal neuron dendritic spines. Eur J Neurosci 22:1793-1798.

Ueda Y, Doi T, Tokumaru J, Mitsuyama Y, Willmore LJ (2000) Kindling phenomena induced by the repeated short-term high potassium stimuli in the ventral hippocampus of rats: on-line monitoring of extracellular glutamate overflow. Exp Brain Res 135:199-203.

Verkhratsky A (2005) Physiology and pathophysiology of the calcium store in the endoplasmic reticulum of neurons. Physiol Rev 85:201-279.

Viassolo V, Previtali SC, Schiatti E, Magnani G, Minetti C, Zara F, Grasso M, Dagna-Bricarelli F, Di Maria E (2008) Inclusion body myopathy, Paget's disease of the bone and frontotemporal dementia: recurrence of the VCP R155H mutation in an Italian family and implications for genetic counselling. Clin Genet 74:54-60.

Villa A, Podini P, Clegg DO, Pozzan T, Meldolesi J (1991) Intracellular Ca2+ Stores in Chicken Purkinje Neurons - Differential Distribution of the Low Affinity-High Capacity Ca2+ Binding-Protein, Calsequestrin, of Ca2+ Atpase and of the Er Lumenal Protein, Bip. Journal of Cell Biology 113:779-791.

Walton PD, Airey JA, Sutko JL, Beck CF, Mignery GA, Sudhof TC, Deerinck TJ, Ellisman MH (1991) Ryanodine and inositol trisphosphate receptors coexist in avian cerebellar Purkinje neurons. J Cell Biol 113:1145-1157.

Zhao H, Steinberg GK, Sapolsky RM (2007) General versus specific actions of mild-moderate hypothermia in attenuating cerebral ischemic damage. J Cereb Blood Flow Metab 27:1879-1894.

Zhao X, Alvarado D, Rainier S, Lemons R, Hedera P, Weber CH, Tukel T, Apak M, Heiman-Patterson T, Ming L, Bui M, Fink JK (2001) Mutations in a newly identified GTPase gene cause autosomal dominant hereditary spastic paraplegia. Nat Genet 29:326-331.

Zuchner S et al. (2004) Mutations in the mitochondrial GTPase mitofusin 2 cause Charcot-Marie-Tooth neuropathy type 2A. Nat Genet 36:449-451.

FIGURE LEGENDS

Figure 1. Potassium-induced reversible ER fission.
(A) Representative images of ER structure of a pyramidal neuron dendrite. The panels show the appearance of ER structure at the indicated stages of the experiment. Initially, ER is continuous and rapidly fragments during 1.5 minute exposure to 50 mM K^+. At 5 min of recovery the ER fragments have partially fused and within 15 minutes of perfusion with aCSF, ER regained continuity without any signs of neuronal damage. (B) Normalized average FRAP signal over time in untreated neurons (blue), the same set of neurons after 1.5 min of exposure to 50 mM K^+ (orange) and ~15 min after washing out high-potassium with aCSF. Photobleaching was performed in time between the arrows. Error bars are SEM, n=51. (C) Box plot of τ_{eff} values in untreated neurons (blue) and the same neurons after exposure to 50 mM K^+ in aCSF (orange) and ~15 min after washing out high-potassium with aCSF (purple). The line in the box is the median and the box represents the 25-75 percentiles. Whiskers extend to the extreme values as long as they are within a range of 1.5 x box length. The circles indicate the outliers. Scale bar in all panels: 10 μm.

Figure 2. Extracellular calcium is necessary for potassium-induced ER fission.
(A) Representative images of ER structure of a pyramidal neuron dendrite. The panels show the appearance of ER structure at the indicated stages of the experiment. After perfusion for 5 min with Ca^{2+} free aCSF the ER is continuous. ER structure did not change noticeably during the initial 1.5 minute exposure to 50 mM K^+ in Ca^{2+} free aCSF. The slice was continuously perfused with 50 mM K^+ in Ca^{2+} free aCSF and neither at 10 minutes nor at 20 minutes did we score any sign of ER fission. At 20 minutes after prolonged exposure to high potassium, some ER structural change can be observed, but no signs of ER fragmentation. (B) Normalized average FRAP signal over time in untreated neurons perfused with Ca^{2+} free aCSF (blue), the same set of neurons after 1.5 min of exposure to 50 mM K^+ in Ca^{2+} free aCSF (orange) and 15 min after prolonged exposure to 50 mM K^+ in Ca^{2+} free aCSF (purple). Photobleaching was performed in time between the arrows. Error bars are SEM, n=35. (C) Box plot of τ_{eff} values in untreated neurons (blue) and the same neurons after 1.5 minute exposure to 50 mM K^+ in Ca^{2+} free aCSF (orange) and 15 min after prolonged exposure to 50 mM K^+ in Ca^{2+} free aCSF (purple). The line in the box is the median and the box represents the 25-75 percentiles .Whiskers extend to the extreme values as long as they are within a range of 1.5 x box length. The circles indicate the outliers. Scale bar in all panels: 10 μm.

Figure 3. NMDA receptor activation contributes to potassium-induced ER fission.
(A) Representative images of ER structure of a pyramidal neuron dendrite in a slice preincubated and perfused with 50 μM D-AP5. The panels show the appearance of ER structure at the indicated stages of the experiment. The initially observed ER continuity was maintained during the 1.5 minute exposure to 50 mM K^+ in aCSF in the presence of 50 μM D-AP5. No alterations in ER structure could be seen during recovery in aCSF with 50 μM D-AP5 at 5 or 15 minutes. (B) Normalized average FRAP signal over time in untreated neurons perfused with aCSF with 50 μM D-AP5 (blue), the same set of neurons after 1.5 min of exposure to 50 mM K^+ in aCSF with 50 μM D-AP5 (orange) and ~15 min after washing out high-potassium with aCSF with 50 μM D-AP5 (purple). Photobleaching was performed in time between the arrows. Error bars are SEM, n=33. (C) Box plot of τ_{eff} values in untreated neurons in

aCSF with 50 μM D-AP5 (blue) and the same neurons after exposure to 50 mM K^+ in aCSF with 50 μM D-AP5 (orange) and ~15 min after washing out high-potassium with aCSF with 50 μM D-AP5 (purple). The line in the box is the median and the box represents the 25-75 percentiles. Whiskers extend to the extreme values as long as they are within a range of 1.5 x box length. The circles indicate the outliers. Scale bar in all panels: 10 μm.

Figure 4. Potassium-induced reversible ER fission at 30°C hypothermia condition.
(A) Representative images of ER structure of a pyramidal neuron dendrite. The panels show the appearance of ER structure at the indicated stages of the experiment. Initially, ER is continuous at 35°C and 30°C and there is no detectable difference in ER structure in normo- and hypothermia conditions. ER rapidly fragments during 1.5 minute exposure to 50 mM K^+ at 30°C. At 5 min of recovery at 30°C aCSF the ER fragments have partially fused and ER regained continuity within 15 min without any signs of neuronal damage. (B) Normalized average FRAP signal over time in untreated neurons at 35°C (green) and 30°C (blue), the same set of neurons after 1.5 min of exposure to 50 mM K^+ at 30°C (orange) and ~15 min after washing out high-potassium with 30°C aCSF. Photobleaching was performed in time between the arrows. Error bars are SEM, n=36. (C) Box plot of τ_{eff} values in untreated neurons at 35°C (green) and 30°C (blue) and the same neurons after exposure to 50 mM K^+ in aCSF at 30°C (orange) and ~15 min after washing out high-potassium with 30°C aCSF (purple). The line in the box is the median and the box represents the 25-75 percentiles. Whiskers extend to the extreme values as long as they are within a range of 1.5 x box length. The circles indicate the outliers. Scale bar in all panels: 10 μm.

Supplementary Figure 1. Coexpression of EGFP and RedER in transgenic mouse hippocampal neuron.
The Z-stack collapsed image shows the coexpression of cytosolic EGFP and RedER in soma (A) and dendrites (B) of CA2 hippocampal neuron of organotypic slice culture from transgenic mouse used in study. Scale bar in all panels: 10 μm.

Supplementary Figure 2. Schematic representation of experimental paradigms.
The schematic image represents the detailed timeline of experimental procedures. (A) Experiments with K^+ induced ER fission and fusion. (B) Experiments with Ca^{2+} free aCSF. (C) Experiments with D-AP5. (D) Experiments with mild hypothermia conditions.

Supplementary Figure 3. ER fission-fusion is repeatable.
The series of collapsed Z-stack images show the repeatability of K^+ induced ER fission and subsequent fusion upon K^+ removal. The experimental procedures were followed as described in results section for K^+ induced depolarisation, with additional step at the end of the procedure, where slices were challenged for the second time to 1.5 min exposure to K^+aCSF. The removal of K^+ led again to regain of ER continuity. The comparison of fragmented ER morphology between first and the second ER fragmentation reveal highly repetitive pattern of ER fission. Scale bar in all panels: 10 μm.

Supplementary Figure 4. The τ_{eff} comparisons between the experimental groups.
The incubation of neurons in Ca^{2+} free neurons as well as in D-AP5 contributes to decrease τ_{eff} values indicating increase of ER continuity (A). The values differ between neurons perfused for 5 minutes with (data from Figure 1C) or without (data from Figure 2C) calcium. Similarly, the presence of D-AP5 lowers τ_{eff} value (data from Figure 3C). ER fragmentation is a temperature sensitive process (B). Neurons exposed to K^+aCSF at 30°C have higher τ_{eff} value compared to neurons at 35°C (data from Figure 1C and 4C). The line in the box is the median and the box represents the 25-75 percentiles. Whiskers extend to the extreme values as long as they are within a range of 1.5 x box length. The circles indicate the outliers.

Supplementary Table 1: Different variants of aCSF used in the study.
The table shows the components of different variants of aCSF used in the study.

Supplementary Video 1: Potassium-induced reversible ER fission.
The video shows the reversible ER fission in CA2 hippocampal neuron in slice expressing RedER. The neuron was treated as described in results section. The video starts exactly at the moment where K^+ACSF is introduced to imaging chamber. After 20 seconds, the first sign of fragmentation can be detected. After 1.5 minute of exposure to K^+, the slice was washed with ACSF and the subsequent recovery of ER continuity could be observed. The video was recorded with frequency 0.75 Hz and is

being displayed in 25 fps in 2 frame step. The video has been exported in .mov format. Scale bar = 10 µm.

Paper II; Figure 1

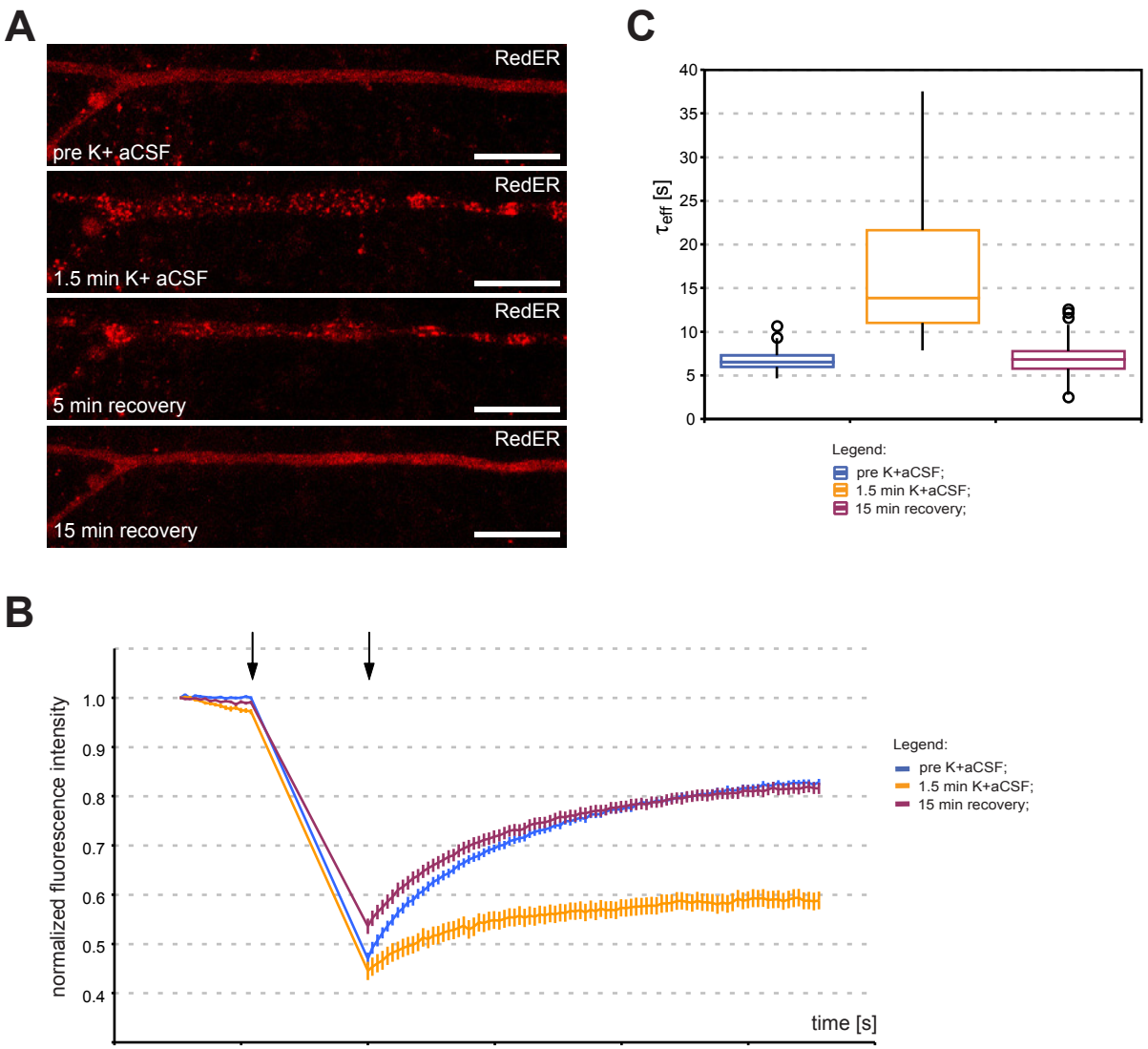

Paper II; Figure 2

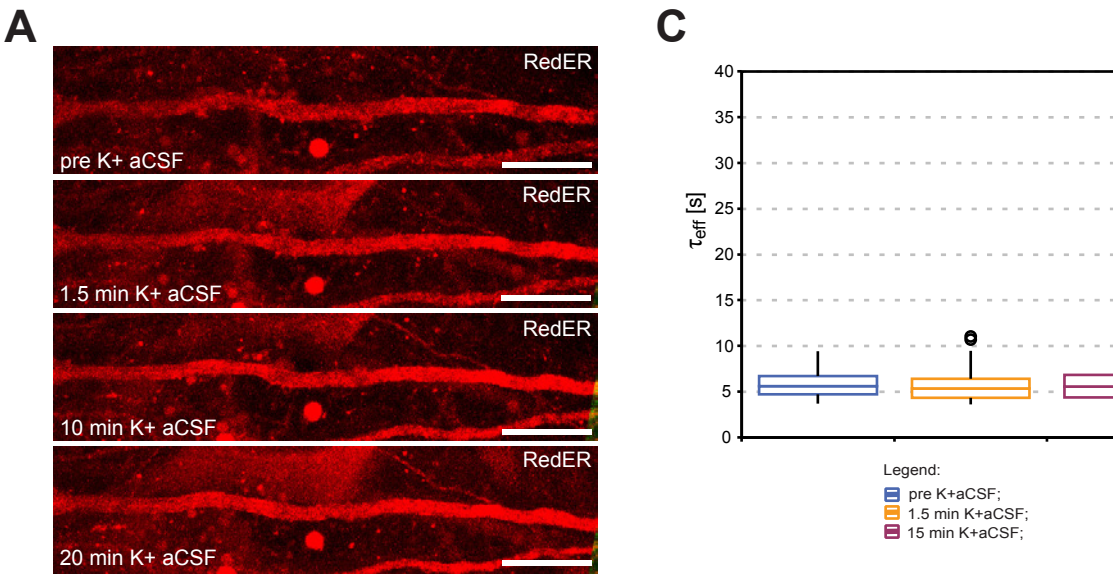

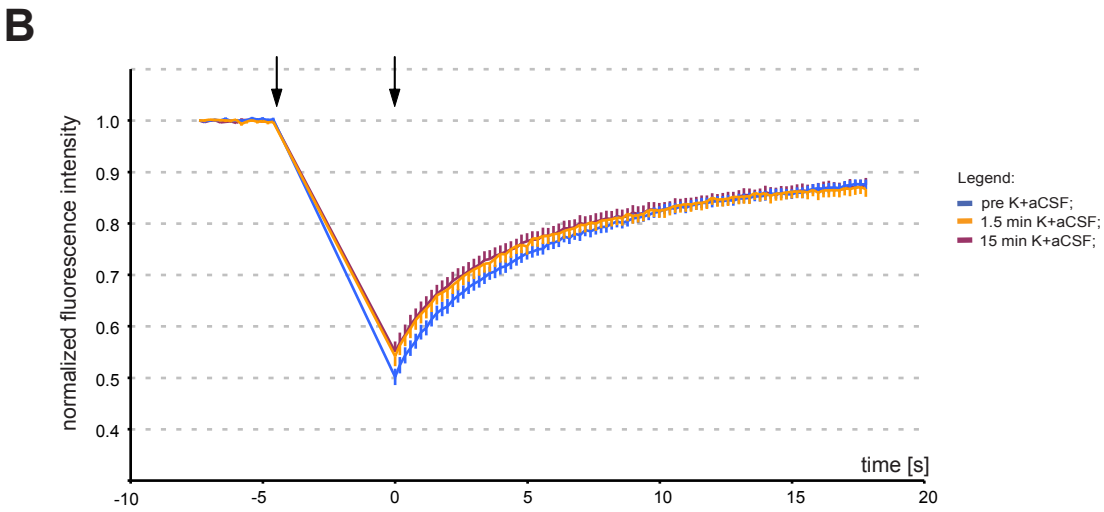

Paper II; Figure 3

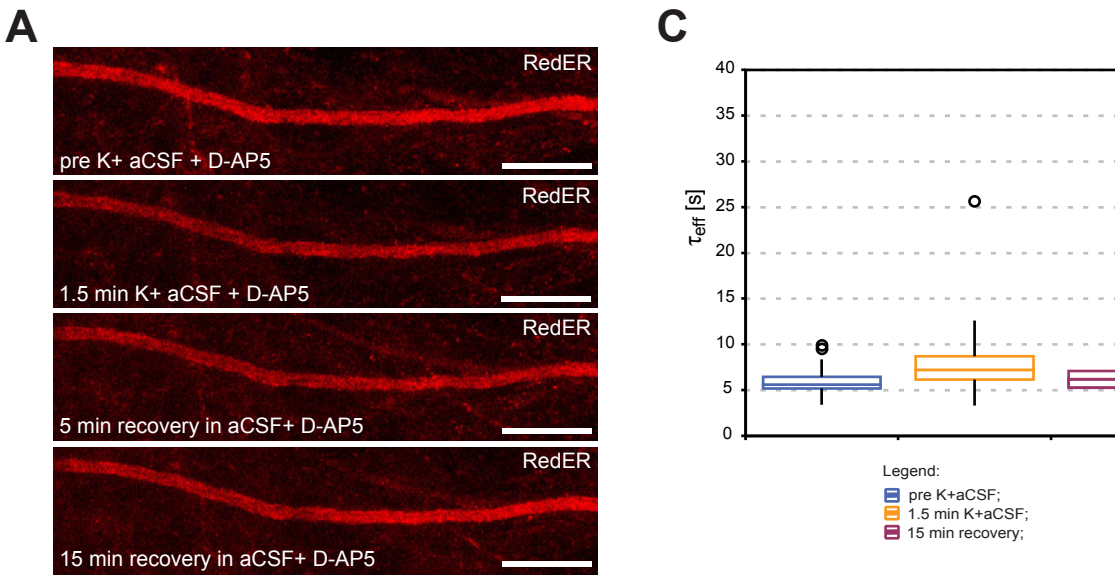

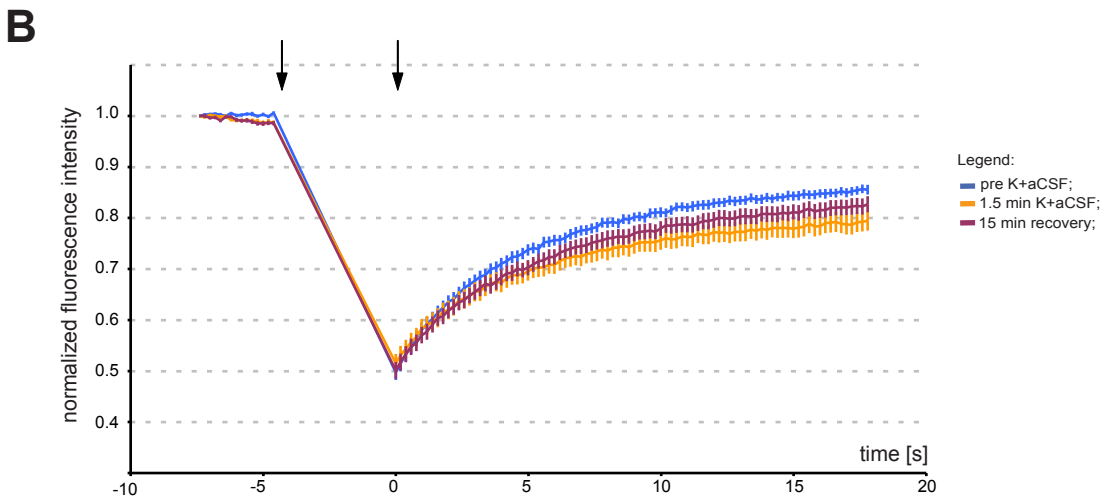

Paper II; Figure 4

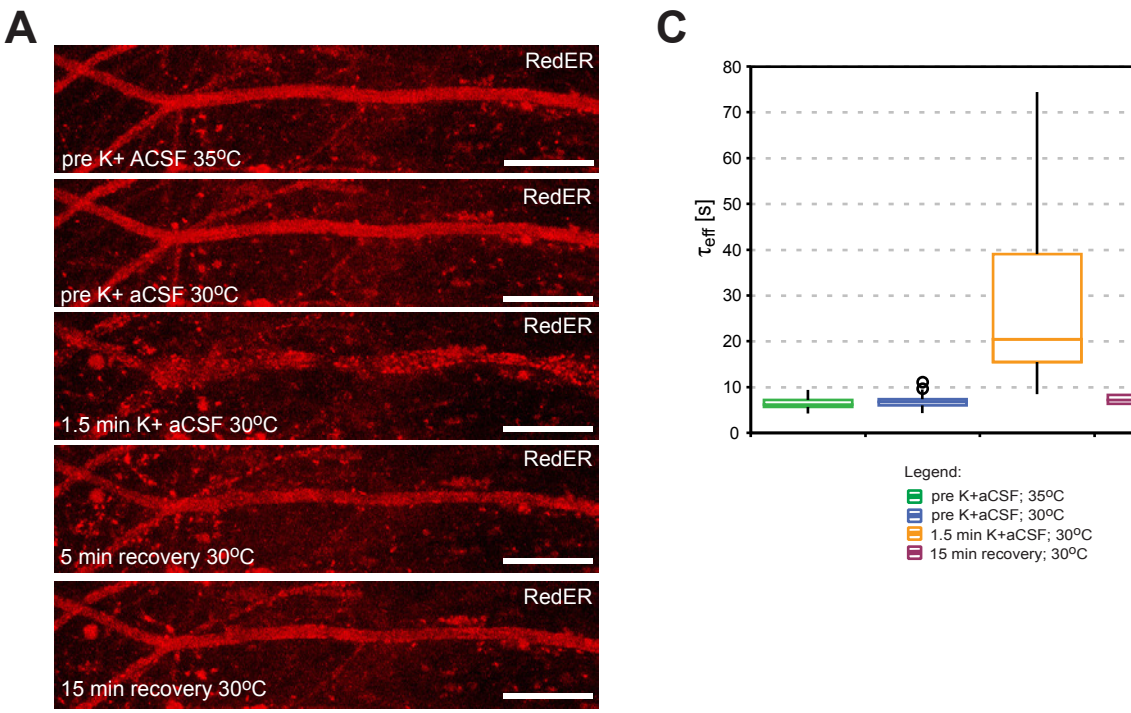

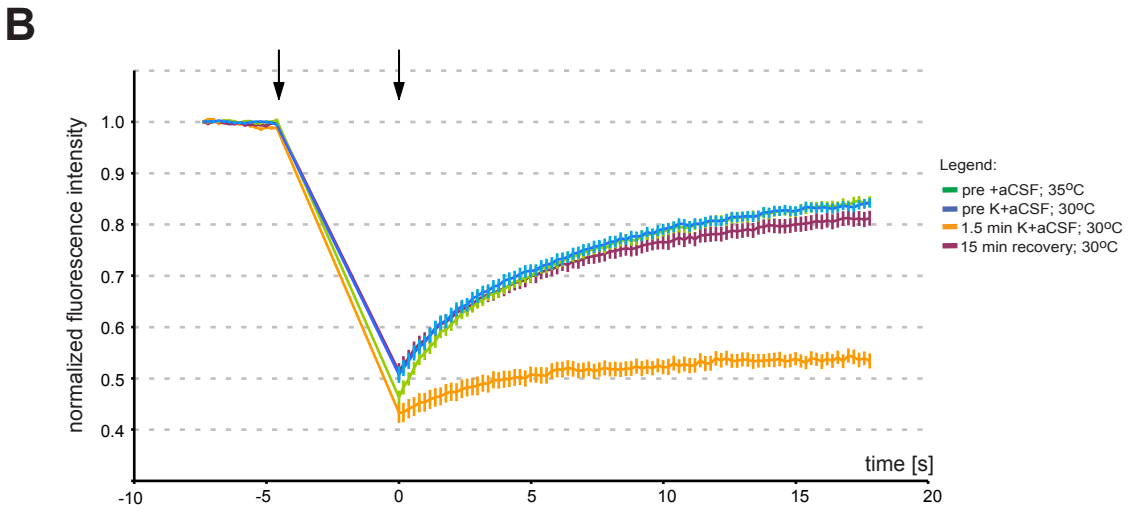

Paper II; Supplementary Figure 1

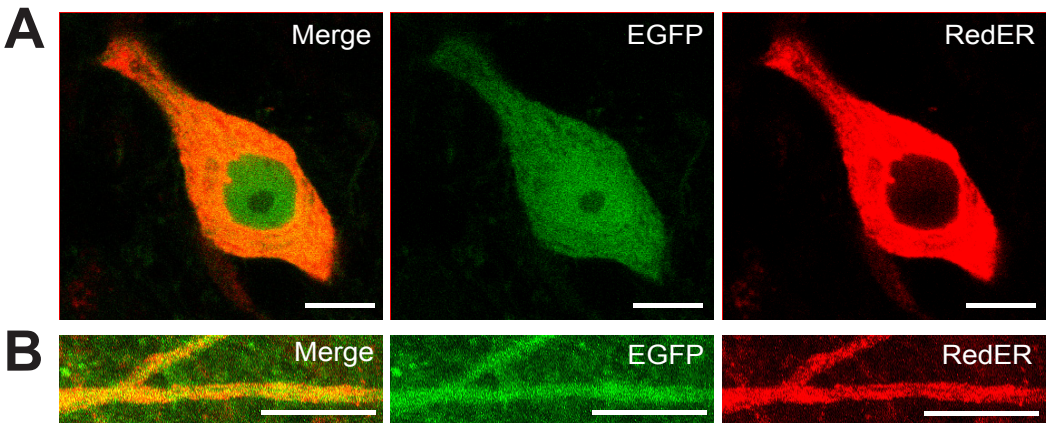

Paper II; Supplementary Figure 2

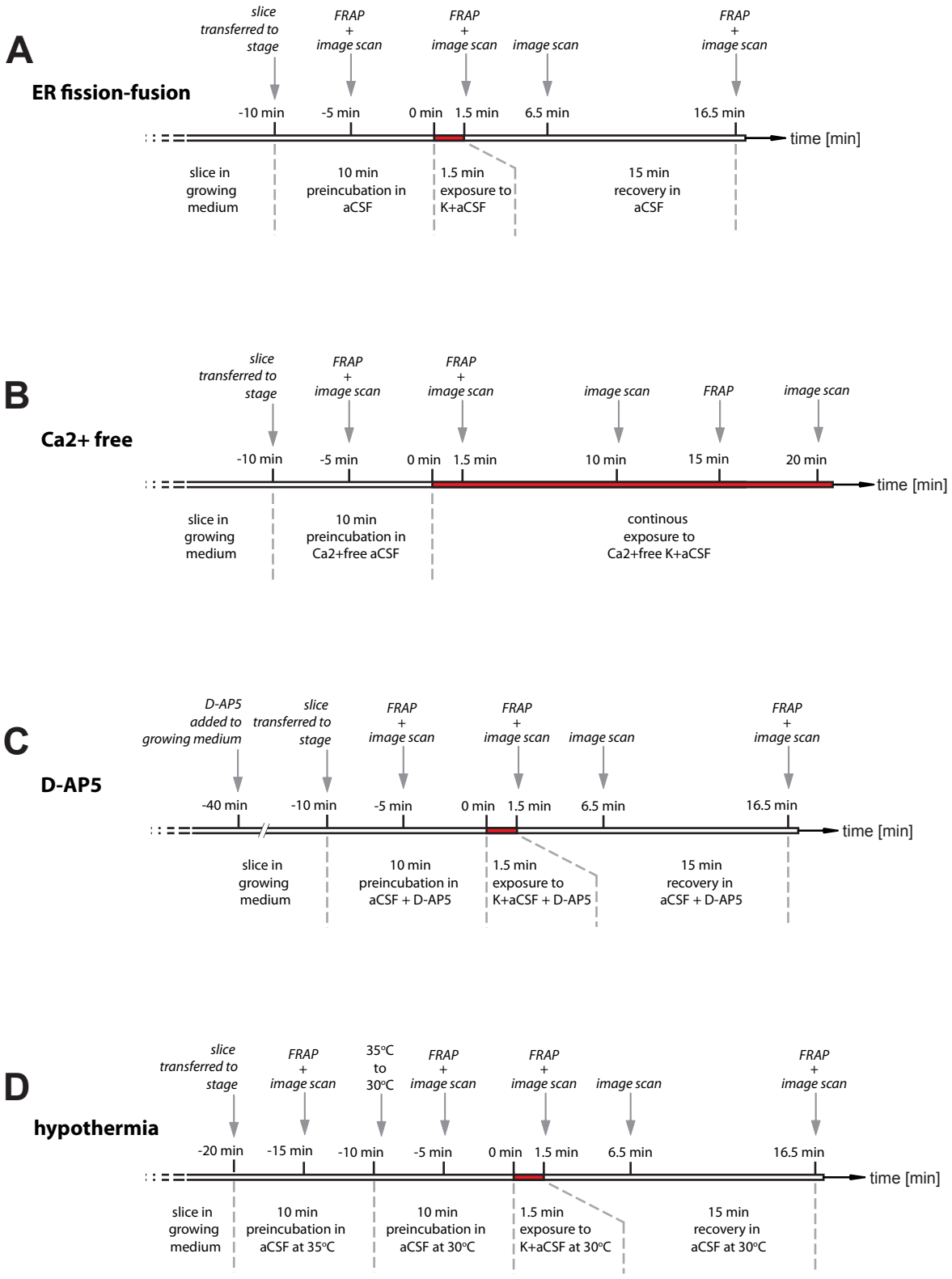

Paper II; Supplementary Figure 3

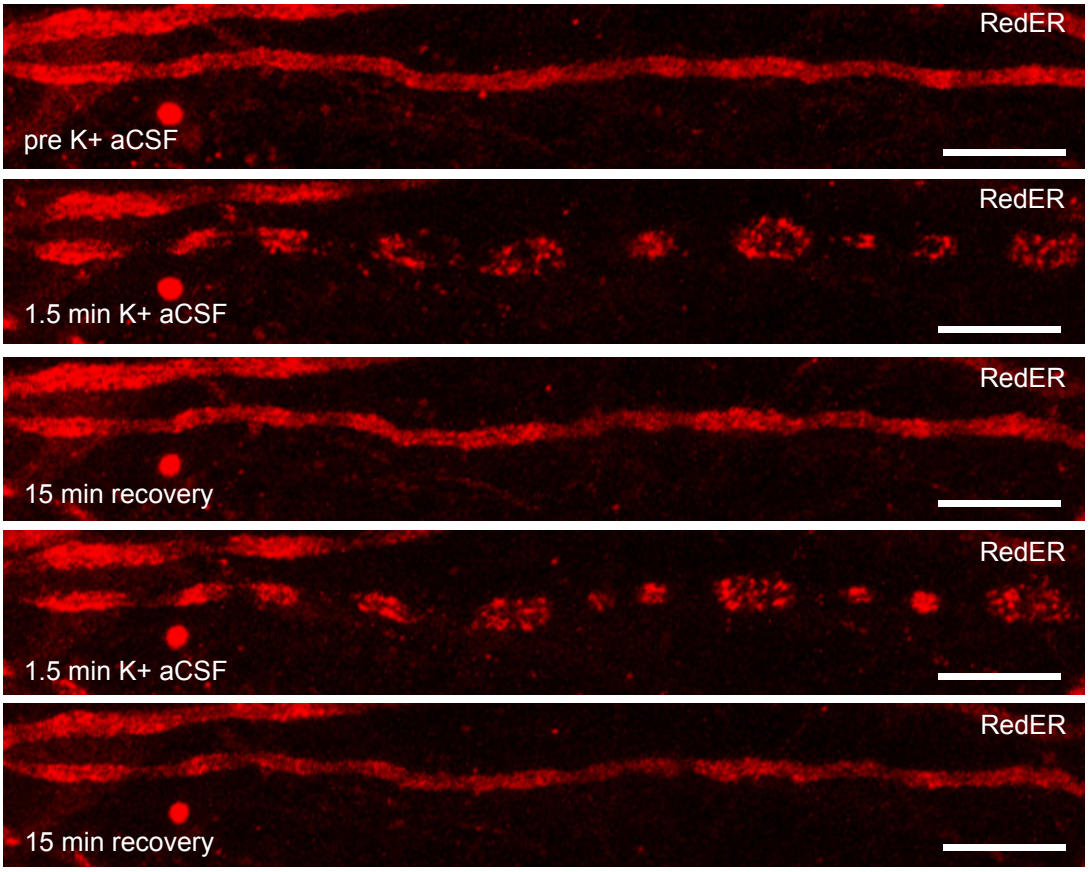

Paper II; Supplementary Figure 4

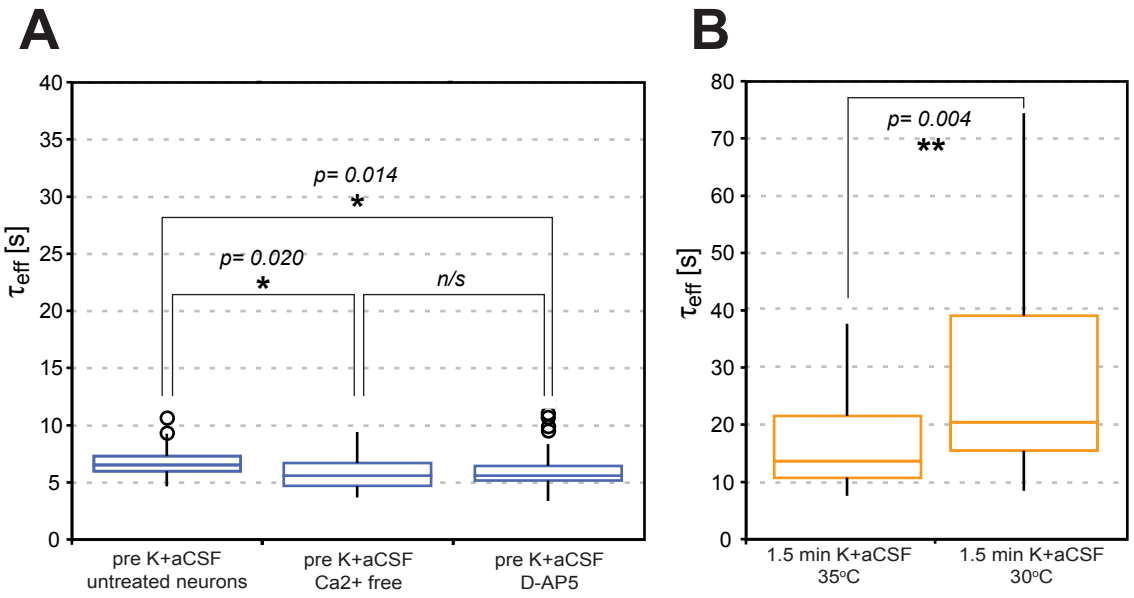

Paper II; Supplementary Table 1

Abbreviation	Description	NaCl [mM]	KCl [mM]	CaCl2 [mM]	EGTA [mM]	MgSO4 [mM]	NaH2PO4 [mM]	NaHCO3 [mM]	glucose [mM]
aCSF	artificial cerebrospinal fluid	119	2.5	2.5	-	1.3	1	26	11
K^+aCSF	high potassium artificial cerebrospinal fluid	71.5	50	2.5	-	1.3	1	26	11
$Ca2^+$ free aCSF	calcium free artificial cerebrospinal fluid supplemented with EGTA	119	2.5	-	20	1.3	1	26	11
$Ca2^+$ free K^+aCSF	calcium free high potassium artificial cerebrospinal fluid supplemented with EGTA	71.5	50	-	20	1.3	1	26	11

PAPER III MANUSCRIPT

Rapid Endoplasmic Reticulum fragmentation in cortical neurons of the mouse brain following cardiac arrest. An in vivo study.

Krzysztof Kucharz[1], Tadeusz Wieloch[1] and Håkan Toresson[1]
1: Laboratory for Experimental Brain Research, Department of Clinical Sciences Lund, Lund University, Sweden

Address correspondence to:
Hakan Toresson; Associate Professor, PhD;
e-mail: hakan.toresson@med.lu.se

Tadeusz Wieloch; Professor of Neurobiology, PhD;
Laboratory for Experimental Brain Research, Department of Clinical Sciences Lund, Lund University, BMC A13, 221 84 Lund, Sweden. Tel: +46 46 222 0600; Fax: +46 46 222 0615;
e-mail: tadeusz.wieloch@med.lu.se

ABSTRACT

Endoplasmic reticulum (ER) is typically a continuous structure, which can undergo rapid reversible fragmentation in response to NMDA receptor-mediated intracellular calcium signaling. We have earlier demonstrated this process in isolated neuronal cultures and in organotypic hippocampal slices cultures. Here we used for the first time, 2-photon laser scanning microscopy (2PLSM) to study the dynamic changes of ER structure in the cerebral cortex of the living mouse. We generated a transgenic mouse expressing enhanced green fluorescent protein targeted to the ER (EGFP-ER) under the Thy-1 promoter thereby selectively expressing the protein in the dendrites of cortical pyramidal neurons. ER structural dynamics (i.e. altered continuity) was assessed by Fluorescence Recovery After Photobleaching (FRAP). In the unchallenged state ER was continuous as evident by both ER morphology and by the FRAP. Furthermore, we found a robust fragmentation of ER into multiple small globular structures as well as loss of FRAP, when cardiac arrest was induced by intravenous KCl injection. The ER was intact for approximately one min after cardiac arrest. Once fragmentation occurred the process was rapid (<10 seconds). We conclude that (1) it is possible to study the ER in the living rodent by 2PLSM, (2) the ER displays a dynamic structural plasticity that can monitored and studied brain disease and injury models as well as (3) in studies of neuronal networks.

INTRODUCTION

Three-dimensional reconstructions depict neuronal endoplasmic reticulum (ER) as a continuous organelle which in dendrites comprises predominantly of complex network of tubules and sac-like structures (cisterns) (Martone et al., 1993; Terasaki et al., 1994; Spacek and Harris, 1997).
The ER is multifunctional organelle, involved in protein synthesis and quality control, cellular stress responses and importantly, calcium homeostasis (reviewed in: (Burdakov et al., 2005; Paschen and Mengesdorf, 2005; Verkhratsky, 2005)). In particular, neuronal ER is one of the key regulators of Ca2+ signaling in the cell, acting as the major store and intracellular source of releasable Ca2+, being of great importance for synaptic transmission and plasticity (Verkhratsky and Petersen, 2002).
The continuous ER lumen permits an efficient, cytosol independent, transport of proteins and diffusion and equilibration of ions within the cell (Dayel et al., 1999; Choi et al., 2006; Jones et al., 2009). It is therefore feasible that decreasing the continuity ER would have an impact on its functions. In fact, ER architecture is dynamic and displays the ability of rapid morphological changes, which results in reduction of ER lumen continuity. We have previously shown that sublethal or lethal stimulation of NMDA receptor (NMDAR) triggers rapid loss of ER continuity (fragmentation, hereafter also called fission), which under sublethal stimulation can be followed by subsequent fusion. Bath application of NMDA or glutamate triggers

reversible ER fission in primary neuronal cell cultures (Kucharz et al., 2009). Furthermore, massive cell depolarisation induces temporary ER fission in hippocampal organotypic slice cultures. NMDAR gated extracellular calcium entry is necessary for ER fission to occur, while the temperature plays important role in regulating the degree of ER fragmentation (Kucharz et al., *unpublished*).

It is well established that during stroke, brain trauma and epilepsy neurons are exposed to rapid increase of synaptic glutamate levels, which leads to NMDAR overstimulation and cellular calcium ion overload (reviewed in: (Lau and Tymianski, 2010)). The link between NMDAR mediated calcium ion entry into cells and ER fission raises the question whether it occurs in the living brain.

In the present study we used 2PLSM to analyze ER dynamics in the brain of the anesthetized transgenic mice expressing ER-targeted Enhanced Green Fluorescent Protein (EGFP). The loss of ER continuity was assessed by image scans, 3D image reconstructions of ER, and fluorescence recovery after photobleaching (FRAP) analysis before and after cardiac arrest. To investigate the rapid loss of ER continuity in the brain we used potassium-induced cardiac arrest model of cerebral ischemia. Global cerebral ischemia leads to a depletion of ATP stores (Lowry et al., 1964), inhibiting extrusion of cytosolic calcium out from the neuron or into intracellular stores. Hence intracellular calcium levels are dramatically elevated 1-2 minutes after cessation of blood flow (Hansen, 1985; Xie et al., 1995). Using the global ischemia paradigm we demonstrate for the first time the occurrence of ER fission *in vivo* and show that marked ER structure remodeling in the living brain can occur in <10 seconds.

MATERIALS AND METHODS

Generation of Thy1-EGFP-ER transgenic mice:

For analysis of dynamic ER structural changes in vivo the transgenic B57 black 6 (C57BL/6) mice, expressing ER-specific marker, were used. The mice expressed Enhanced Green Fluorescent Protein targeted to ER (EGFP-ER hereafter also called GreenER) under Thy1 promoter. The transgene construct was created using EGFP gene containing calreticulin ER-targeting sequence and KDEL ER-retention sequence (gift from Thomas Oertner; Friedrich Miescher Institute). The ER-targeted EGFP was amplified with XhoI restriction site-containing primers and after sequence verification cloned into the XhoI site of the pThy-1.2 vector (gift from Joshua R. Sanes Washington University). We assessed the fluorescence signal strength and the cellular expression patterns among three generated transgenic lines and we chose the Thy1-EGFP-ER-7b line for our further studies.

The cranial window surgery:

All animal handling procedures were approved by the Malmö/Lund ethical committee. The surgery was based on the method developed by Anthony Holtmaat and colleagues (Holtmaat et al., 2009) with minor modifications. Briefly, Thy1-EGFP-ER mice were anesthetized with 3.5% isoflurane in a oxygen/nitrous oxide (30:70) gas mixture, and transferred onto custom modified operating stage. The temperature of animal during surgical procedures was maintained at 37^{o}C. The temperature was monitored using YSI-451 rectal thermistor probe connected to TC-1000 Mouse Proportional temperature unit controlling the 08-13013 mouse small heating pad (Linton Instrumentation, Norfolk, UK).

The animal head was shaved and mounted onto a stereotactic head frame. The eyes were lubricated with Viscotears (Novartis, Switzerland). Subsequently, animals were injected subcutaneously with Temgesic (dosage: 0.1mg/kg, active substance: buprenorfin, Schering-Plough, Germany) and isoflurane was decreased to 1.8-2%. The shaved skin was washed with chlorhexidine and iodine. The scalp and periosteum was removed and Marcaine (2.5mg/ml: bupivacain, AstraZeneca, UK) was applied to the surface of the scar. Subsequently the animal was injected with Rimadyl (dosage: 5mg/kg, active substance: carprofen, Pfizer) and Dexafort (dosage: 2mg/kg, active substance: dexamethasone, Intervet, Netherlands). The exposed edges of the scar scull was covered with a thin layer of tissue adhesive (Vetbond, 3M) and a 4 mm diameter area was encircled on the anterior part of right parietal lobe to mark the location for cranial window. The craniotomy was performed over approximately 30 minutes with a dental drill within the previously demarcated area. To prevent tissue damage due to excessive heating, the scull was flushed every 5 minutes with cold saline. The bone flap was carefully removed to leave the dura intact and to prevent excessive bleeding. Immediately after opening of the cranium, the surface of the brain was covered with a haemostatic absorbable gelatin sponge (Spongostan®, Ferrosan, Denmark) wetted with saline to preserve humidity. Sterile liquid

low melting agarose (Promega) was applied to the brain surface and the sterile 5 mm diameter coverglass (Karl Hecht GmbH & Co KG "Assistent", Germany) was positioned on top of the cranial opening. The rim of the circular coverglass was covered with Vetbond and the surface of the scull was coated with dental cement in order to firmly position the cranial window. Subsequently, using dental cement, a custom-made titanium bar was attached in order to stabilize the head during imaging procedures (Supplementary Figure 1).

Animal preparation for imaging:

For cardiac arrest induction by potassium chloride injection during the imaging, a vein catheter was inserted. Following the surgical procedures, the animal head was mounted to the custom-built imaging stage insert by the titanium bar (Supplementary Figure 2). The rectal temperature was maintained at 37^{o}C. The animal was spontaneously breathing 1.8-2% isoflurane in N2O/O2 (30:70) gas mixture during imaging.

In vivo imaging setup:

The *in vivo* imaging was carried out with multiphoton Zeiss LSM 7 MP upright laser scanning microscope using W-Plan Apochromat 20x/1.0 DIC Vis-IR water immersion objective (Carl Zeiss, Germany). EGFP was excited using Mai Tai DeepSee Ti:Sapphire pulse laser (Spectra-Physics, Newport, USA) tuned to 900 nm and the signal was collected by Gallium-Arsenide-Phosphide (GaAsP) detector. The images and time-lapse recordings were acquired in 8-bit color depth. The Z-stack images were projected using maximum intensity projection (in Figure 2, to assess ER continuity) or semi transparent intensity projection (in Figure 1, to assess the details of ER morphology). The data was exported from ZEN 2010 (Carl Zeiss, Germany) imaging software as .mov; .tiff or uncompressed .jpg format.

FRAP analysis:

Fluorescence Recovery After Photobleaching (FRAP) was utilized to assess ER continuity before and after induction of cardiac arrest. From each mouse used in the study, 10 randomly chosen dendrites (>150 µm below cortex surface) with typical ER morphology were used for analysis. The GreenER was excited using Mai Tai DeepSee Ti:Sapphire pulse laser (Spectra-Physics) tuned to 900 nm and the signal was collected using the GaAsP detector. The mean fluorescence intensity signal was recorded using W-Plan Apochromat 20x/1.0 DIC Vis-IR water immersion objective from a 2 µm x 2 µm selected region of interest (ROI) on a dendrite for 10 scanning cycles bleached for 15 cycles with 900 nm Mai Tai laser and FRAP curve was recorded for 90 cycles.
The parameters used for collecting the time-lapse images for FRAP mean signal calculations were adjusted for each animal used in the study. The data was normalized to the initial signal fluorescence intensity = 1 and presented as a mean ± SD.

Potassium chloride induced cardiac arrest:

The cardiac arrest was induced during imaging by lethal injection of 0.5 ml 2 M KCl through a venous catheter.

RESULTS

GreenER expression and inclusion criteria:

The GreenER was expressed under control of Thy1 promoter in a subfraction of cortical neurons and the morphology of ER defined by GreenER signal did not differ from those observed in our previous studies in primary neuronal cultures (Kucharz et al., 2009) and hippocampal slice cultures (Kucharz et al., *unpublished*). The ER in neurons defined by GreenER signal appeared continuous with no abnormalities in morphology such as blebbing or vacuolar structures, although scattered isolated globular structures could be seen (Figure 1). We selected structures in dendrites of molecular layer I or external granular layer II of cerebral cortex with typical ER morphology expressing GreenER.

In vivo ER fission in the mouse brain:

Z-series of image scans confirmed the continuous appearance of the ER in dendrites (Figure 2a; Supplementary Video 1). Subsequently, an intravenous bolus injection of 0.5 ml of 2 M KCl via a vein catheter was performed, which resulted in immediate cardiac arrest. ER fission occurred within 1-2 minutes after injecting KCl, and loss of continuity, occurred within seconds (Figure 2b; Supplementary Video 2). The fragmented ER appeared as a string of small, disconnected beaded structures (Figure 2c; Supplementary Video 3).

Assessing ER fission *in vivo* by FRAP analysis:

To confirm ER fragmentation phenomenon *in vivo* we carried out FRAP analysis on dendritic ER of cortical neurons. Due to the secondary effects related to phototoxic damage occurring during high power multiphoton bleaching step and high frame rate of time-lapse recording of signal recovery, the parameters of collecting the FRAP signal data, such as the time interval between scans, bleaching laser power and iterations were adjusted separately for each mouse used in study.
The dendritic signal from GreenER in one animal prior to cardiac arrest displayed high degree of FRAP signal recovery reaching above 67% of initial signal strength and thus, confirming the continuous structure of ER (blue graph, Figure 3). Subsequently, cardiac arrest was induced and the continuity of ER lumen was assessed 2 minutes thereafter. The FRAP signal was collected again from neurons in the same brain area as prior to cardiac arrest, and the neurons exhibited loss of FRAP (red graph, Figure 3), confirming the reduction in ER lumen continuity. A similar dynamic fission phenomenon was seen in additional two investigated animals (data not shown). ER fission after cardiac arrest was not localized to isolated neurons but a global process occurring in essentially all neurons expressing GreenER (Figure 4).

DISCUSSION

The aim of the study was to show that ER fragmentation, observed previously in primary neuronal cultures (Kucharz et al., 2009) and hippocampal slices (Kucharz et al., *unpublished*) also occurs in neurons in the brain of a living rodent.
Multiphoton *in vivo* imaging of neurons has become an increasingly useful method in neuroscience to study dynamic events in the living rodent brain such as spine morphology and calcium homeostasis under normal or disease conditions (Misgeld and Kerschensteiner, 2006). Here we demonstrated for the first time the *in vivo* images of the endoplasmic reticulum of dendrites of pyramidal neurons in the outer layers of the mouse cortex. Until now, there have not been any studies, which directly assess ER morphology and its dynamics under normal or pathological conditions *in vivo*.
For this purpose we carried out 2PLSM imaging on mice expressing ER targeted fluorescent protein GreenER. In our previous studies we used transgenic mice expressing RedER (Kucharz et al., *unpublished*) to monitor changes of ER morphology in slices, however, in current experimental protocol EGFP was the fluorophore of choice, since the excitation and emission properties of EGFP render GreenER more suitable for 2PLSM.
The overall neuronal ER morphology, delineated by GreenER signal in mouse transgenic Thy1-EGFP-ER-7b line used in this study, did not differ from the one observed previously in organotypic slice cultures expressing RedER (Kucharz et al., *unpublished*), therefore the 7b line was chosen for further ER analysis. However, we observed scattered fluorescent globular structures, the origin of which remains to be identified.
The gross morphology of the dendrites as evident by 2PLSM in the living mouse was similar to that displayed in cultured neurons (Kucharz et al., 2009) and tissue cultures (Kucharz et al., *unpublished*). Also, we found that in basal conditions, ER lumen is continuous. The Z-series of image scans and 3D image reconstruction depict ER continuity, which was later confirmed by FRAP signal analysis. This result was in accord with our previous findings (Kucharz et al., 2009, Kucharz et al., *unpublished*) that ER displays high degree of FRAP signal recovery and also confirms previous reports on ER continuity in neurons by other methods (Jones et al., 2009).
To stimulate a robust change of the ER structure we induced global cerebral ischemia by cardiac arrest. Cardiac arrest results in an immediate loss of cerebral blood flow and subsequently depletion of tissue glucose and high-energy phosphate compounds such as ATP and PCr (Lowry et al., 1964), leading eventually to depolarization of neuronal plasma membranes in the brain (Hansen, 1985). The shortage of energy supply leads to inhibition of cellular glutamate uptake and inhibition of extrusion of calcium ions from neuronal cytosol, with a subsequent increase in synaptic glutamate levels (Benveniste et al., 1984; Globus et al., 1988) and intracellular calcium levels (Silver and Erecinska, 1992). Noteworthy, the depolarization of cell membranes takes 1-2 minutes after cessation of blood flow to the brain. As expected, ER fission did not occur immediately after cessation of blood flow, and ER morphology appeared intact within the first 1-2 minutes after cardiac arrest. Once ER fragmentation occurred, which corresponded to the previously reported time-course of calcium entry into brain cells (Silver and Erecinska, 1992), preferentially neurons, it was rapid.
The presence of ER fission *in vivo*, and its occurrence on the same time-scale as calcium

entry into neurons during ischemia strengthens our previous findings where we identified the glutamate-mediated NMDA receptor-stimulated calcium entry as the mechanism triggering ER fragmentation (Kucharz et al., 2009; Kucharz et al., *unpublished*). The loss of ER continuity was rapid, and the morphology of fragmented ER lumen resembled the one observed previously in hippocampal slice cultures upon depolarisation of neurons. The Z-stack image scans and 3D reconstruction of ER morphology analysis confirmed the fragmented state of ER, which was further validated by FRAP analysis. The fragmentation of ER was not restricted to selected neurons. Loss of ER continuity was a global process, observed in all cortical neurons.

The experimental model used previously to study ER fission phenomenon in primary neuronal cultures or organotypic slices showed that fragmentation was uniquely mediated by NMDA receptor mediated calcium ion entry into neurons. In contrast to these experimental conditions, global ischemia is associated with loss of ATP synthesis and subsequently to an influx of calcium ions into cells. Calcium ions therefore most probably also contribute to ER fission during global ischemia, but the detailed mechanisms of the fission process still need to be determined.

The significance of dramatic ER structural changes in physiology and disease were discussed in details in our previous works (Kucharz et al., 2009; Kucharz et al., *unpublished*). Our current study demonstrates that ER fission occurs in the brain of a living rodent during ischemia, and is therefore of relevance for brain pathology. In our previous studies, we showed that ER fission is reversible. The reversibility of ER fission was not assessed in the current study, since the cardiac arrest model used was terminal. Also, from our present experiments we cannot state if ER fission process is detrimental or beneficial. In our earlier studies in tissue cultures, ER fission induced by high potassium was augmented by decreasing temperature from 35°C to 33°C, suggesting that fragmentation is protective (Kucharz et al., *unpublished*). The reversibility of ER fission and its correlation with cell survival in vivo during ischemia will be assessed in future experiments in models of transient global or focal brain ischemia.

We conclude that it is possible to study the ER in subcellular resolution in the living rodent by 2PLSM, that the ER displays structural plasticity, which can be monitored and studied in models of brain disease and injury as well as in studies of neuronal networks.

ACKNOWLEDGEMENTS

We would like to acknowledge Anthony Holtmaat for his comments and help concerning the cranial window surgery procedures, Kerstin Beirup for invaluable and excellent technical assistance and Sol daRocha and Carin Sjölund for help in establishing the mice transgenic lines. This study was supported by the Swedish Research Council (nr 08644), the EU 7th workprogram through the European Stroke Network (grant No 201024), The Pia Ståhl Foundation, The Swedish Brain Fund, and The Segerfalk Foundation.

REFERENCES

Benveniste H, Drejer J, Schousboe A, Diemer NH (1984) Elevation of the extracellular concentrations of glutamate and aspartate in rat hippocampus during transient cerebral ischemia monitored by intracerebral microdialysis. J Neurochem 43:1369-1374.

Burdakov D, Petersen OH, Verkhratsky A (2005) Intraluminal calcium as a primary regulator of endoplasmic reticulum function. Cell Calcium 38:303-310.

Choi YM, Kim SH, Chung S, Uhm DY, Park MK (2006) Regional interaction of endoplasmic reticulum Ca2+ signals between soma and dendrites through rapid luminal Ca2+ diffusion. J Neurosci 26:12127-12136.

Dayel MJ, Hom EF, Verkman AS (1999) Diffusion of green fluorescent protein in the aqueous-phase lumen of endoplasmic reticulum. Biophys J 76:2843-2851.

Globus MY, Busto R, Dietrich WD, Martinez E, Valdes I, Ginsberg MD (1988) Effect of ischemia on the in vivo release of striatal dopamine, glutamate, and gamma-aminobutyric acid studied by intracerebral microdialysis. J Neurochem 51:1455-1464.

Hansen AJ (1985) Effect of anoxia on ion distribution in the brain. Physiol Rev 65:101-148.

Holtmaat A, Bonhoeffer T, Chow DK, Chuckowree J, De Paola V, Hofer SB, Hubener M, Keck T, Knott G, Lee WC, Mostany R, Mrsic-Flogel TD, Nedivi E, Portera-Cailliau C, Svoboda K, Trachtenberg JT, Wilbrecht L (2009) Long-term, high-resolution imaging in the mouse neocortex through a chronic cranial window. Nat Protoc 4:1128-1144.

Jones VC, Rodriguez JJ, Verkhratsky A, Jones OT (2009) A lentivirally delivered photoactivatable GFP to assess continuity in the endoplasmic reticulum of neurones and glia. Pflugers Arch 458:809-818.

Kucharz K, Wieloch T, Toresson H (*unpublished*) Reversible ER fission in hippocampal pyramidal neurons in organotypic hippocampal slices is dependent on extracellular Ca2+ and NMDA receptor activation. *Manuscript*

Kucharz K, Krogh M, Ng AN, Toresson H (2009) NMDA receptor stimulation induces reversible fission of the neuronal endoplasmic reticulum. PLoS One 4:e5250.

Lau A, Tymianski M (2010) Glutamate receptors, neurotoxicity and neurodegeneration. Pflugers Arch 460:525-542.

Lowry OH, Passonneau JV, Hasselberger FX, Schulz DW (1964) Effect of Ischemia on Known Substrates and Cofactors of the Glycolytic Pathway in Brain. J Biol Chem 239:18-30.

Martone ME, Zhang Y, Simpliciano VM, Carragher BO, Ellisman MH (1993) Three-dimensional visualization of the smooth endoplasmic reticulum in Purkinje cell dendrites. J Neurosci 13:4636-4646.

Misgeld T, Kerschensteiner M (2006) In vivo imaging of the diseased nervous system. Nat Rev Neurosci 7:449-463.

Paschen W, Mengesdorf T (2005) Endoplasmic reticulum stress response and neurodegeneration. Cell Calcium 38:409-415.

Silver IA, Erecinska M (1992) Ion homeostasis in rat brain in vivo: intra- and extracellular [Ca2+] and [H+] in the hippocampus during recovery from short-term, transient ischemia. J Cereb Blood Flow Metab 12:759-772.

Spacek J, Harris KM (1997) Three-dimensional organization of smooth endoplasmic reticulum in hippocampal CA1 dendrites and dendritic spines of the immature and mature rat. J Neurosci 17:190-203.

Terasaki M, Slater NT, Fein A, Schmidek A, Reese TS (1994) Continuous network of endoplasmic reticulum in cerebellar Purkinje neurons. Proc Natl Acad Sci U S A 91:7510-7514.

Verkhratsky A (2005) Physiology and pathophysiology of the calcium store in the endoplasmic reticulum of neurons. Physiol Rev 85:201-279.

Verkhratsky A, Petersen OH (2002) The endoplasmic reticulum as an integrating signalling organelle: from neuronal signalling to neuronal death. Eur J Pharmacol 447:141-154.

Xie Y, Zacharias E, Hoff P, Tegtmeier F (1995) Ion channel involvement in anoxic depolarization induced by cardiac arrest in rat brain. J Cereb Blood Flow Metab 15:587-594.

FIGURE LEGENDS

Figure 1. The expression of GreenER *in vivo*.
(A). The image shows the projected Z-stack of dendrites of typical pyramidal neuron expressing GreenER in outer layer of the cortex in Thy1-EGFP-ER-7b transgenic mouse line. The arrow indicate a blood vessel. (B). A fragment of dendritic ER in (A). Scale bar in all panels = 20 μm.

Figure 2. Dendritic ER fission in cortical neurons *in vivo* following the cardiac arrest.
The images show typical ER morphology defined by GreenER and its dynamic structural changes in dendrites of pyramidal neurons in superficial cortex layer in response to cardiac arrest. (A). The projected Z-stack of image scans show that dendritic ER in *in vivo* in its basal state is continous. (B). Cessation of blood flow results in rapid reduction in ER continuity occuring within <10 seconds after first minute of cardiac arrest. (C). Z-stack of image scans shows ER in its fragmented state, 3 minutes after cardiac arrest. Scale bar in all panels: 20 μm.

Figure 3. FRAP analysis of dendritic ER fission in cortical neurons *in vivo* following the cardiac arrest.
Normalized average FRAP signal over time in dendrites of neurons in three animals subjected to cardiac arrest (A, B, C). The graphs show FRAP signal recovery before (blue), and loss of FRAP (red) after the 2 minutes of cardiac arrest. Photobleaching was performed in time between the arrows. Time = 0 was set to when photobleaching ends and fluorescence starts to recover. The recovery of FRAP signal from dendritic ER before the cardiac arrest indicates ER continuity, while loss of FRAP demonstrates a fragmented structure of ER. Error bars are SEM, n = 12 neurons.

Figure 4. The ER fission is a global phenomenon in pyramidal neurons of cerebral cortex.
The projected Z-stack of images shows the fragmented state of dendritic ER in neurons of outer layer of cerebral cortex (dimensions of projected area: X=900 µm x Y=450 µm x Z=120 µm) following the cardiac arrest. Scale bar: 100 µm.

Supplementary Figure 1.
Picture and schematic representation of the head of the Thy1-EGFP-ER-7b transgenic mouse subseqently to cranial window surgery. Legend: (1) titanium bar; (2) dental cement; (3) anestesia delivery; (4) removed scalp surface; (5) cranial window; (6) anesthetized mouse.

Supplementary Figure 2.
Picture and schematic representation the Thy1-EGFP-ER-7b transgenic mouse in the *in vivo* imaging stage setup. Legend: (1) titanium bar mount; (2) anestesia gases delivery; (3) water immersion objective; (4) water applied on top of cranial window; (5) anesthetized mouse; (6) heating pad; (7) imaging pad insert; (8) rectal thermal probe.

Supplementary Video 1. 3D reconstruction of continous ER *in vivo*.
The animation shows the 3D reconstruction of continous ER structure in dendrite in pyramidal neurons of superficial cortex layer before the cardiac arrest.

Supplementary Video 2. Timelapse recording of ER fragmentation *in vivo*.
The timelapse recording shows the rapid ER fission occuring after the first minute of cardiac arrest. The timer starts at the beginning of the video, 60 seconds after cardiac arrest. The ER fragmented rapidly, and the first signs of ER fission can be observed at 18th second of recording while at 31st second ER displays no detectable signs of continuity. The images were collected at 0.22 Hz, the movie is encoded to 20 frames per second. Scale bar = 20 µm.

Supplementary Video 3. 3D reconstruction of fragmented ER *in vivo*.
The animation shows the 3D reconstruction of fragmented ER morphology in dendrite in pyramidal neurons of superficial cortex layer 2 minutes after the cardiac arrest.

Paper III; Figure 1

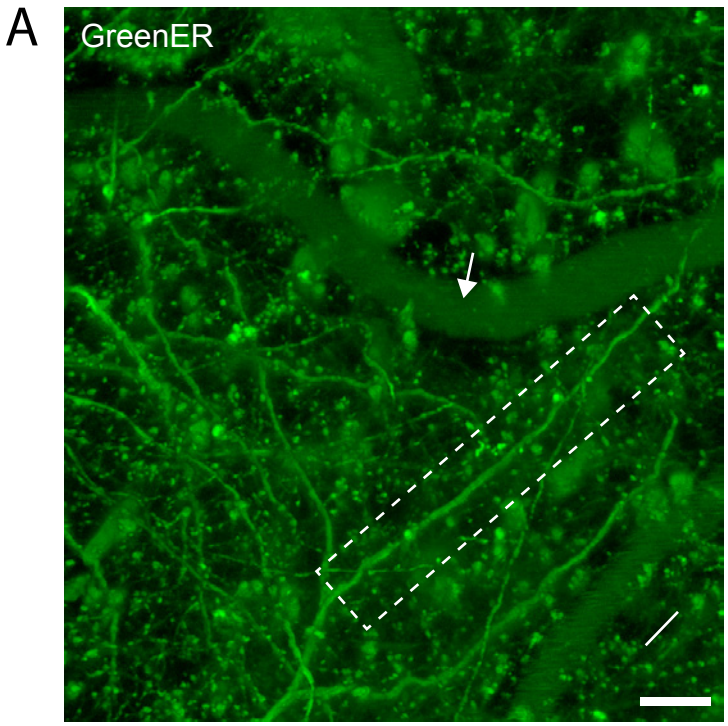

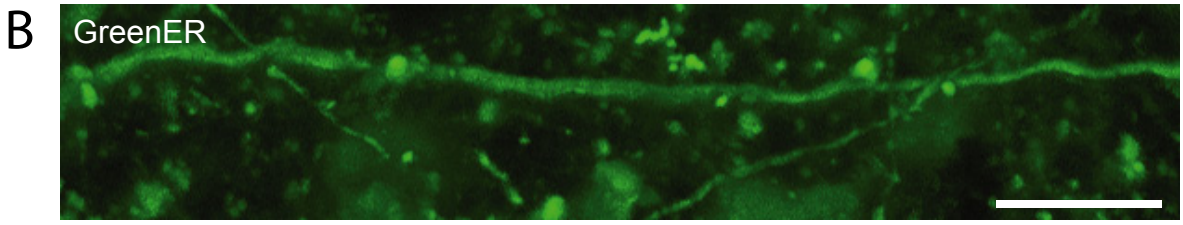

Paper III; Figure 2

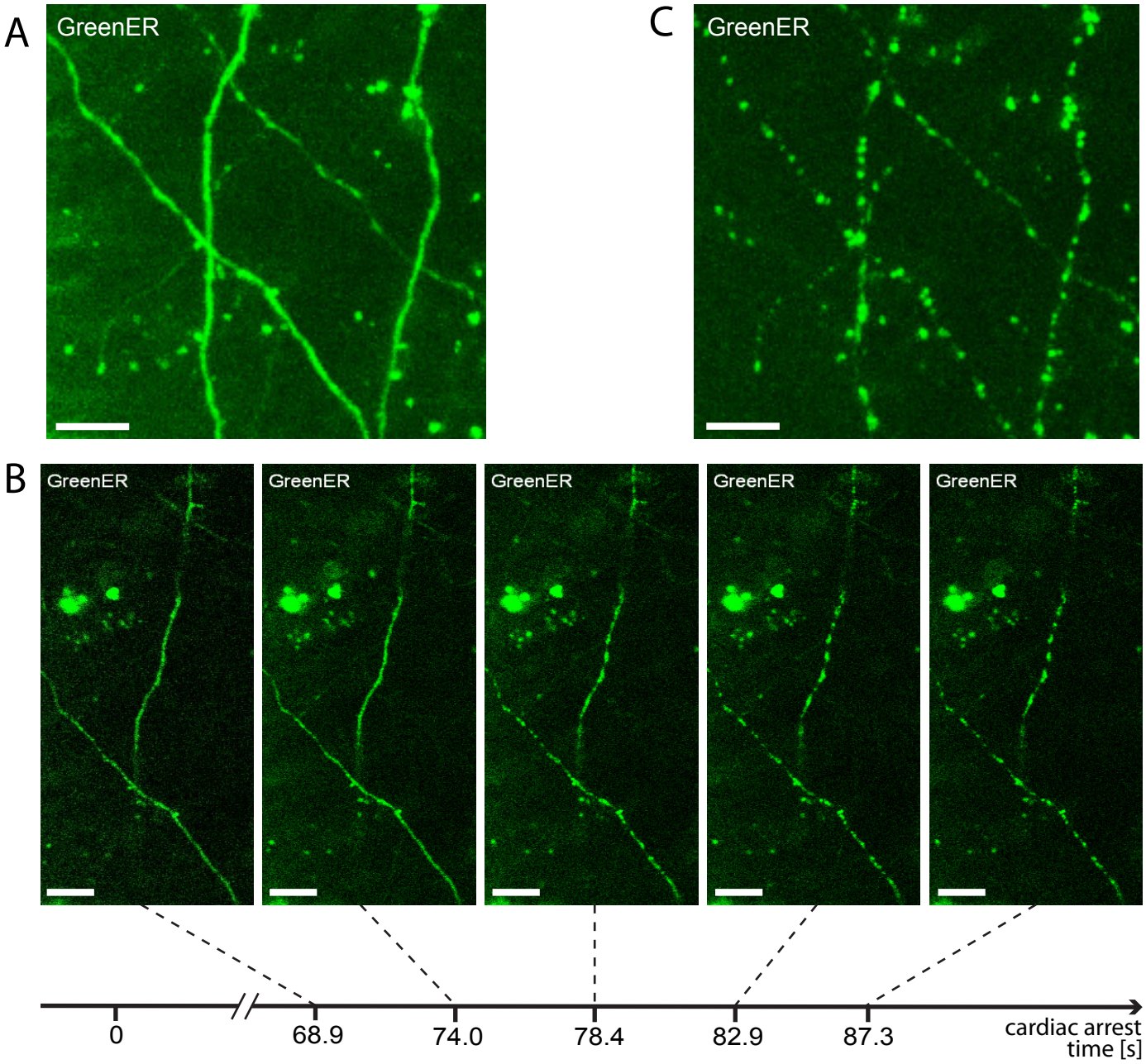

Paper III; Figure 3

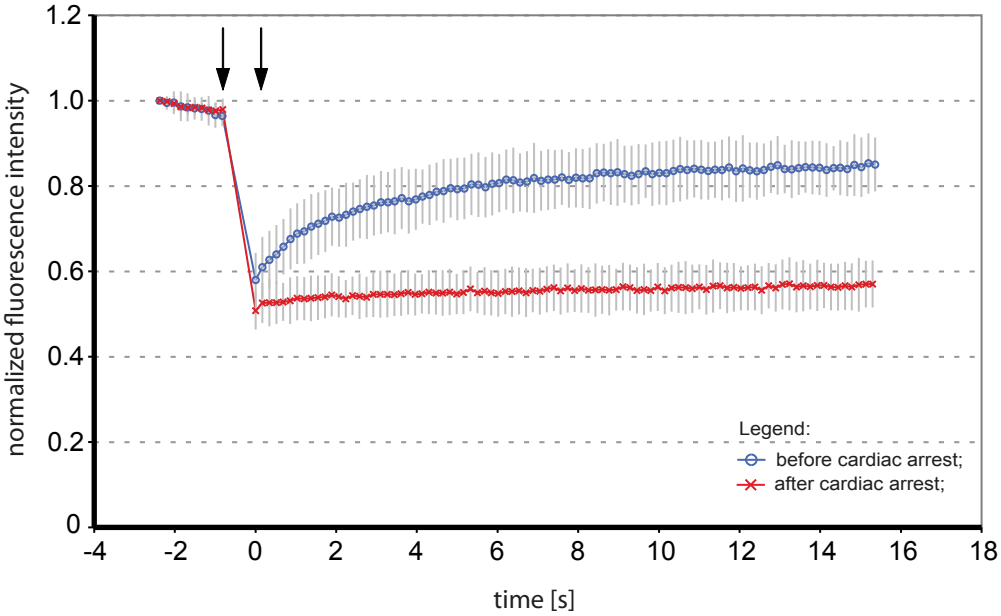

Paper III; Figure 4

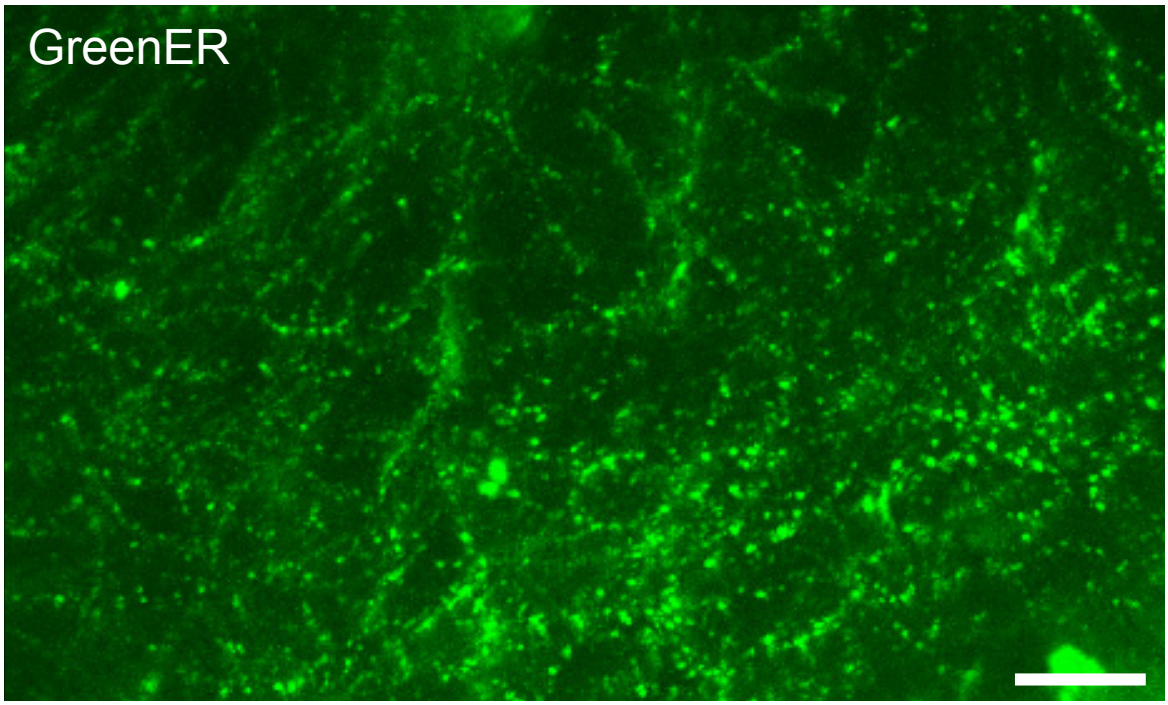

Paper III; Supplementary Figure 1

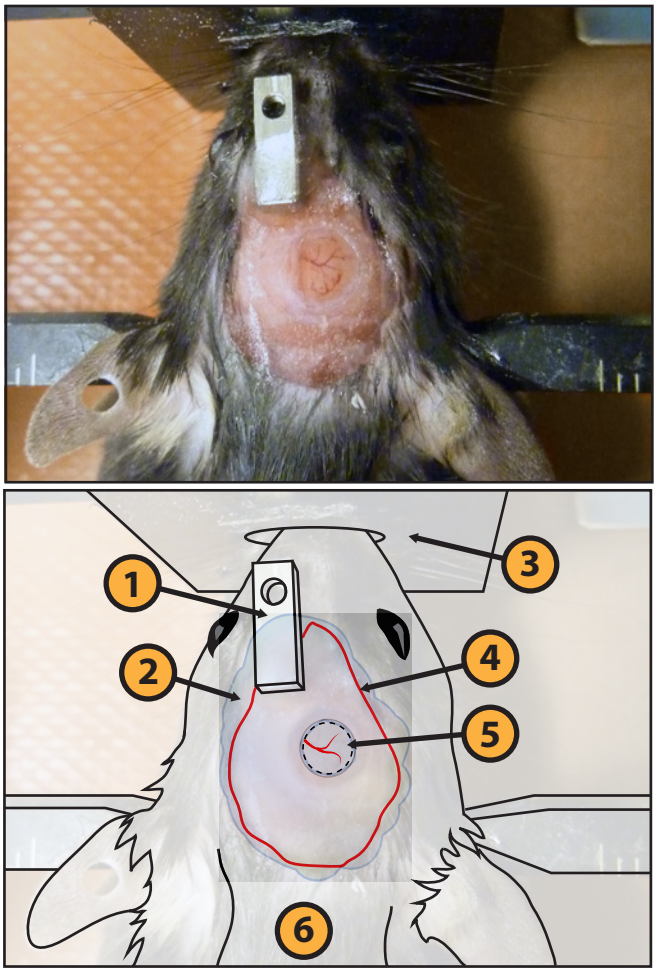

Paper III; Supplementary Figure 2